The realisation of the solar chimney inlet guide vanes

Cobus van Dyk

12929840

Thesis presented in partial fulfilment of the requirements for the degree of Master of Civil Engineering at the University of Stellenbosch.

Study leader: Prof. G.P.A.G. van Zijl

April 2004

DECLARATION

I, the undersigned, hereby declare that the work contained in this thesis is my own original work and has not previously in its entirety or in part been submitted at any university for a degree.

SYNOPSIS

Up to this point in time research on the South African solar chimney, proposed for a site in the Northern Cape, comprised of determining the structural integrity of the chimney structure, as well as airflow calculation, finding the optimal shape for the airflow channels. Not much work had been done on the realisation of the foundation of the global structure, i.e. how the cardinal parts are optimized in an integrated system.

The inlet guide vanes (IGV's) should be central in such research efforts, being the main support of gravitational and lateral wind load on the chimney structure, as well as its important role in channelling air and creating pre-swirl of the airflow onto the turbine blades. However, little detailed research – research to actually determine and fix the many variables of the IGV's and integration with surrounding parts – had been performed!

In this thesis as many of these variables as possible are investigated – ranging from structural integrity with regard to compressive and shear strength through optimizing structure eigenfrequency to economic feasibility. The outcome of this study is conceptual solutions regarding the geometry of the IGV structures in order for it to support the chimney while minimizing material volume.

Finite element methods are used to create insight into the behaviour of the IGV's and force transferring structures, incorporating external factors such as lateral wind and gravitational loads to determine the optimal shape of these structures.

This study is valuable for researchers on the solar chimney, serving as a reference from where to design and secure the variables of the global structure, and eventually building the solar chimney.

Keywords: Solar chimney, inlet guide vanes, solar power, massive concrete structures, structural realisation, finite element application, structure optimisation.

OPSOMMING

Tot op hede het die navorsing op die Suid Afrikaanse sonskoorsteen, wat beplan word vir konstruksie in die Noordkaap, bestaan uit die bepaling van die integriteit van die struktuur asook lugvloei berekeninge om die optimale vorm van die lugvloei kanale te lewer. Min werk is gedoen om die fondasies van die globale struktuur, dus hoe die kardinale dele geïntegreer is in die gesamentlike sisteem, te ondersoek.

Die inlaat lei lemme behoort sentraal te lê in sulke navorsingspogings aangesien dit die hoof ondersteuner en verspreider van gravitasie en laterale windlaste op die skoorsteen struktuur is. Dit speel ook 'n integrale rol in die kanalisering van invloeiende lug om dit vooraf 'n vorteks beweging te gee vir 'n optimale invalshoek op die turbine lemme. Min gedetaileerde navorsing – navorsing om die verskeie onbekende faktore rondom die inlaat lei lemme en die omliggende strukture te bepaal – is tot op hede gedoen.

Hierdie tesis mik om soveel moontlik van hierdie veranderlikes – wat reik van struktuur integriteit met betrekking tot die samedrukkings- en skuifsterktes in die materiaal tot die eie-frekwensies en ekonomiese vatbaarheid van die struktuur – vas te stel. Die uitkoms van hierdie studie is konseptuele oplossings vir die geometrie van die inlaat lei lem strukture wat terselfdertyd die totale struktuur se materiaal volume minimiseer.

Eindige element metodes word gebruik om insig in die gedrag van die inlaat lei lemme en ander strukture wat krag oordra, te genereer. Die metodes inkorporeer soveel as moontlik van die eksterne faktore soos gravitasie en laterale windlas om die optimale geometrie vir die betrokke struktuur te bepaal.

Hierdie studie is waardevol vir navorsers oor die sonskoorsteen en dien as 'n bron waaruit verdere ontwerp en die vasstel van veranderlikes in die globale struktuur gedoen kan word met die oog op die uiteindelike daarstelling van 'n sonskoorsteen.

ACKNOWLEDGEMENTS

Professor G.P.A.G. van Zijl, my study leader.

Professor Reinhard Harte and Matthias Andres, Bergische Universität Wuppertal.

My father and engineering inspiration, Louis van Dyk, for his enthusiasm as well as the many hours of diligent proof reading.

Carl Kirstein, my mede visionêr en pelgrim. Mag ons drome vir Afrika en die wêreld realiseer.

Robert Kellerman, for all his support and enthusiasm.

D.F. Fyfer, Antoon de Klerk, Stephanus de Kock en al die ander Afrika magnate.

Lord Jesus Christ who always, always stands with me.

TABLE OF CONTENT

APPENDICES

LIST OF FIGURES AND TABLES

FIGURES Description of figure page

TABLES **Description of table** **page**

KEY TO THE USE OF THIS REPORT

References are depicted in square brackets. They are not numbered in the order of their appearance in the report but are numbered according to their alphabetical position in the "References" at the end of the thesis.

Appendices are located at the end of this thesis after the "References" pages.

When passages from literature are quoted, the text might be slightly adapted for more comfortable reading. These changes are made in italic text.

Many references are made to full colour figures. Where reference is made to a specific colour in a figure the corresponding shade in greyscale format is provided in brackets.

The input and geometry files for the models used in the FE analyses, in digital format, are handed in with the report.

CHAPTER 1: INTRODUCTION

1.1 Why solar power?

Electricity is a basic necessity in modern everyday life. The search for energy converting, electricity-generating mechanisms continues unabated. Through kinetics the bicycle dynamo generates electricity, dry cells provide power in order to listen to music on a CD-Discman and coal, oil, gas and nuclear are successfully used in providing energy for generating electricity; and many other ingenious scientific achievements attained energy-generating status on the world energy market. The earth also provides mankind with many resources, once thought of as inexhaustible.

Recently, however, mankind has had to start facing the consequences of his selfish consummation of the very resources that keep him alive. The fact is that the waning coal and oil/gas deposits in the world will soon have to be replaced by an alternative sustainable energy source.

Figure 1-1. Possible energy sources: fossil fuels, ocean currents, lightning and wind turbines [21, 27, 24, 28].

For the past fifty years the dream of a high efficiency, low cost electricity generator that acts in harmony with nature kept scientists busy. Wind power, wave action and even lightning, as seen in *Figure 1-1*, are all sparks of interest in the search for an alternative energy source. The shortage of water to justify more hydro-electricity plants, the abandonment of wave-generated electricity due to high cost and low efficiency, as well as public resistance to nuclear energy motivate the search towards other sustainable energy sources.

Conspiracy theory has it that such revolutionary "clean" sciences had been in existence for years but remains smothered by the economical power-monopoly of the fossil fuel gods. The looming cloud

predicting the depletion of these energy sources will, however, demand drastic action to be taken soon, forcing these hidden technologies to come to the fore.

The future of this earth and mankind depends to a great extent on the ability to slow down the population increase in the "Third World" by civilized means [22]. The key is to increase the standard of living and to overcome the inhumane poverty and deprivation. To achieve this by traditional means will not suffice any longer as exemplified by the following paradox: those countries where agriculture provides more than 20% of the gross national product are those also stricken by starvation. Development requires mechanisation and energy. Energy consumption increases proportional to the gross national product or prosperity while simultaneously the population growth decreases exponentially. This phenomenon is graphically displayed in *Figure 1-2*.

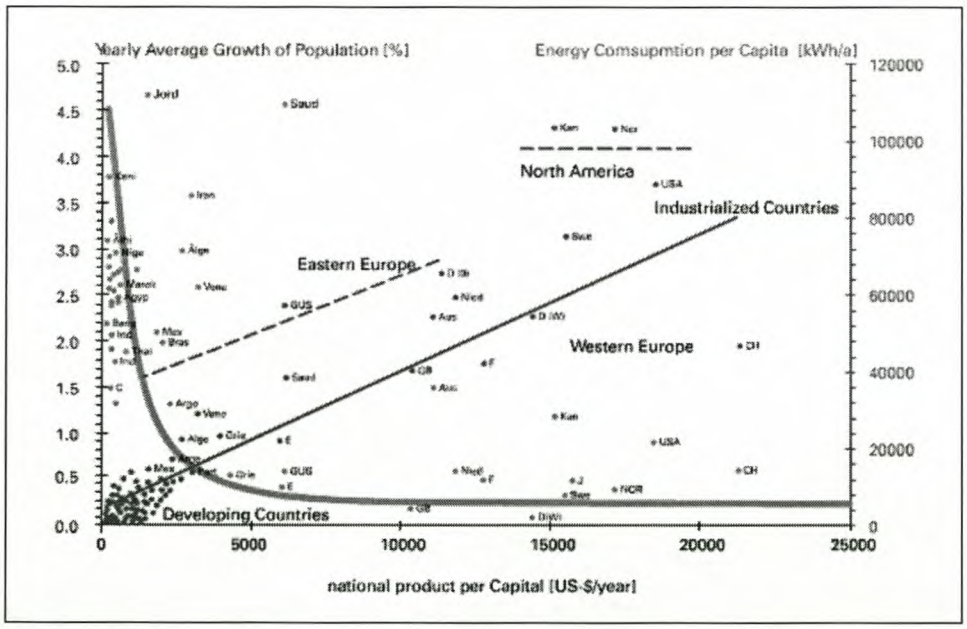

Figure 1-2. Energy consumption depicted relative to the gross national product and the population growth of countries [22].

Many developing countries possess hardly any energy sources while their population doubles every 15 to 30 years [22]! The results are seen in civil wars and fundamentalism. If these developing countries could only be provided with a humane and viable energy source satisfying their minimum energy requirements, the global energy consumption will drastically increase. Unfortunately it proves impossible to supply such an enormous amount of energy without an ecological breakdown (poor countries cannot afford environmental protection) or safety hazards (these countries are not acquainted with the necessary safety requirements for nuclear power plants) and without a rapid depletion of natural resources at the expense of future generations!

However, many of these countries have an abundance of sunshine, especially in their desert areas, and thus have an abundant source of solar radiation [22]. This is common knowledge, already stated in Agenda 21 of the United Nations conference on Sustainable Development that took place in Rio de Janeiro in June 1992 (the Rio Declaration On Environment And Development, see [26]), but few parties are doing anything about it – it must be a well-kept secret that large-scale solar energy utilization is possible today and that it is affordable and competitive!

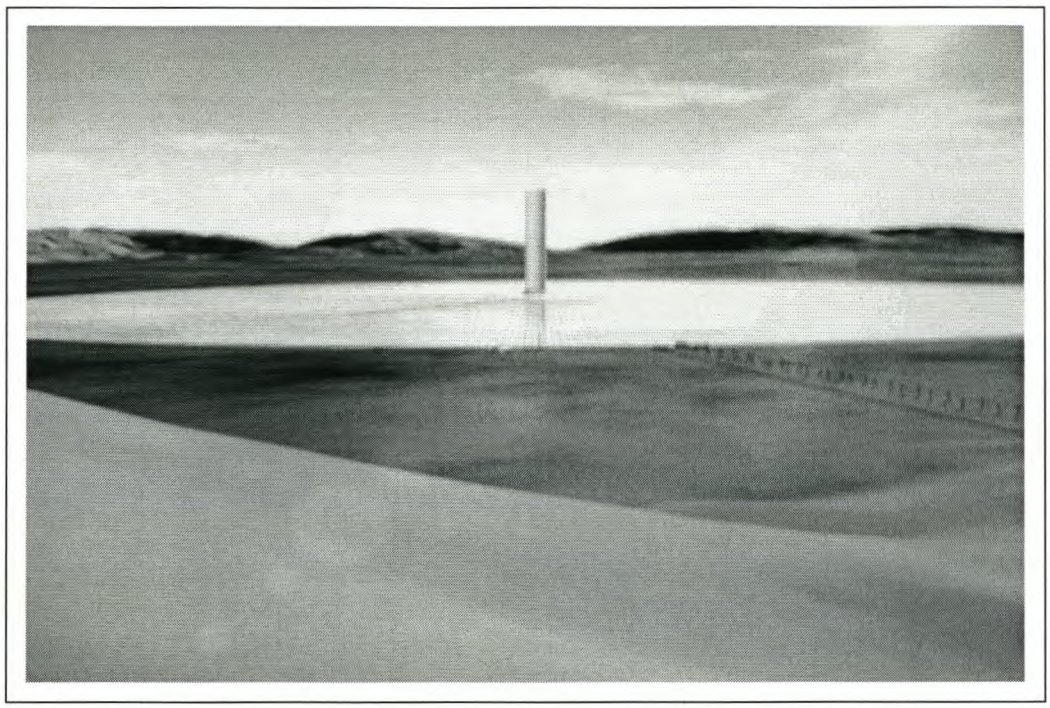

Figure 1-3. The solar chimney... [32]

1.2 The solar chimney

The sun, the earth's main energy source, has been the subject of many research projects and even commercial action, with installations such as solar panels being widely available today. Recent scientific breakthrough in South Africa claims the production cost of these solar panels can be lowered to a tenth of that of the panels commercially available up until now [31]. The sun still remains the biggest prospect toward finding feasible solutions for our energy crisis.

1.2.1 Enter: the solar chimney

The solar chimney (refer to *Figure 1-3*) had proved itself to be one of the main contenders in the race toward finding an alternative energy source for the 21st century. SolarMission AG, a German

solar-energy propagating company, states that "... within the field of solar thermia, two power plant technologies have emerged which promise the greatest economic success: the Parabolic Trough and the Solar Chimney ..." [23].

A consequential prospect of the solar chimney in developing countries is that raw material and labour costs will be much lower than in the first world, so that initial capital outlay will decrease significantly. Although the initial cost will still be great, low maintenance costs and high, continuous energy output rates may prove it to be both an effective and feasible solution [10].

1.2.2 Principle and working of the solar chimney

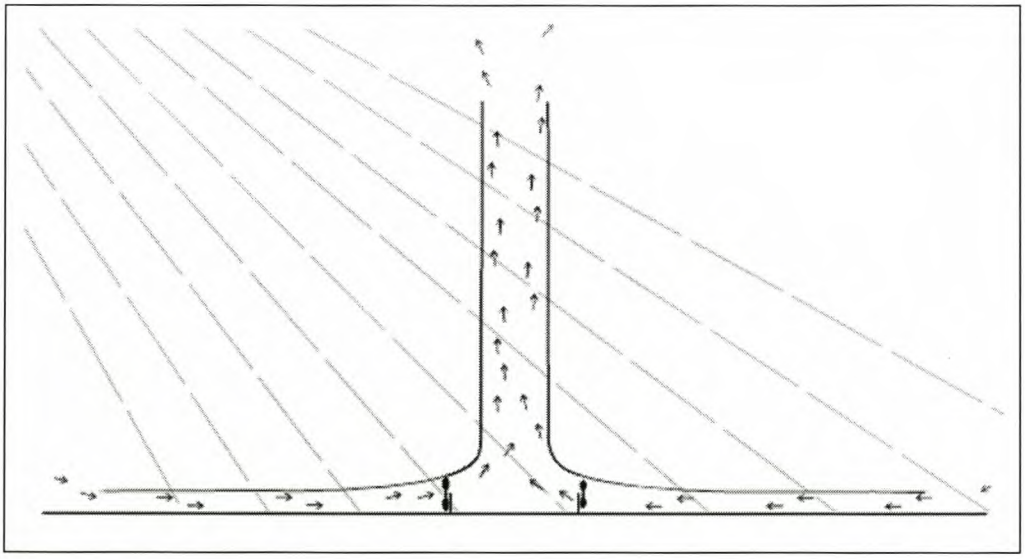

Figure 1-4. The solar chimney in principle: glass roof collector, chimney and wind turbine [22].

The solar chimney operates like a hydroelectric power plant using hot air instead of water (*Figure 1-4* – note: this figure depicts a variation in the turbine setup, where several turbines with horizontal axes, placed around the chimney base, are used). Air is heated beneath a large glass roof. The roof is slightly inclined toward its centre, causing the heated air to rise, thus entering a vertical tube placed at the centre of the roof. An up-draught is created. Inside the tube a wind turbine with an electrical generator transforms kinetic energy into electricity.

Contrary to solar power plants with reflecting mirrors, the glass roof collector of a solar chimney operates 24 hours continuously. The earth, heated during the day, radiates at night, upholding the air flow toward the chimney. Furthermore, generation continuity can be guaranteed by placing

watertight tubes, filled with water, under the roof. The water heats up during the daytime and emits its heat at night. These tubes are filled only once; hence no further water is needed.

1.2.3 Dimensions of the solar chimney

In order for the solar chimney system to convert electric energy from solar radiation (heat energy) significant wind velocities must be reached inside the collector (kinetic energy) to cause continual movement of the turbine. A high pressure system is created at the base of the chimney through the convergence and hence compression of the air. Air diffuses from the high pressure air volume to the lower pressure at the top of the chimney. The continual cycle of air moving under the glass roof is caused by the upward inclination of the roof toward the centre of the system working in combination with the vertical convection of the heated air, and by the momentum (once the cycle is initiated) of the mass of air moving. The immense size of the collector determines the stability, continuity and magnitude of the force exerted on the turbine blades. Larger dimension of the glass roof ensures greater volumes of air moving, effecting greater momentum and, consequently, greater force on the turbine. *Figure 1-5* displays that the taller the chimney and/or the greater the collector diameter, the greater the annual energy production [10]. Therefore it is these immense dimensions of the solar chimney that makes it effective and feasible as an energy source.

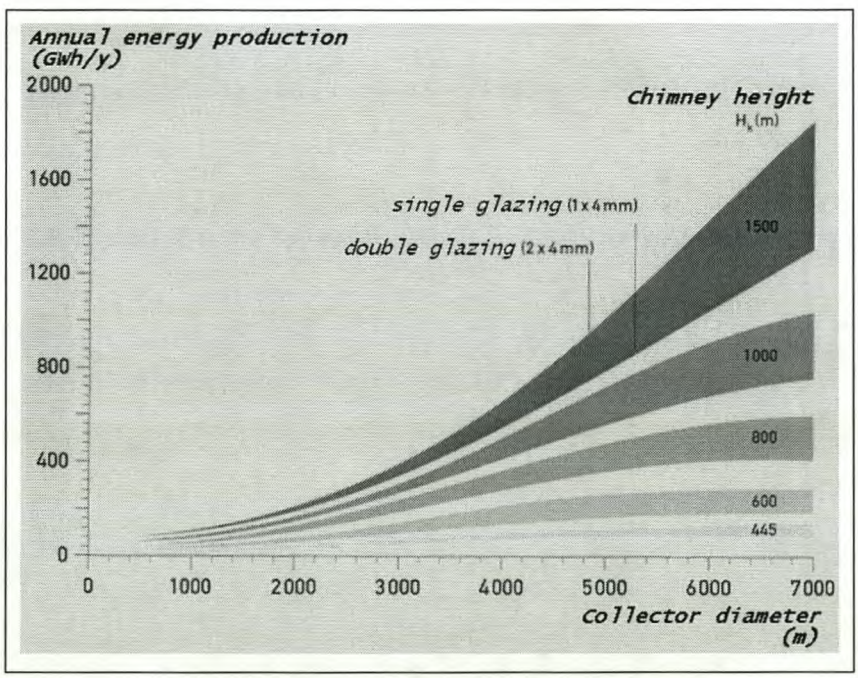

Figure 1-5. The amount of energy generated by solar chimneys is dependent on its dimensions. The figure shows values for collectors with single and double glazing glass [10].

A demand for an output of 200 MW was put forward for the design of a solar chimney proposed for the Northern Cape, South Africa [13]. The proposed geometry of the solar chimney system includes a 1500-metre tall chimney shell; 160 meters in diameter and flaring slightly toward the top, as well as a glass roof collector with a diameter of 6.9 kilometres (*Figure 1-6*). A summary of the global dimensions follows:

<u>Chimney</u>	
Chimney height:	1500 m
Diameter, $D_{base,inner}$:	160 m
Diameter, $D_{base,outer}$:	164.4 m
Diameter, $D_{top,inner}$:	170.5 m
Diameter, $D_{top,outer}$:	171 m
Chimney-enclosed sectional flare:	14 %
Wall thickness, t_{bottom}:	2.2 m
Wall thickness, t_{top}:	0.25 m
<u>Collector</u>	
Collector diameter:	6.9 km
Collector inlet height:	10 m
Collector height at chimney base:	60 m

The "flare" mentioned above is an outward tapering of the chimney toward its top, proposed in documentation [16].

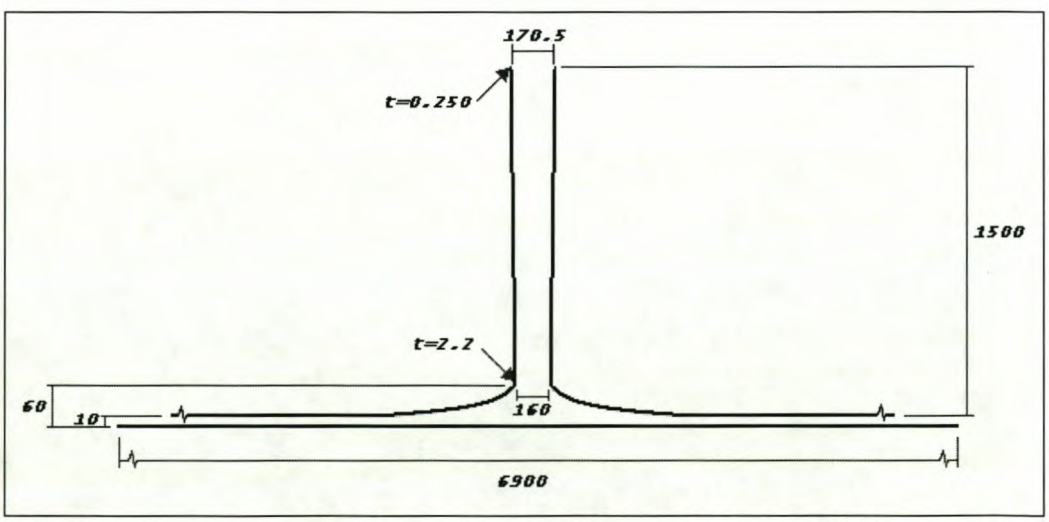

Figure 1-6. Global dimensions of the solar chimney (dimensions are in metres).

1.2.4 Introducing the inlet guide vanes

With reference to *Figure 1-7*, the heart of the solar chimney system lies at the bottom of the chimney shell where the collector and chimney meet. The moving air flows radially inwards from the exterior environment through the collector, past the inlet guide vanes, and upwards. The turbine, which is also situated here, rests on a cone. The cone, in combination with the inlet guide vanes, directs the air before it hits the blades of the turbine, giving it a pre-rotation or "pre-swirl".

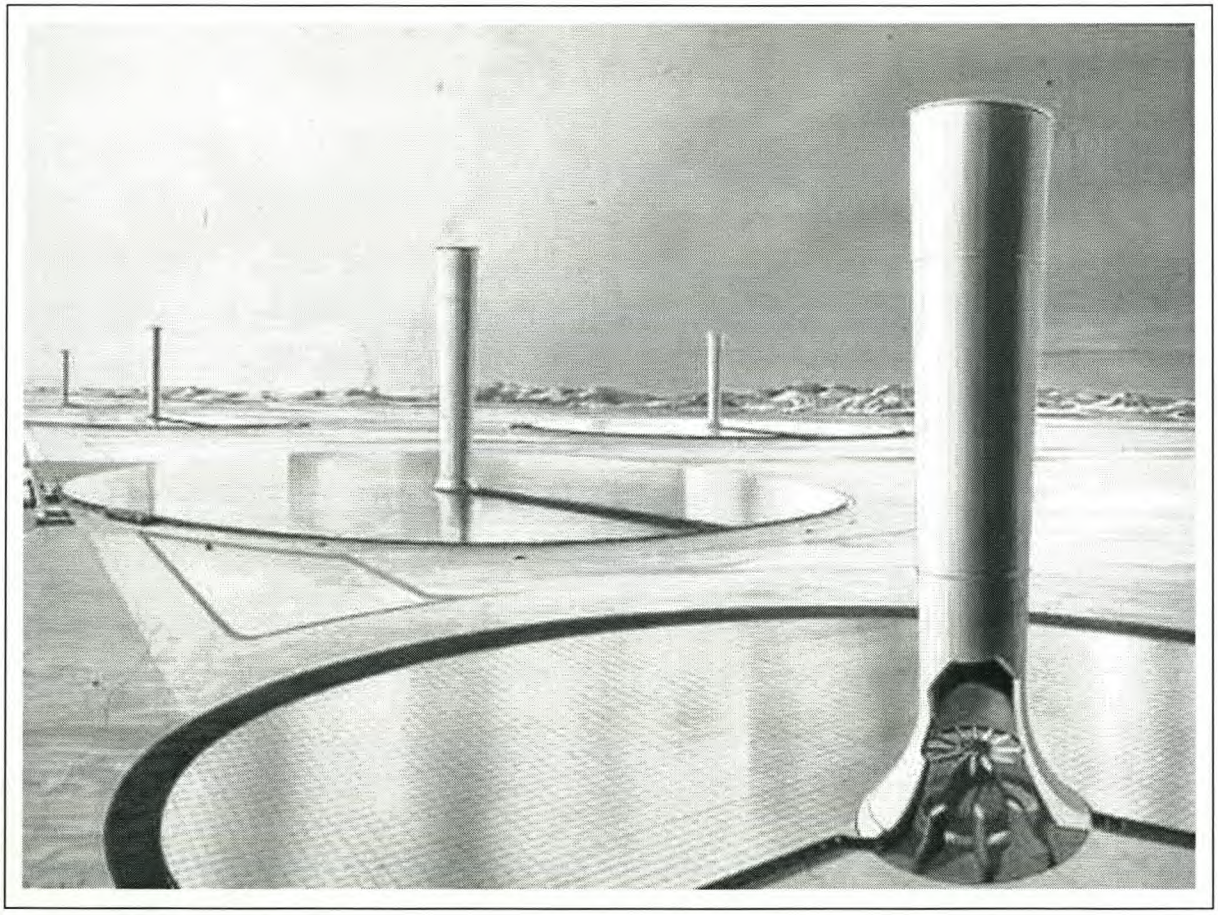

Figure 1-7. An artist's impression of the future – a solar chimney farm. The chimney base is cut open, revealing approximate positions of the inlet guide vanes, the turbine and the turbine cone [8].

These vanes have a crucial role to play in the dynamics of the solar chimney serving as aerodynamic guides to the air. The possibility exists to utilize these vanes further for the cardinal role of structural columns supporting the chimney, transferring the massive gravitational and wind loads of the chimney to the foundation of the system. The vanes will then fulfil a dual role: primarily supporting the chimney while re-directing the inflowing air. For the purpose of this thesis the structural role is considered to be the primary.

The structural function of the inlet guide vanes is the topic of the research reported in this thesis.

1.3 The inlet guide vanes

1.3.1 Background

Until now research on the South African solar chimney, proposed for a site in the Northern Cape, has addressed various widespread topics, such as the structural integrity of the chimney structure, as well as air flow calculation towards the optimal shape for the airflow channels. Little work has been done on the realisation of the global structure, i.e. how the key parts are optimized in an integrated system and, as implied in the previous paragraph, the structural role of the inlet guide vanes (IGV's) should lie central to such research efforts.

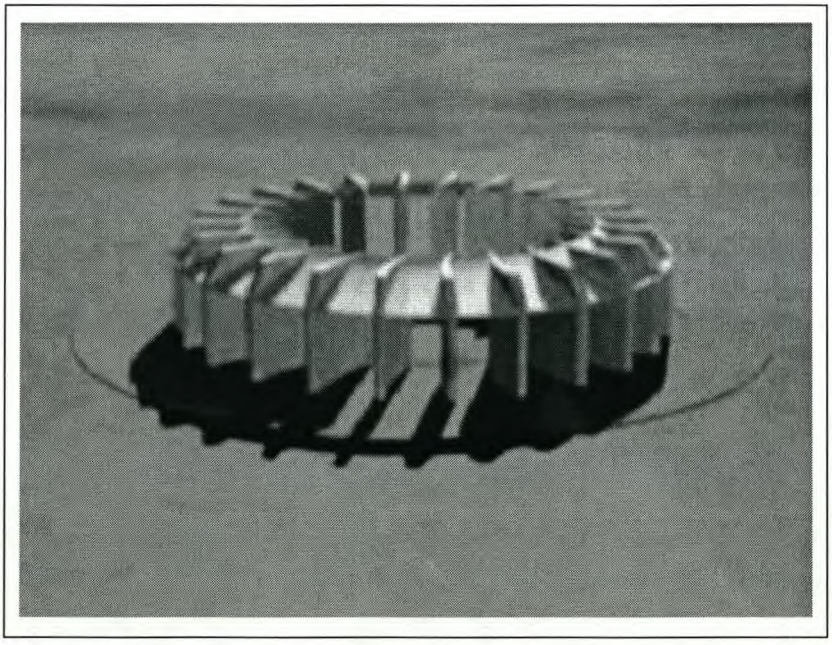

Figure 1-8. An artist's impression of the supporting columns of the chimney: structurally sound, space generating, aerodynamically shaped structures [32].

1.3.2 What is expected of an inlet guide vane structure?

The IGV is to be primarily a structural entity. The main forces acting on the chimney are gravity and wind-induced pressure. The chimney, acting like a cantilever under lateral wind forces (refer to *Table A-1* of *Appendix A* for values of these forces), needs a vessel transferring these forces to the

foundation. The structure must be able to support all forces acting on it – mainly compressive forces, but also tensile forces, shear forces and moment action – while remaining stable.

Secondly, the IGV's are space managing structures, creating and sustaining suitable ducts/guides for the through flow of incoming air (see *Figure 1-8*) toward the turbine and its supporting cone.

The third, and very significant, function of an IGV is not structural but aerodynamic in essence. An IGV serves to create a pre-swirl of the air approaching the turbine in order for it to attack the turbine blades at the optimal angle. In order for it to fulfil this function, the IGV must be aerodynamically shaped.

Finally, the IGV's act as connection point between the collector and the chimney. It must allow the geometry of the collector to "flow" into the geometry of the chimney, creating airtight channels in the solar chimney for unobstructed air flow past the IGV's, via the cone-structure into the chimney.

The above-mentioned requirements are structural in nature, dictating the design of the IGV's. More detailed requirements, which this thesis will briefly touch on, entail facets concerned with the financial and practical feasibility of the structure.

1.4 Scope of this thesis

1.4.1 Summary of the problem

The challenge at hand is to formulate a concept that will satisfy all requirements for the IGV as set out above – a structurally sound, space generating, aerodynamically shaped structure that is able to transfer all loads exerted on it while remaining stable. The solution must be economically viable.

1.4.2 Constraints before the research process starts

The research was mainly directed towards the structural aspects of the IGV's using values determined during previous research, or literature studies, as given inputs. These values were transferred to constraints that the IGV's have to satisfy. Instances are clearly indicated where used.

Only static analyses with linear material properties are considered in order to provide a foundation from which in-depth dynamic analyses with non-linear material can be studied in future. Non-linear

geometrical effects are considered in most instances. Dynamic analyses are not considered in much detail in this research effort.

Geotechnical aspects such as soil stiffness characteristics are not incorporated into this study.

In conclusion, this study is conceptual in nature.

1.4.3 Layout of the report

The research followed a logical process, reflected in the layout of the report, which is as follows:

1. The report commences in *Chapter 2* with a summary of the literature study performed in the duration of the research. After previous research performed on IGV's is reported, deep beam theory, as well as typical column theory and design, is summarised.
2. The detailed IGV geometry used in this research is presented in *Chapter 3*. Current IGV concepts are investigated, weighed up and criticized.
3. This is followed by *Chapter 4* where the forces acting on the IGV, as well as consequent internal action, are predicted and studied.
4. With this foundation in place conceptual solutions to the problem are formulated and reported in *Chapter 5*.
5. The concept is also tested in *Chapter 5*. Resultant stress and deformation patterns as well as eigenfrequency are the limit state parameters. ABAQUS finite element (FE) software [17], amongst others, is used for this process.
6. A geometrical optimization as well as a brief cost comparison is done in *Chapter 6* improving different concept models.

1.5 Additional motivation

Before reporting the details of the research effort the author would like to quote the following paragraphs, written by Carl Kirstein [29] as additional background in this introductory section. It is from the section he composed as the motivation for the research he is conducting on the airflow characteristics surrounding the inlet guide vanes of the solar chimney. Kirstein writes (additions to his text in *italics*):

> "The Republic of South Africa is not the scientific breadbasket it could be due to lack of funds and the consistent emigration of graduates as they finish studying. The solar chimney project helps to change

that by drawing graduates from other countries and keeping *our own* graduates because it is highly advanced and multi-disciplined. It involves applying theories that were inapplicable previously, it involves developing new manufacturing and construction techniques and it gives opportunity to investigate convalescence of the environment with the assistance of man-made structures. The disciplines involved in the project at the moment are disciplines of engineering (with the exception of chemical engineering), environmental impact researchers, project managers, marketing researchers, human resources and politicians. As the project develops even more disciplines would get involved. Its attraction is also that due to the *immense* scale of the project nearly everything done on it is unique.

Eventually when the solar chimneys are being built, the cost of producing such a structure would decrease with each one erected. This will cause many of these plants to be built throughout Africa and in all the desert areas of the world. Doing so creates many job opportunities and strengthens the economy of our country and that of the countries in which it is being built. The plants would initially boost the tourism to the country that has such a structure, improving the economy even more.

The motivation of this project is therefore primarily to make the solar chimney more feasible and attractive. As soon as the full potential for this plant is realized beyond its power generating abilities, the development of the project will be supported ardently..."

and

"...Fossil fuels are non-renewable and produce emissions that are damaging to the environment. Nuclear plants produce radioactive waste that may be hazardous to store or dispose of. These considerations have lead to the emphasis on 'clean' (non-polluting) energy. The energy sources that are considered clean are natural sources like solar radiation, wind and flowing water."

"Environmentalists may argue that such a large structure that causes large displacements of air will somehow affect the weather adversely. However, research to investigate the environmental impact of the solar chimney has thus far not revealed any indication of undesirable effects.

The capital expenditure of such a structure would be high, but not significantly higher than a nuclear power plant of the same power output. When the solar chimney's layout is finalized and standardized, the cost of producing each new plant would be less than the previous one, but the main advantage of the solar chimney over the other power plants is the *low* operational costs. A local inhabitant trained on site, for instance, ran the pilot plant at Manzanares *(an experimental solar power plant – chimney of 194 metres – completed in 1989 [22])*. The solar chimney would require some maintenance but in general, very few staff members will be needed to operate and maintain the plant in comparison to any other power plant. Therefore the economical motivation is to have the chimney pay for its capital expenditure in a few years and from then on produce energy more economically than other existing power plants.

> A significant amount of the capital expenditure is embedded in the cost of materials. Therefore the transition section *(i.e. the topic of the present research)* should be optimised to give the best combination of strength, efficiency and cost. This project ... endeavours to lay a foundation on which any future designs on the inlet could be built and evaluated."

These paragraphs summarise the pre and post-construction benefits this project could have to Southern Africa and the world. And, as mentioned earlier, the future of this earth and mankind depends to a great extent on his ability to slow down the population increase in developing countries by the increase of living standards [22].

The solar chimney endeavours to resolve this crisis.

CHAPTER 2: LITERATURE STUDY AND PRELIMINARY DISCUSSION

Finding documentation on the solar chimney is not an easy, if indeed at all possible, task. Due to it being a sensitive, contentious subject, information is not readily available. Most researchers and companies are protecting the information known to them.

Basic conceptual information on the solar chimney is available through authors like Prof. Jörg Schlaich, the initiator of worldwide research efforts, through his book *The Solar Chimney: Electricity from the Sun* [10]. Several authors investigated the feasibility of the solar chimney (or parts of it) as a workable energy generating entity, focusing on the thermodynamics (Kröger and Buys, [3]), air flow (Von Backström [15]), turbine performance (Gannon [1]) and the global impact of the prospected power plant (Schlaich [10 and 11]). To the author's knowledge only two research efforts surrounding or incorporating the inlet guide vanes have been (and are being) performed and reported, namely the work by Dr. Anthony J. Gannon on the turbine performance, *Solar Chimney Turbine Performance* [1], and a continuation of his work by Carl Kirstein [29] in which he furthered the research by Dr. Gannon. Kirstein's work is to be published in 2004.

Structural aspects of the inlet guide vanes are yet to be defined, although limited proposals have been made by Gannon [1] on the shape of the section, the layout and number of IGV's. Also, some video clips have been released for marketing purposes [19, 32]. ("References" from video material were never during this research used to determine dimensions or other facts, but are rather used during the conceptualization process, directing and furthering it.) There is therefore a great void in the structural development of the solar chimney, making this research effort an unchartered and, consequently, a very exciting one.

2.1 Inlet guide vanes

The functioning of general IGV's, followed by the solar chimney IGV's, is briefly described in order to introduce the structural aspects and optimisation parameters of these structures.

2.1.1 General inlet guide vanes

Inlet guide vanes provide an efficient method for the re-direction of airflow into centrifugal compressors such as those found in gas turbines, thermo-compressors and turbojets (*Figure 2-1*).

The guide vanes realize energy savings through the lowering of the inlet pressure drop and the impartation of a whirl motion (the term "pre-swirl" is preferred in this thesis) to the gas before it enters the compressor impeller [25].

Each vane is designed as an aerofoil to minimize its resistance to airflow in the fully open (zero rotation angle with the radial plane) position. IGV's use unique cambered wing airfoil vane designs to add the whirl motion to the air. With un-cambered, straight vanes there is more air resistance and less whirling action [20].

IGV's can be rotatable, i.e. the angle with the radial plane can be varied so that they open on a loss-of-air situation (leading edge is longer than trailing edge). This keeps the compressor from entering a state of surge on loss of air. The movable vanes are constructed and positioned in such a way that the inlet air to the impeller eye is caused to swirl in the direction of impeller rotation. The flow angle to the impeller eye increases as the vanes are closed and with increased angle (with the radial direction) the first stage impeller is required to do less work resulting in higher system efficiency. As the entering flow angle of the air is varied, a new head characteristic curve is produced for each angle of flow. This type of control results in increased efficiency at partial load conditions (that is, when the load is not at its maximum) [20].

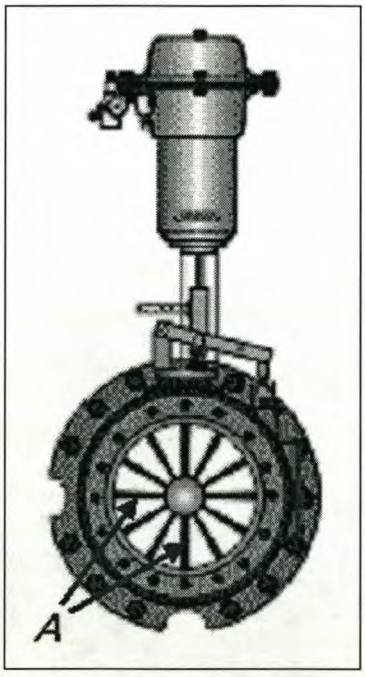

Figure 2-1. An application of inlet guide vanes (radially positioned structures, "A" in the figure) as found in a micro-turbine system providing onsite electricity [25].

2.1.2 Solar chimney inlet guide vanes

In his thesis Dr. Gannon [1] poses the question whether a successful compromise can be found between the two functions of the radial flow inlet guide vanes of the turbine, namely providing the optimum amount of pre-swirl and supporting the chimney structure. His research focussed on the former of the two functions, proposing an optimal aerodynamic shape, height, layout, amount and an optimal range of angles through which the IGV's may be rotated.

Gannon proposes a concept whereby the chimney base supports are used as inlet guide vanes to introduce pre-swirl onto the turbine. Values of a few of the design parameters he assumed during his research included a chimney height of 1500 metres, a chimney inner diameter of 160 metres and an overall energy output of 200 MW.

Amount [1]

The amount of IGV's was fixed after an optimisation procedure showed that, in the laminar flow criterion chosen by Gannon to be used in the IGV blade airflow analyses, the blade aspect ratio was very low resulting in long flow passages. It was decided to increase the number of IGV's. This resulted in shorter flow passages and higher aspect ratio blades. In the final part of the design process a system with 18 IGV's with rotatable trailing sections, to maintain high efficiency over a wide operating range, were proposed.

Rotation [1]

The IGV is to be rotated about its vertical axis by a fixed angle of between 0 and 22.5 degrees in order to optimally re-direct the airflow. These rotated chimney supports would improve the torsional stiffness of the chimney base.

Height [1]

From a structural perspective the height of the IGV's should be made as low as possible without constricting the air flow. Low IGV's would increase the velocity at the base of the chimney as the inlet area would be smaller. However, the advantage of high IGV's is that there would be a large flow contraction in the duct section, resulting in an accelerating flow that would be resistant to separation on the outer wall of the IGV.

Blade profile [1]

To obtain optimal air flow along the exit angles of the IGV span, a twist in the previously constant IGV plan-section is wished for (see *Figure 2-2*). This would require the construction of the high chimney supports with a twist – a challenging task! Consequently, Dr. Gannon proposes the IGV

plan-section to be constant to "make their construction simpler and *to make* them more effective as supports for the chimney."

The choice of the blade profile happened early in the design process when it was decided to use existing aerofoil profiles for the inlet guide vanes, mainly to keep the design variables on the solar chimney concept to a minimum. For existing profiles experimental data exists, stating values for the lift and drag coefficients that have been demonstrated to work in many applications. Consequently, a NACA 4-digit blade profile was proposed and used in his research [1].

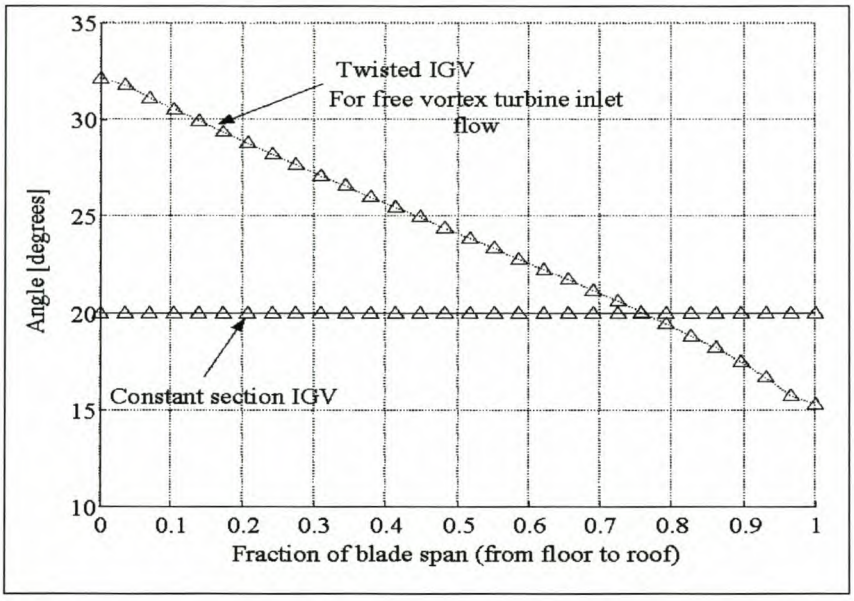

Figure 2-2. Exit flow angles for the optimal air flow case and constant section IGV [1].

Final geometry [1]

Figure 2-3 displays the final global geometry proposed by Gannon. Note that the turbine diffuser is not a solid wall but is merely a proposed form specially shaped for creating the optimal air pressure around the turbine and post-turbine regions.

Research performed by Carl Kirstein [29] aims at homing in on the optimal IGV height and angle. His research is currently in its final stages.

Sustaining through flow of air [1]

Apart from its structural purpose the IGV's are space-managing structures, as was mentioned briefly in *Chapter 1 paragraph 1.3.2*, creating and sustaining suitable ducts/guides for the through flow of incoming air toward the turbine and its supporting cone. The layout, section, angle and height of the IGV's are important parameters to form an air through-flow section suitable for the generation of

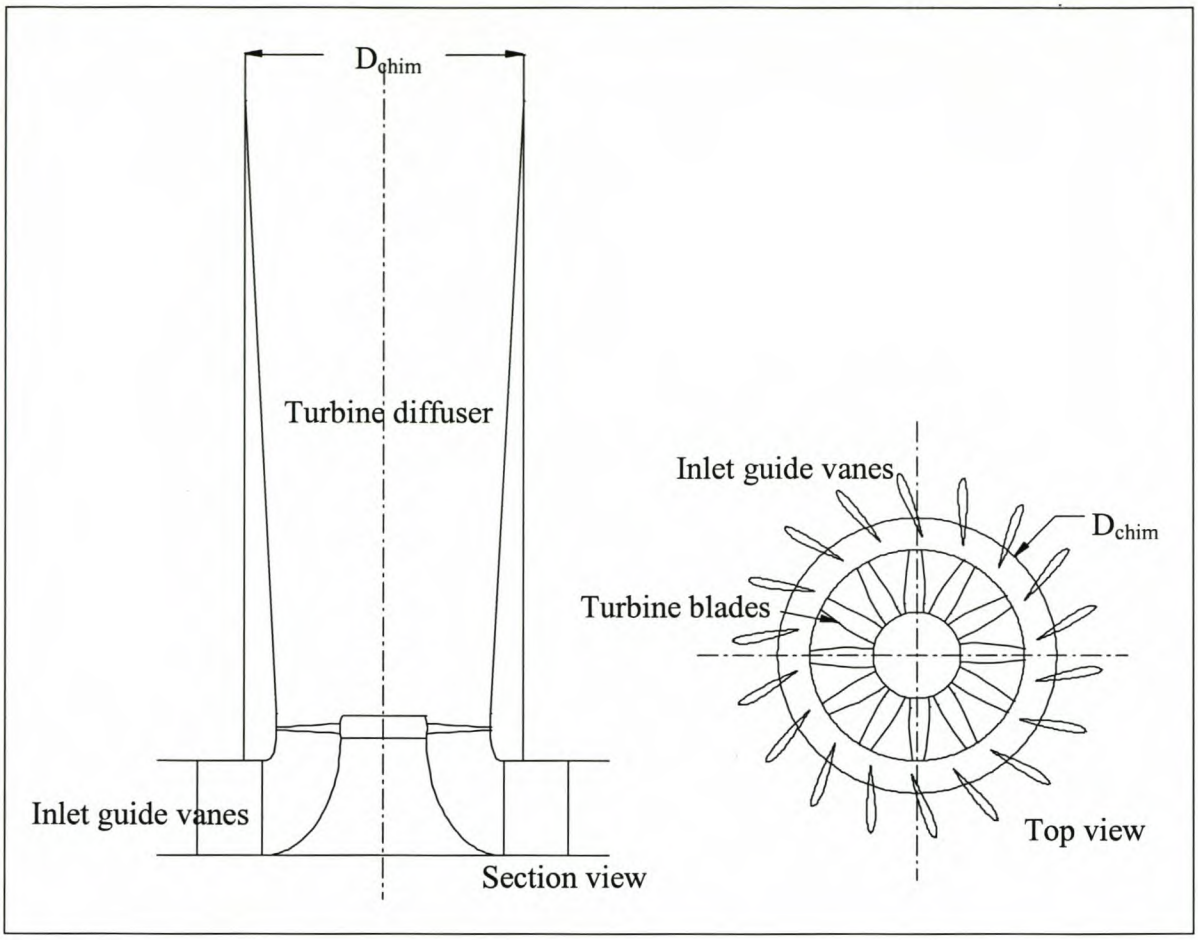

Figure 2-3. Section and top view of solar chimney turbine [1].

optimal wind velocity and pre-swirl. The continuity of this through-flow velocity determines, to a great extent, the effectivity of the solar chimney as a system.

2.2 Forces on the IGV

Previous research investigated the forces acting on the chimney structure [14]. Wind extrapolation models were used to determine the wind velocity and pressure at the appropriate heights because of the lack of prescriptions in loading codes and of meteorological information on speeds at these great heights. Three wind extrapolation models were investigated and the most conservative result, that is, the wind velocity distribution with the highest values, reaching 108 m/s at the maximum height of 1500 m, was used in further application. *Table A-1* in *Appendix A* give the wind velocity values corresponding to the conservative model.

Consider *Figure 2-4a*. The curve gives the values for the pressure coefficient at positions around the chimney, both for rough and smooth surfaces. The corresponding coefficients for smooth surfaces were used in the determination of the wind pressure. The calculations for determination of the wind forces are reported in *Appendix A*. The effect of this non-uniformly distributed pressure on an unstiffened chimney is displayed in *Figure 2-4b*.

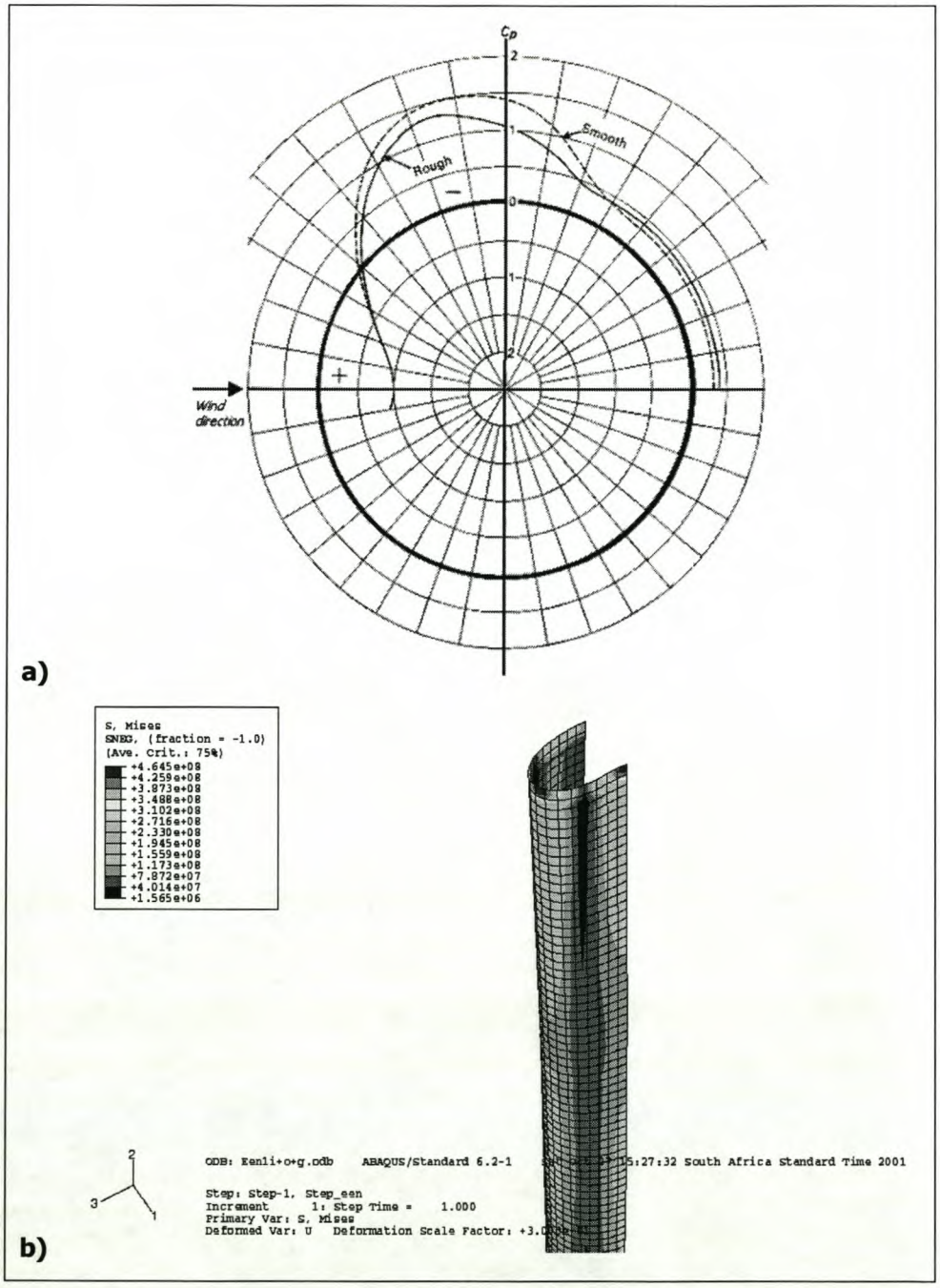

Figure 2-4. Wind pressure: a) the pressure distribution due to wind from the direction as shown [8] causing b) large deformations in the chimney shell [14].

A finite element (FE) model of the chimney structure was set up [14] with ABAQUS FE-software [17] and the wind load applied. The analysis results indicate the non-uniform wind pressure to be very significant, coercing the thin-shelled chimney structure into a bean shape (ovalisation), making it an ineffective air-channel and a structure susceptible to buckling because of the distortion of its regular circular shape. Special conceptual tension structures, acting as ring stiffeners, have been proposed to sustain the cylindrical form. The analyses showed that the current proposal is not sound, as local low frequency resonance of stiffener parts will be excited. Nevertheless, an improved design, which will sustain the cylindrical form under static wind pressure, has been proposed for the purpose of this study, while local vibrations of the stiffener parts have been ignored for the time being. This is an issue earmarked for further research.

The ovalling behaviour was the focus of the previous research by Van Dyk [14] and effects like resonant lateral oscillation were predicted not to be excited under the wind load causing the ovalisation. Hence, the dynamic response was not further considered in that research.

Limit state design

The partial safety factor for the ultimate limit state (ULS) of concrete in compression is 0.45, i.e. it limits compressive stresses to 0.45 times the characteristic concrete strength [2]. The factor is in fact a combination of a simplification of the compression constitutive behaviour and the material factor of 1.5 for concrete. The simplified compressive law comprises a parabolic stress-strain relation up to 2/3 of the ultimate resistance (fcu). Subsequently, perfect plasticity is assumed at that limit of 2/3 f_{cu} until failure at a strain level of 0.0035. The combined limit state factor of 2/3 x 1/1.5 = 0.45 is implemented in this thesis.

2.3 Structural theories and tools

During IGV design a few structural theories and tools prove to be valuable. These are

- deep beam theory, as parts of the structure, including the IGV-chimney intersection, can be seen as very deep beams (*Figure 2-5*);
- basic column theory, where the IGV is assumed to be a short, eccentrically loaded column (*Figure 2-5*);
- column interaction diagrams – a useful tool to initialise the conceptualisation process.

The following sections are devoted to a summary of these theories and tools.

2.3.1 Deep beam theory

The following section on deep beam theory is summarised from *Reinforced Concrete Structures* by R. Park and T. Paulay [6].

Introduction

When the span to depth ratio of simply supported beams is less than 2, or less than 2.5 for any span of a continuous beam, it is customary to define these beams as deep. Such structures are encountered in rectangular suspended containers such as silos, in foundation walls supporting strip footings and in shear wall structures that resist lateral forces in buildings. The traditional principles of stress analysis are neither suitable nor adequate to determine the strength of deep reinforced concrete beams.

With the midspan moment being $wl^2/8$ (where w = distributed load [N/m] and l = span length [m]), the usual extreme fibre stress at midspan of a square panel with a span/depth ratio of 1 would be

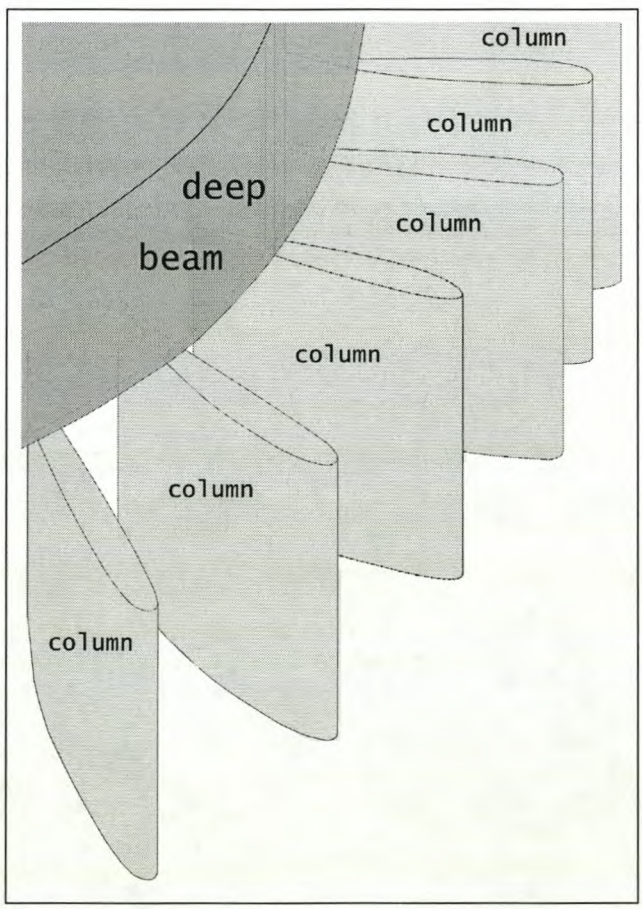

Figure 2-5. The base of the chimney structure – a type of continuous deep beam – resting on the IGV's – a type of column.

$$f_{tension} = f_{compression} = \frac{6M}{bh^2} = 0.75\frac{w}{b} \qquad (2\text{-}1)$$

where f = stress
M = resultant moment
b = width of beam
h = depth of beam

The middle figure in *Figure 2-6* (span to depth ratio = 1) displays the fact that the tensile stresses at the bottom fibre of this beam are more than twice this value. Similar deviations occur for the distribution of shear stresses. For the determination of principal tensile stresses, the vertical stresses, particularly at the support points of the beam, are of great importance. The dimensions of the bearings of the beams in *Figure 2-6* would affect the principal stresses, which can be very critical in the immediate vicinity of these supports. Stiffening ribs and extended columns at these supports would markedly influence the stress patterns.

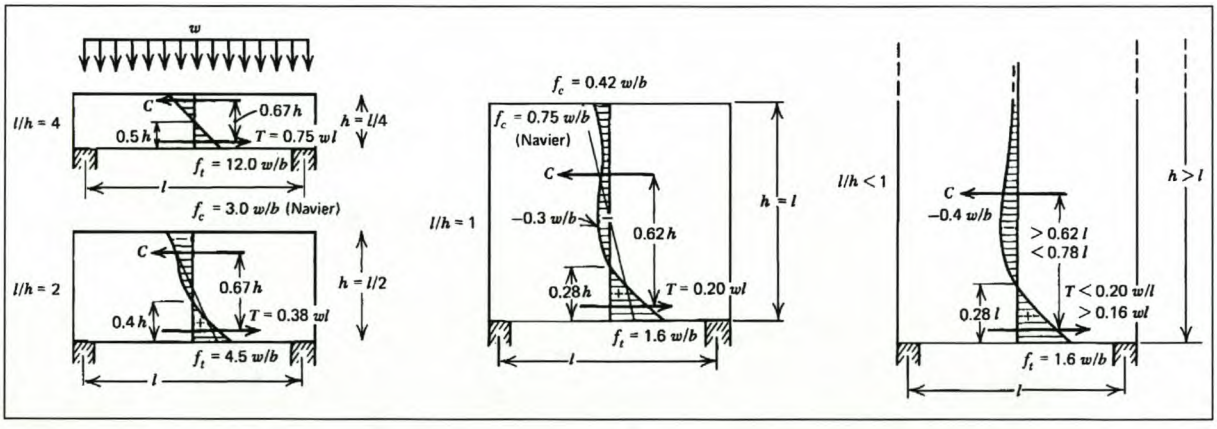

Figure 2-6. Distribution of flexural stresses in homogenous simply supported beams [6].

The application of the load would be more or less uniformly distributed – the gravity load being in the form of bearing pressure applied at the top surface of the beam as seen in *Figure 2-6*. This causes vertical compressive stresses, which the concrete can usually resist without difficulty, opposed to other cases (silos) where the weight to be supported may have to be suspended from the bottom edge of the beam, necessitating extra reinforcement. The compressive stresses in the concrete are seldom critical but still solutions often fail to take into account the two most important aspects of deep beam design, namely the anchorage requirements for the reinforcement and the considerable increase of diagonal compressive stresses near supports after the onset of cracking.

Due to the fact that the steel demand for these structures is seldom large, approximate design techniques have been developed that cover most load cases and boundary conditions. These techniques also account for the concrete cracks in the tension zones.

Note that only gravity loads are examined in the paragraphs following.

Continuous deep beams

Continuous homogenous deep beams show a great deviation from the linear pattern of stress profiles across the midspan and support sections of non-deep beams. The internal lever arm of the axial force stress resultants decreases rapidly as the span to depth ratio of the beams approach unity (see *Figure 2-6*). In particular, the tension force over the support region (i.e. negative moment) can be closer to the compression edge than to the tension edge of the beams. This is an important feature of deep beams and must be kept in mind, even though the internal lever arms will increase in both the negative and positive moment zones after cracking, and especially when yielding of the flexural steel has set in.

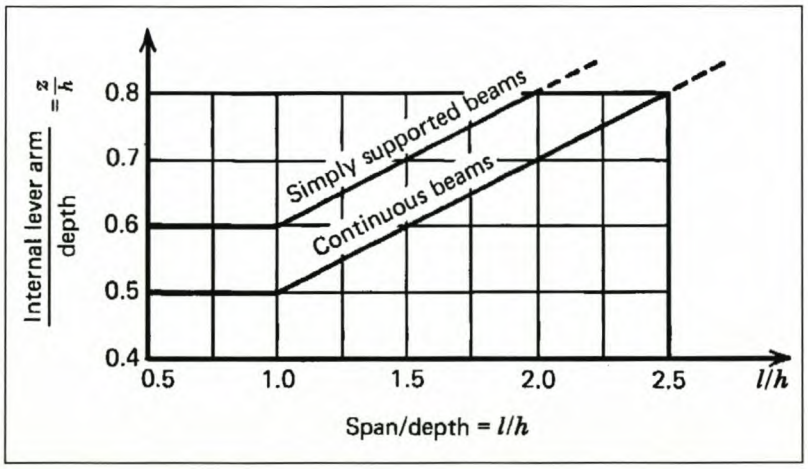

Figure 2-7. Internal lever arm of deep beams [4].

The shear stresses, when combined with the vertical compression stresses originating from bearing at the supports, will generate steeply inclined principal compressive stresses. This suggests that shear is transferred mainly by, so called, "arch" action.

To simplify the flexural steel computations the Comité Européen du Béton-Federation, in their *International Recommendations For The Design And Construction Of Concrete Structures*, suggests that the internal lever arm z be computed for both the negative and positive moments as

$$z = \frac{l}{2}; when \frac{l}{h} < 1 \qquad (2\text{-}2)$$

Figure 2-7 depicts the values for the lever arm length for simply supported and continuous beams. Bending moments may be calculated as for slender beams – that is, $wl^2/12$ and $wl^2/24$ of the continuous spans, for the support and midspan moments respectively. In a cracked beam the internal lever arm is likely to be smaller over the support than at midspan. *Equation 2-1* does not show this but the apparent discrepancy is compensated for because the actual moments at the supports are smaller than those predicted by the customary analysis with the midspan moment for a cracked beam, correspondingly, being larger than the $wl^2/24$.

Steel reinforcement

The midspan (positive) reinforcement should be arranged exactly as for simply supported beams, all bars anchored at or passing through the supports. Detailed reinforcement design is often neglected but is not reported here as the detailing falls outside the scope of this research.

Shear resistance

The compressive forces due to flexure are rarely critical in deep beams, but the possibility of lateral buckling of the compression zone in thin walled beams may need to be examined. It is important to protect the compression zone over the support where diagonal compression due to shear concentration may be critical. Satisfactory shear behaviour can be expected if the maximum shear force is limited to

$$V_{\max} \leq 0.08\varphi b_w h f_{cu}^{'} \qquad (2\text{-}3)$$

where $h \leq l$

φ = 0.85

b_w = beam width

h = beam height

f_{cu} = concrete yielding strength

Recommendations for shear strength of deep beams are restricted to simply supported beams with a clear span to depth ratio of less than five, provided the beams are loaded on the top face and supported on the bottom face. It is postulated that the shear capacity of a member is obtained by the superposition of the capacity of the concrete and that of the web reinforcement. Recognition of

the reserve shear capacity of a deep beam without web reinforcement led to the development of the semi-empirical expression

$$v_c = \left(3.5 - 2.5\frac{M_u}{V_u d}\right)\left(1.9\sqrt{f_{cu}'} + 2500\rho_w \frac{V_u d}{M_u}\right) \le 6\sqrt{f_{cu}'}; \frac{V_y d}{M_u} \le 1.0 \qquad (2\text{-}4)$$

where v_c = shear capacity of concrete
M_u = ultimate moment
V_u = ultimate shear force
V_y = yielding shear force
d = effective depth of concrete stress block
ρ = density of web material
(Note that all quantities in the above formula are in imperial units with stresses in psi.)

The derivation of the web reinforcement's contribution toward shear resistance is based on the shear friction concept – shear stresses causing a sliding type of failure along a well-defined plane, and because of external tension or shrinkage a crack may form along such a plane even before shear occurs. Thus the possibility for shear transfer by aggregate interlock and dowel action arises. It is assumed that when a steep diagonal crack develops shear displacements occur. The resulting increase in crack width then fully mobilizes all reinforcement crossing such a crack. The component of the yield force acting at right angles to the inclined crack assumedly supplies the required clamping force for the shear friction mechanism to operate. This way horizontal web reinforcement significantly contributes toward the shear strength of the web provided the bending moment at the section considered is small. From an experimental derivation of the relationship between the inclination of the diagonal crack and the span to depth ratio with the acceptance of the apparent coefficient of friction of 1.0 along the potential diagonal failure crack, it was shown that the shear capacity of the steel must be

$$v_s = v_u - v_c = \left[\frac{A_v}{12s}\left(1 + \frac{l_n}{d}\right) + \frac{A_{vh}}{12s_h}\left(11 - \frac{l_n}{d}\right)\right]\frac{f_y}{b_w}; v_u = \frac{V_u}{b_w d} \qquad (2\text{-}5)$$

where v_s = shear capacity of steel
A_v = area of vertical reinforcement
s = distance between vertical reinforcement members
l_n = effective section length
A_{vh} = area of horizontal reinforcement

s_h = distance between horizontal reinforcement members

f_y = yielding strength of steel

Arch mechanism

In slender beams the diagonal cracking load sets the limit to the useable shear strength in the absence of web reinforcement. When suitably introduced into a deep beam, a load in considerable excess of the diagonal cracking load can be carried because of the great stiffness and strength of the arch mechanism. Eventually crack widths become excessive; nominal shear stresses must therefore be limited (*Equation 2-3*). Gravity load, introduced along the top edge of the beam, is disposed of mainly by arch action. The load will naturally choose to dispose of itself through the stiffer of two possible resisting systems and in deep beams the arch is always stiffer than the truss mechanism.

2.3.2 Column theory

Columns are structural elements used primarily to support compressive loads. They can be classified, amongst others, as short or slender: a short column is one in which the ultimate load at a given eccentricity is governed only by the strength of the materials and the dimensions of the cross section. With a slender column the ultimate load is also influenced by slenderness, producing additional bending because of transverse deformations. Kong and Evans [2] states that it is sufficient to define a short column as one in which the length is not more than 15 times the minimum lateral dimension. Since the aspect ratio (the ratio of the height to the minimum width) of the IGV is nearly never more than approximately 10 it will be assumed to be a short column. Present load cases are both axial (around the weak axis) and eccentric (around the strong axis). The aspect ratio around the strong axis should never be bigger than five.

Columns with high aspect ratios as well as great transverse force and/or end moments are classified as "slender". The only known transverse action along the height of the IGV is the force due to incoming air flow which is approximately 300 000 smaller than the largest vertical downward force acting in on the IGV. Also assuming the imperfections in the IGV geometry and material to be small it cannot be classified as a slender column.

The subject is introduced to the reader starting elastically. Subsequently the ULS is described which is used extensively in the design process.

Axially loaded short reinforced concrete columns – elastic behaviour

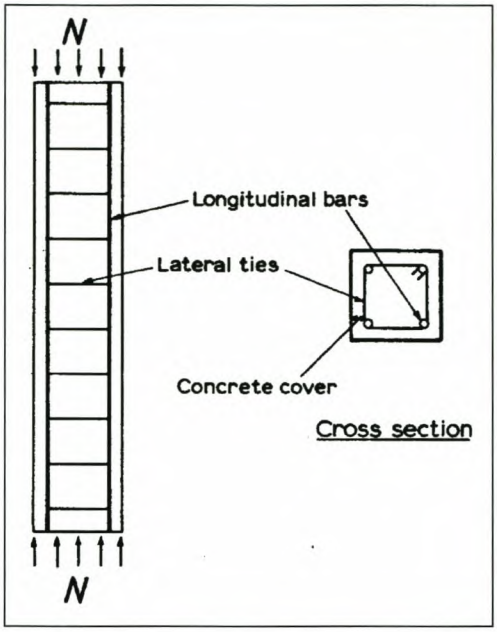

Figure 2-8. A typical reinforced concrete column subjected to an axial load *N*, showing the layout of reinforcement A_{sc} [2].

When the stresses in the concrete and the reinforcement are sufficiently low the stress/strain relationship may be considered linear and the usual elastic theory applies. The axial load resistance is calculated by the *Equation 2-6* (see *Figure 2-8*):

$$N = f_{cu} A_c + f_s A_{sc} \tag{2-6}$$

where N = axial load resistance
f_{cu} = yielding compressive stress in the concrete
f_s = yielding compressive stress at coinciding strain in the longitudinal reinforcement
A_c = cross-sectional area of the concrete
A_{sc} = cross-sectional area of the longitudinal reinforcement

Equation 2-6 can be re-written to give the required concrete yield stress as

$$f_c = \frac{N}{A_c + \alpha A_{sc}} \tag{2-7}$$

where $\alpha = \frac{E_s}{E_c}$ = ratio of the material modulii and

$$\frac{f_c}{E_c} = \frac{f_s}{E_s}$$ (concrete strain = steel strain)

This, of course, applies for elastic behaviour and limits the concrete stress to the linear-elastic range. If the limit is exceeded a larger section is required.

Axially loaded short reinforced concrete columns – hygral behaviour

The above equations may give the false impression that the stresses f_{cu} and f_s in a column are uniquely defined once the load N is specified. In fact it is almost impossible to determine these stresses accurately. This is because of the effects of creep and shrinkage of the concrete. Note, however, that in practice f_{cu} is usually much less than that given in *Equation 2-7*.

The detailed concrete behaviour due to creep and shrinkage falls outside the scope of this thesis due to its conceptual nature. However, for a detailed definition of and a discussion on the dynamics of creep and shrinkage refer to the publication by Kong and Evans [2].

Eccentrically loaded short reinforced concrete columns – uni-axial bending [2]

Purely axially loaded columns occur rarely in practice because some bending is almost always present, brought about by, amongst others, the slight initial crookedness of columns, the manner in which loading is applied by beams and slabs, and the moments introduced by continuous construction. The analysis of reinforced concrete members under combined bending and axial load may be based on the same assumptions as those in the general theory for axial short column theory and theory for ultimate flexural strength in beams. Bending about one major axis of the section only (uni-axial bending) is considered in this section through the study of *column interaction diagrams* and the theory behind it.

Column interaction diagrams

At this stage non-linear behaviour of the material is considered. The ULS criteria are introduced for further application in this study. In the design of eccentrically loaded columns engineers make extensive use of design charts called column interaction diagrams. These diagrams prove to be a helpful tool during this study, especially during the cost optimisation process; hence some time will be taken to get an insight into the properties of these diagrams and the principles governing their construction.

Consider a plain concrete section (*Figure 2-9*) subjected to an axial load N and a bending moment M. The section in the figure is at incipient failure with strain and stress distributions as shown. The depth of the concrete stress block is equal to 0.9x with $0.9x \leq h$. From the equilibrium equation (applying the British loading code partial safety factors γ_m, which for the ultimate limit state (ULS) of collapse are 1.5 and 1.15 for concrete and reinforcement, respectively)

$$N = 0.45 f_{cu} b d_c = 0.405 f_{cu} b x \tag{2-8}$$

where N = axial load resistance
f_{cu} = yielding compressive stress in the concrete
b = section width
d_c = maximum depth of concrete stress block
x = effective section depth

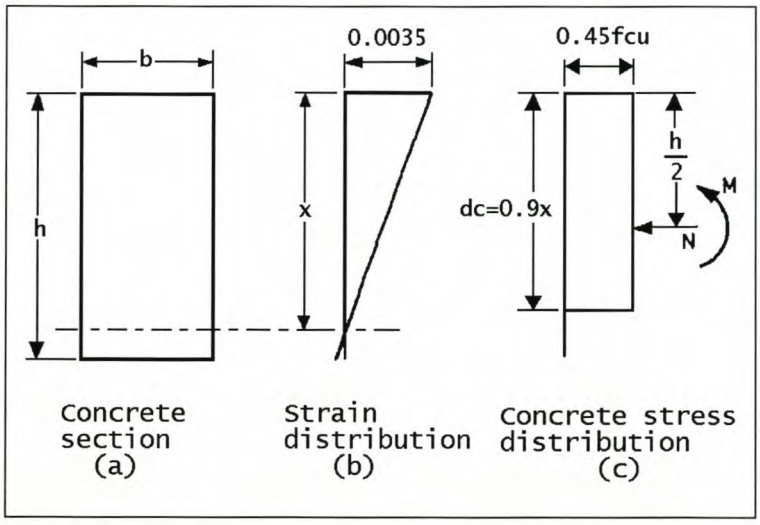

Figure 2-9. Plain concrete section (a) subject to an axial load *N* and a bending moment *M* with corresponding strain distribution (b) and stress distribution diagrams [2].

And by taking moments about the mid-depth of the section

$$M = N\left(\frac{h}{2} - \frac{d_c}{2}\right) = 0.203 f_{cu} b x (h - 0.9x) \tag{2-9}$$

where h = height of the section

These equations can be expressed in dimensionless form for later application in the column interaction diagrams:

$$\alpha_{concrete} = 0.405\frac{x}{h} \tag{2-10}$$

$$\beta_{concrete} = 0.203\frac{x}{h}\left(1 - 0.9\frac{x}{h}\right) \tag{2-11}$$

Thus for x/h = 0.1, $\alpha_{concrete}$ = 0.0405 and $\beta_{concrete}$ = 0.0185; for x/h = 0.2, $\alpha_{concrete}$ = 0.0810 and $\beta_{concrete}$ = 0.0333 and so on. By successively assigning different values to x/h the complete $\alpha_{concrete}$ against $\beta_{concrete}$ curve may be constructed (*Figure 2-10*). Each point on this curve represents a state of incipient failure, an "envelope" fencing off the points representing safe combinations of N and M (inside the curve) while those outside the envelope represent combinations where failure will occur.

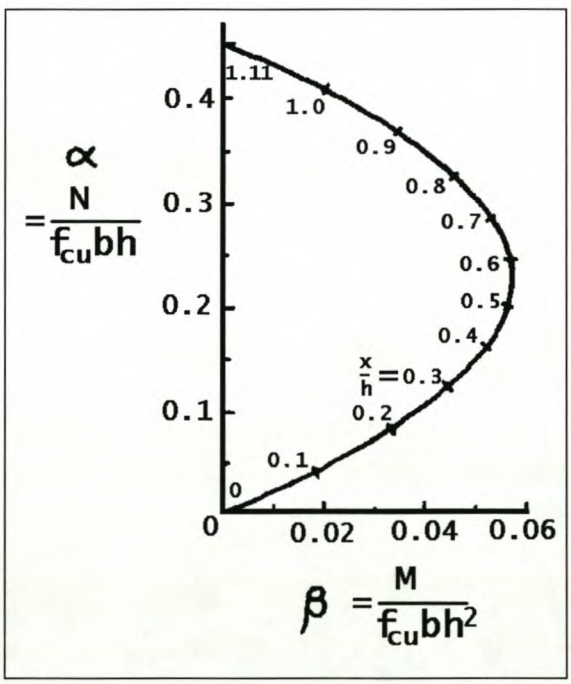

Figure 2-10. Column interaction diagram of a plain concrete section [2].

Consider the effect of compressive and tensile reinforcement steel areas A_{s1} and A_{s2}. The axial strength of the column becomes

$$N = 0.405 f_{cu} bx + 0.87 A_{s1} f_{s1} + 0.87 A_{s2} f_{s2} \tag{2-12}$$

And for the moment

$$M = 0.203 f_{cu} bx(h - 0.9x) + A_{s1} f_{s1}\left(\frac{h}{2} - d_1\right) + A_{s2} f_{s2}\left(\frac{h}{2} - d_2\right) \qquad (2\text{-}13)$$

The contribution of the reinforcement steel in the adapted column interaction diagram can clearly be seen in *Figure 2-11*:

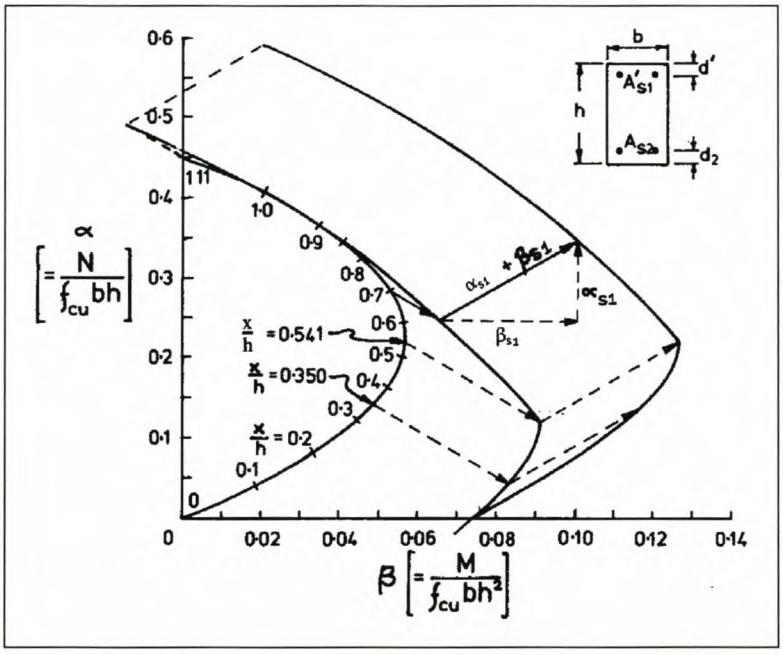

Figure 2-11. Column interaction diagram of a reinforced concrete column [2].

Once again points inside the curve represent safe combinations of N and M while those outside represent unacceptable combinations. For more insight into the principles governing the construction of column interaction diagrams, refer to Kong and Evans [2].

A practical example

Figure 2-12 and Table 2-1 displays an end result of how the section geometry axial force and bending moment combinations – blue line (greyscale: line on the right) – calculated in the table are optimized to enclose the actual axial force/moment combinations present along the circumference of the chimney base – the yellow line (greyscale: line on the left). Note the column headings in *Table 2-1* where calculations toward the optimal section and reinforcement steel for the IGV at 30 meter height were made:

f_{cu} = concrete strength

% As1 and % As2 = percentage of area reinforcement steel used

h = height of section

b = width of section

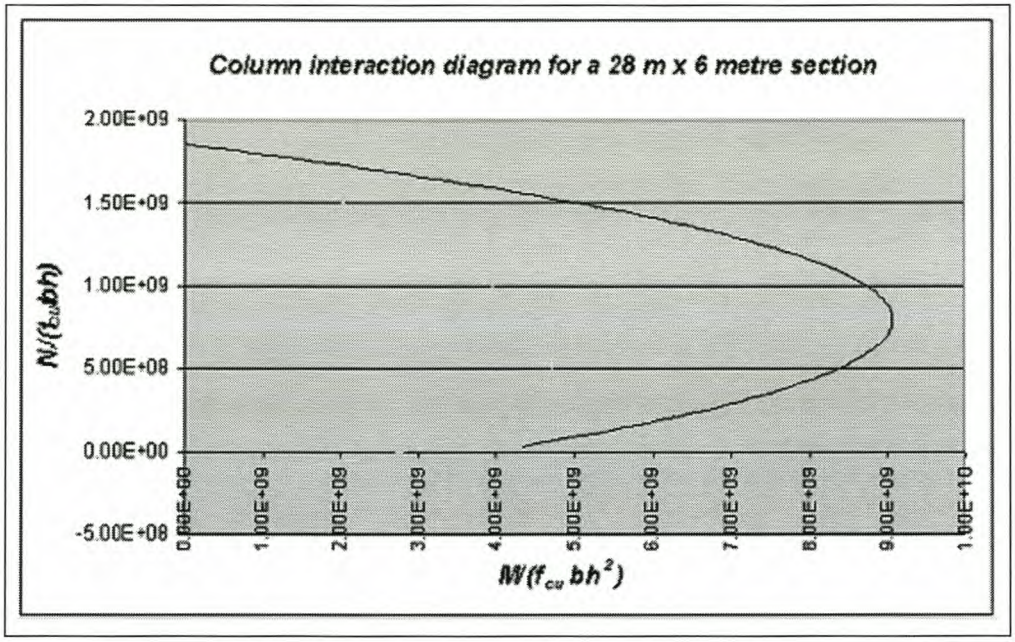

Figure 2-12. A practical example of column interaction diagram.

For 30m-level

fcu	h	b	x	fs1	%As1	As1	d'	fs2	%As2	As2	d	N	M
2.3E+07	28	6	1.87	4.50E+08	0.0015	0.252	4.2	4.50E+08	-0.003	-0.42	4.2	2.87E+07	4.34E+09
2.3E+07	28	6	3.73	4.50E+08	0.0015	0.252	4.2	4.50E+08	-0.003	-0.42	4.2	1.33E+08	5.51E+09
2.3E+07	28	6	5.60	4.50E+08	0.0015	0.252	4.2	4.50E+08	-0.003	-0.42	4.2	2.37E+08	6.57E+09
2.3E+07	28	6	7.47	4.50E+08	0.0015	0.252	4.2	4.50E+08	-0.003	-0.42	4.2	3.42E+08	7.41E+09
2.3E+07	28	6	9.33	4.50E+08	0.0015	0.252	4.2	4.50E+08	-0.003	-0.42	4.2	4.46E+08	8.09E+09
2.3E+07	28	6	11.20	4.50E+08	0.0015	0.252	4.2	4.50E+08	-0.003	-0.42	4.2	5.50E+08	8.59E+09
2.3E+07	28	6	13.07	4.50E+08	0.0015	0.252	4.2	4.50E+08	-0.003	-0.42	4.2	6.55E+08	8.91E+09
2.3E+07	28	6	14.93	4.50E+08	0.0015	0.252	4.2	4.50E+08	-0.003	-0.42	4.2	7.59E+08	9.05E+09
2.3E+07	28	6	16.80	4.50E+08	0.0015	0.252	4.2	4.50E+08	-0.003	-0.42	4.2	8.63E+08	9.03E+09
2.3E+07	28	6	18.67	4.50E+08	0.0015	0.252	4.2	4.50E+08	-0.003	-0.42	4.2	9.68E+08	8.82E+09
2.3E+07	28	6	20.53	4.50E+08	0.0015	0.252	4.2	4.50E+08	-0.003	-0.42	4.2	1.07E+09	8.44E+09
2.3E+07	28	6	22.40	4.50E+08	0.0015	0.252	4.2	4.50E+08	-0.003	-0.42	4.2	1.18E+09	7.88E+09
2.3E+07	28	6	24.27	4.50E+08	0.0015	0.252	4.2	4.50E+08	-0.003	-0.42	4.2	1.28E+09	7.15E+09
2.3E+07	28	6	26.13	4.50E+08	0.0015	0.252	4.2	4.50E+08	-0.003	-0.42	4.2	1.38E+09	6.24E+09
2.3E+07	28	6	28.00	4.50E+08	0.0015	0.252	4.2	4.50E+08	-0.003	-0.42	4.2	1.49E+09	5.16E+09
2.3E+07	28	6	29.87	4.50E+08	0.0015	0.252	4.2	4.50E+08	-0.003	-0.42	4.2	1.59E+09	3.90E+09
2.3E+07	28	6	31.73	4.50E+08	0.0015	0.252	4.2	4.50E+08	-0.003	-0.42	4.2	1.70E+09	2.47E+09
2.3E+07	28	6	33.60	4.50E+08	0.0015	0.252	4.2	4.50E+08	-0.003	-0.42	4.2	1.80E+09	8.55E+08

Table 2-1. Calculations for determining the column interaction diagram.

2.4 Relevance of structural theories and tools on the IGV's

2.4.1 Relevance of deep beam theory literature study

The chimney base structure is in essence a deep beam with a very low span to depth ratio. As mentioned in the literature study the application depth for specific reinforcement design need not be larger than the span – only the nominal steel applies in areas above that. If the span between IGV centre points is 28 metres then only the lower 28-metre height of the chimney shell needs application of special deep beam reinforcement.

The procedure for shear resistance design outlined in the literature gives valuable insight, firstly, into the mechanisms at work between chimney and IGV and, secondly, into the formulation of detailed shear area and reinforcement design.

The arch phenomenon in deep beams displays the channelling of forces toward the supports. It initiates the possibility for the volume of concrete that is subject to tensile stresses ("below" the arch) to be cut away.

2.4.2 Relevance of column theory literature study

The IGV is a column eccentrically loaded around its strong axis. A negligible bi-axial bending effect, due to transverse forces in the form of air pressure of the incoming airflow and the re-directing of it towards the turbine, exists. (These forces are at their maximum approximately 300 000 times smaller than the vertical forces acting in on the IGV's. The exact magnitude of these lateral forces is still unpublished although already under investigation by Carl Kirstein [29].) Hence the IGV columns will not be classified as bi-axially loaded columns.

The relevance of column theory and especially the column interaction diagrams to this research effort lie in the fact that they are valuable design tools for determining the initial dimensions (before optimising the shape), concrete strength prediction and amount of reinforcement steel. The envelope (line distinguishing the area containing safe load cases from those causing failure) will provide a design limit to be respected when setting out to determine these starting parameters.

2.5 Solar chimney frequency analyses

In order to discuss analysed eigenfrequencies of the global chimney structure and the influence of the IGV's thereon it is necessary to understand the method of excitation of these vibrations. This will be established in the first part of this section by a study on research by Sachs [8].

Secondly, previous research determining the eigenfrequencies of the chimney structure of the solar chimney in order to predict detrimental wind speeds [9, 14] will be reported.

2.5.1 Cross wind oscillation

The causes of crosswind oscillation are the periodic pressure variations arising from the action of vortex shedding on alternate sides of the structure. At a high Reynolds number (this number is proportional to wind velocity) the cylinder is subjected to forces that alternate in direction corresponding to the vortex shedding. If the cylinder is flexible oscillation may result. The oscillation tends to detach the vortices and the vortex shedding locks into the natural frequency of vibration of the cylinder and its elastic support system. The wind velocity that would match this frequency and hence cause oscillation can be found from the following equation:

$$V = \frac{ND}{S} \tag{2-14}$$

where V = critical wind velocity
N = frequency of vortex shedding
D = diameter of tower
S = Strouhal number: a dimensionless factor accounting for the sectional shape of the structure. It may be chosen as 0.2 for circular chimneys.

If a structure is flexible with low damping it responds to the oscillating forces. Oscillating starts as the wind velocity approaches the speed at which the vortex shedding frequency is equal to the natural frequency of the structure. Model tests show that right up to the critical velocity there is very little swaying and that in this zone the vortex development is similar to that arising from a stationary cylinder. At the critical velocity the resonant frequency of the structure is equal to the vortex shedding frequency. Vibrations commence and at the same time begin to control the vortex

shedding. The tests also show that the maximum amplitudes and stresses occur at the critical wind velocity.

Oscillation continues through a zone of critical wind speed and eventually the structure becomes stable when an upper limit is reached at which it is again controlled by wind speed only. In most chimneys only oscillation at the first eigenmode needs to be considered.

2.5.2 Previous research determining the eigenfrequencies of the chimney structure

Research by [9] and [14] determined eigenfrequencies for the chimney structure. [9] approximated the ring stiffener effect (to uphold the circular geometry of the chimney) by fully constraining the rotations of the chimney shell around the vertical axis at the relevant positions on the chimney (72 positions along the circumference on six heights, corresponding to six 72-beam stiffeners [9]). The first eigenmode was found to occur at a frequency of 0.10 Hz.

In research performed by Montag et al. [5] on the Niederaussem cooling tower, completed in Germany in 2000, the designed stiffness of the tower corresponded to eigenfrequencies in the region of 0.7 Hz, falling well outside the relevant resonance inducing wind load conditions determined in the European loading code. Resonance due to wind excitation is also the expected mode of failure for the solar chimney. The author is convinced that 0.7 Hz is not a realistic aim for this structure. Instead, a wind characterisation study for this special structure is essential to ascertain that the low structural frequency will not lead to resonance.

CHAPTER 3: IGV GEOMETRY

This chapter states the structural functionality of the IGV and introduces its geometrical boundaries as they are proposed by Dr. Gannon [1]. Finally, current IGV and force transfer concepts are stated and criticized.

3.1 IGV structural functionality

3.1.1 Structural

For purposes of this research the IGV is assumed to be primarily a structural entity. The chimney structure needs a vessel performing the transfer of forces acting on it to the foundation. The main forces acting on the chimney are gravity and wind-induced pressure. The structure must remain stable under all forces – mainly compressive forces, but also tensile forces, shear forces and moment action. To be able to withstand the great forces acting on the IGV's a special, unique shape is required.

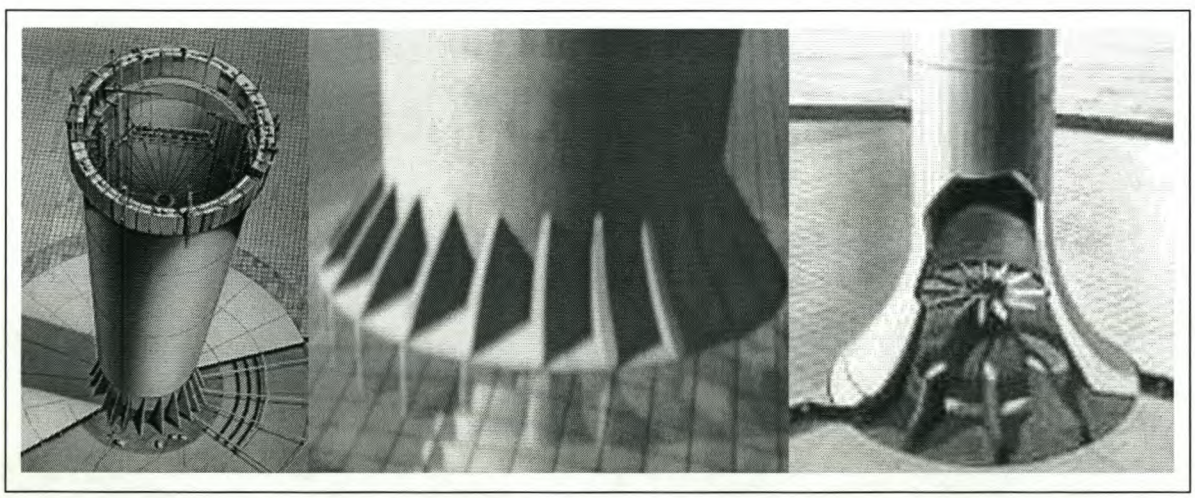

Figure 3-1. Artist's impressions of the integration of the different parts of the solar chimney [22, 32, 22].

Each IGV is to be rotated about its vertical axis by a non-zero angle in order to optimally re-direct the airflow. This rotation will cause an increase in the torsional stiffness of the solar chimney base.

The trailing section will not act as a support structure for the chimney but is utilised merely to re-direct airflow. This characteristic necessitates it to be a non-load-bearing structure, enabling it to

rotate relatively fast according to the systems efficiency needs, and it will therefore not play a structural role.

3.1.2 Structure integration

As mentioned in *Chapter 1 paragraph 1.3.2* the IGV's are the connection point between the chimney and the collector structure. It must allow the geometry of the collector to gradually flow into the geometry of the chimney, upholding airtight channels in the system for unobstructed airflow past the IGV's and via the cone-structure into the chimney. The optimal airflow ducts [1] must be upheld during this integration process. *Figure 3-1* shows different concepts for this integration aspect, as proposed by previous (unknown) researchers.

3.2 IGV geometry

3.2.1 Plan-section

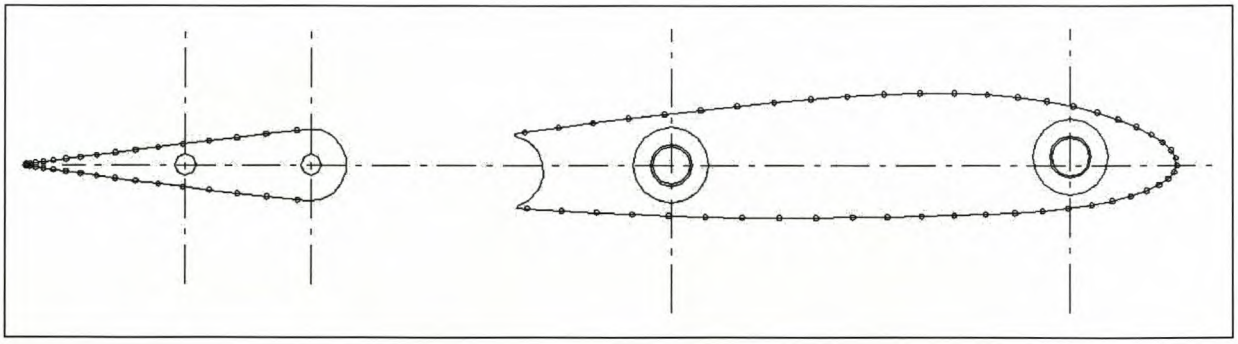

Figure 3-2. The profile of the IGV [29].

From the view point of optimal air flow and turbine effectivity, the plan-section for the IGV is chosen to follow a NACA 4-digit blade profile [1]. *Figure 3-2* displays the profile in plan-view. Note the trailing section, referred to in *paragraph 3.1.1*, on the left in the figure. The proposed sectional dimensions for the IGV, given as fractions of the chord length, are displayed in *Figure 3-3* and tabulated in *Table 3-1*.

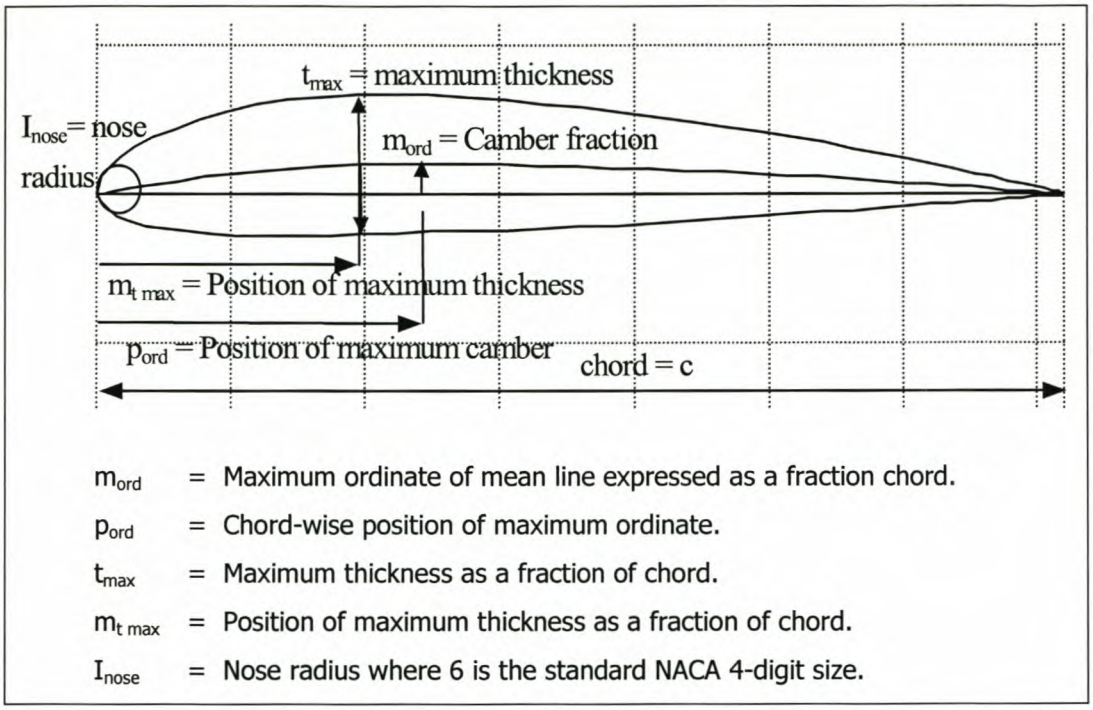

Figure 3-3. Blade profile nomenclature [1].

X (Design vector)	Value	Description
m_{ord}	2.64 %	Maximum camber as a fraction of chord
p_{ord}	29.85 %	Position of maximum camber as a fraction of chord
t_{max}	11.70 %	Maximum thickness as a fraction of chord
$m_{t\,max}$	28.58 %	Position of maximum thickness as a fraction of chord
I_{nose}	5.47	Nose radius relative to NACA 4-digit profile. (6 = standard)

Table 3-1. Blade profile geometry of modified NACA 4-digit profile for IGV's [1].

Although an aspect ratio, h/c (height to chord-length), of 1.42 is proposed [1], resulting in a 40-meter chord length for a 57-meter high IGV, a larger IGV is used in this research effort. To commence the iteration of the concept the full (trailing section included) chord length is chosen as 60 metres.

The work by Gannon [1] mentioned that the trailing section of the IGV must be able to rotate. To accommodate this feature it was decided that the section supporting the chimney (in the first design iterations) shell would be situated 2/3 along the chord-length (40 metres), moving from the leading edge – depicted by the hatched area in *Figure 3-4*.

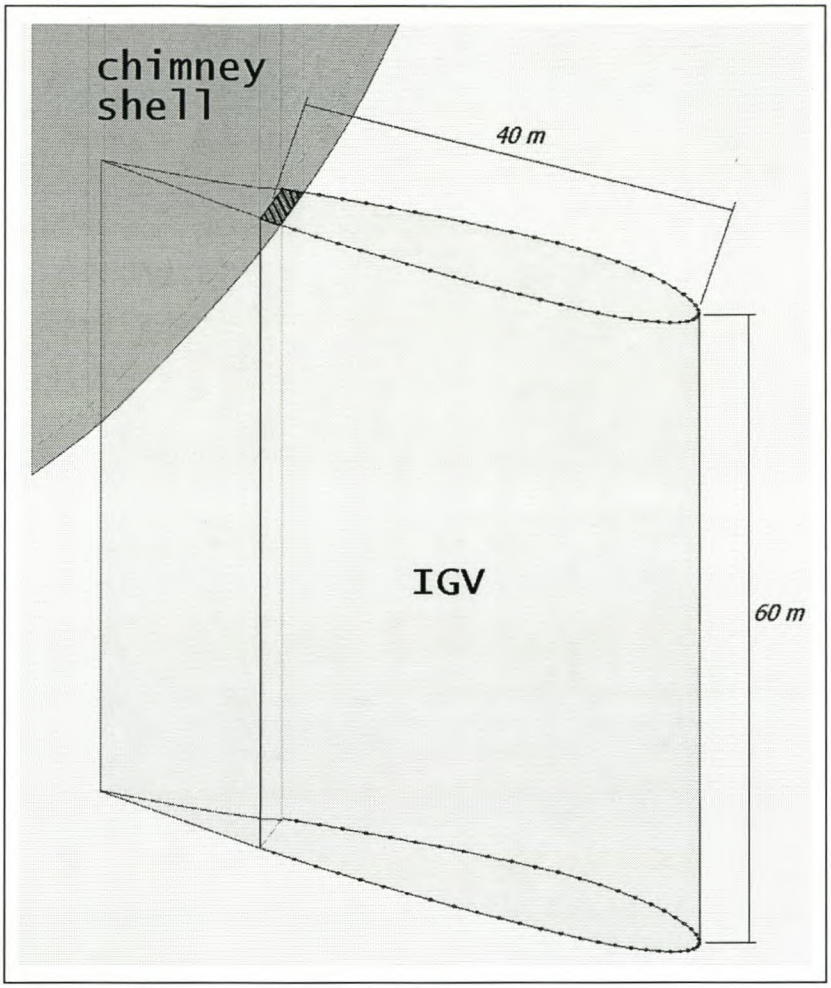

Figure 3-4. IGV height and structural chord length as used in the first iteration analyses.

3.2.2 Height

Table 3-2 presents the results of optimisation [1] with the turbine dimensions expressed as a fraction of the chimney diameter as well as the actual sizes.

The IGV height used in this research is simplified to 60 metres – see *Figure 3-4*.

	D_{chim}	D_{turb}	D_{hub}	H_{IGV}	H_{turb}	U_{tip}
Fraction of chimney diameter	1	0.7991	$0.4*D_{turb}$	0.355	0.444	
Full scale plant value [m]	160	127.9	51.1	56.83	71.03	88.6 $m.s^{-1}$

Table 3-2. Final turbine dimensions and IGV height.

3.2.3 Amount, layout and wall thickness

In this research eighteen IGV's are used in the circumference, as was proposed by Gannon [1].

Figure 3-5 displays the extreme stagger angles of the IGV's. The angle of maximum rotation, measured from the zero turning position (radial) was found to be 22.5 degrees [1].

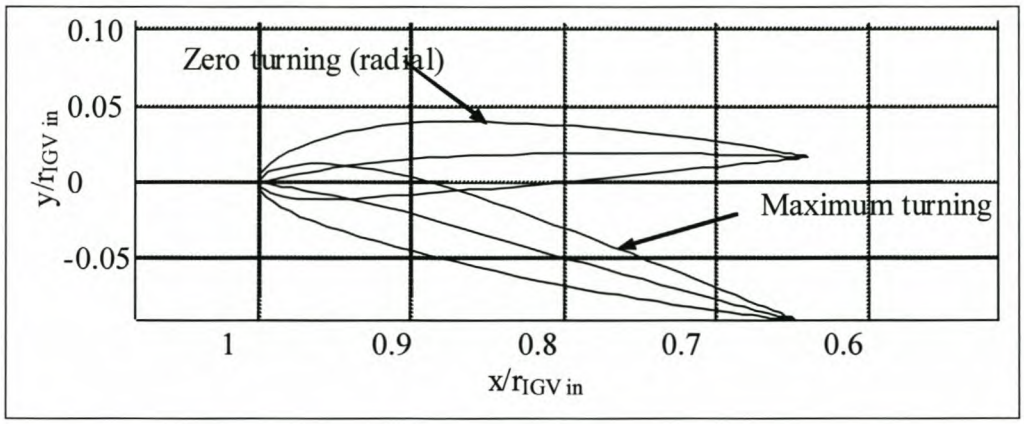

Figure 3-5. Detailed inlet guide vane blade profiles at extreme stagger angles [1].

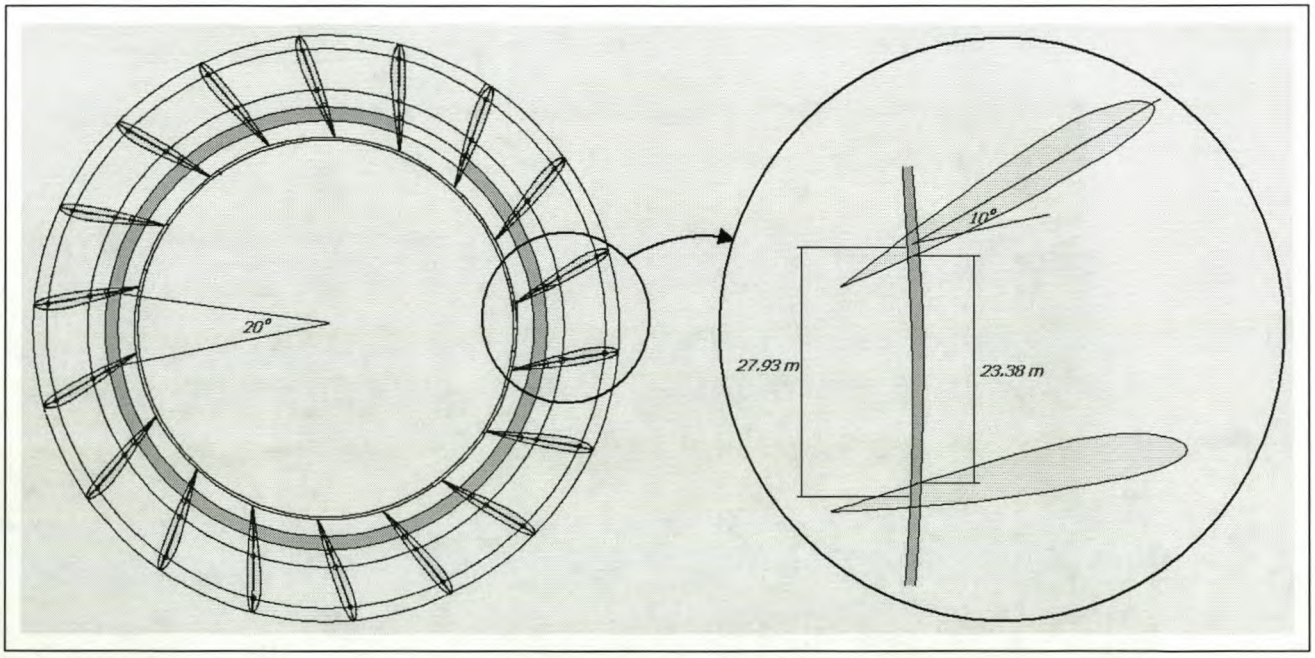

Figure 3-6. Plan view of the layout, amount, rotation and consequent dimensions of the IGV's situated below the chimney.

In this research this rotation angle is chosen as 10 degrees. *Figure 3-6* displays the layout. The circumference of the inside of the chimney shell at chimney base level, where the radius equals 80 metres, is 502.655 metres, resulting in 27.93 metres per IGV, measured from centreline to centreline. The span between two IGV's is 23.38 metres.

The wall thickness of the chimney at the region to be supported (therefore at chimney base level) is 2.2 metres.

3.3 Current designs and criticism

Consider *Figure 3-1*. The three pictures portray two different approaches to the problem of force transfer. (Note that all these concepts are speculative – it could have been created by architects playing around with solid modelling software. It will not be investigated as being factual solutions but only as concepts.) The concepts in the pictures on the left and in the middle aim to transfer forces through so called "fin stiffener" structures while the concept on the right uses an adapted geometry of the shell to establish stability and the transfer of vertical force vectors to inclined vectors.

3.3.1 Fin stiffeners

The fin stiffener structures reach up to a significant height along the chimney shell. They have no area-enlarging transfer section to be able to bear excessive compressive loads between the chimney shell and the IGV but rely on a shear resistant plane at the interaction face between the chimney shell and the fin structure to transfer forces. Possible advantages of this approach are

- Added stability due to a weight increase in the lower region of the solar chimney and due to increase of the plan section up to significant heights of the lower chimney region.
- Relatively straight forward construction method.
- Forces are already transferred from the chimney shell to the fin stiffener structure through a shear resistant interface from a great height implying the distribution of dead weight at lower levels to be over larger areas (fin stiffener sections).

3.3.2 Adapted shell geometry

The base region of the chimney shell in this concept has the distinctive shape – parabolic hyperboloid – of the well-known cooling tower diffracting the vertical forces into inclined vectors and

consequently activating vertical shear action. Implications of the consequent increase in circumference are

- Increase in shell area (greater circumference) to bear compressive or axial load.
- Stability increase due to the parabolic hyperboloid shell shape.
- A possible reduction in the shell thickness due to increased stability.
- Utilisation of the shear resistance of the concrete.
- This geometry implies a greater chimney radius. An increase in the amount of IGV's/transfer structures in order to uphold the pressure increase at greater radii caused by contracting air ducts could benefit the structural state.

3.4 In conclusion

The geometry of the IGV had now been defined – a 60-metre tall, 40-metre long blade shaped structure spaced approximately 28 metres apart around the circumference of the chimney base – and some previously proposed concepts viewed. This, and the forces acting on the structure, investigated in the next chapter, will aid in the conceptualization process. The concepts in the previous section suggests that (undocumented) possibilities as to a solution to the aim of this thesis – the realisation and stability of the inlet guide vanes and force transfer structures – exists. *Chapter 5* investigates two geometries, the one implementing the mentioned fin stiffener concept while the other utilises the compressive strength of concrete through an anvil shaped force transfer section.

CHAPTER 4: FORCES ON AND IN THE IGV

This chapter looks at the forces acting on the inlet guide vanes and the internal reaction to these forces with its consequent interaction with the surrounding structure. Only gravitational and wind forces are considered in this study. For South African design purposes it is assumed that seismic activity is equal to zero. Whereas seismic activity has been registered in regions such as the Western Cape as well as in deep mining regions, the proposed site, near Sishen in the Northern Cape Province, is a seismically inactive region. Although seismic presence will surely change the values of design parameters, one can for South African design purposes assume that seismic activity is equal to zero.

4.1 External forces

Two categories of forces affecting the IGV's can be identified: firstly, great forces are generated in the foundation part of the solar chimney due to wind and gravitational action on the chimney shell. The IGV's support the chimney, transferring these forces to the foundation. The second group of forces are those acting directly on the IGV's, for instance, the pressure due to the incoming airflow, and the re-directing of it, as well as the dead weight of the collector parts near the chimney base. These are comparatively small forces and will not be considered during the initial structural IGV design.

4.1.1 Effect of wind and gravitational load

Previous research by Van Dyk [14] yields a finite element (FE) model of the chimney structure. ABAQUS FE-software [17] was used determining the wind force to be the most significant load. *Chapter 2 paragraph 2.2* reported the effect of the resulting pressure on the chimney shell – large deformations because of ovalisation – and the solution found in the application of ring stiffener structures.

Note that the wind extrapolation model used was the most conservative (*Chapter 2 paragraph 2.2*) and that no safety factors were used during the wind and gravity load calculation. Also, note that wind force acts only on the parts (the chimney and possibly the force transfer section) above the glass roof. Laterally, the structures underneath the roof (IGV's, turbine, cone, etc.) are only loaded with the small pressure due to inflowing air.

The immense height of the chimney raises questions about the wind loads effecting it. Gusts will most probably not occur over the whole chimney height simultaneously, as has been the conservative assumption in earlier work [14], but may be spatially distributed. Gusts from varying directions with varying intensity could also occur, complicating the modelling of the wind load. Such load cases call for mathematical and probabilistic investigation to these wind loads which should be performed to derive a more realistic loading description.

The FE-model [14] is used to determine the reaction forces on elements at the chimney base level. *Figure 4-1* portrays the vertical and lateral forces on the unfolded perimeter, transformed to coordinates locally radial and tangential for each IGV, rotated around its vertical axis by 10 degrees – see *Figure 4-2*. The reaction moments are small relative to the vertical force and only the local tangential moment is considered further.

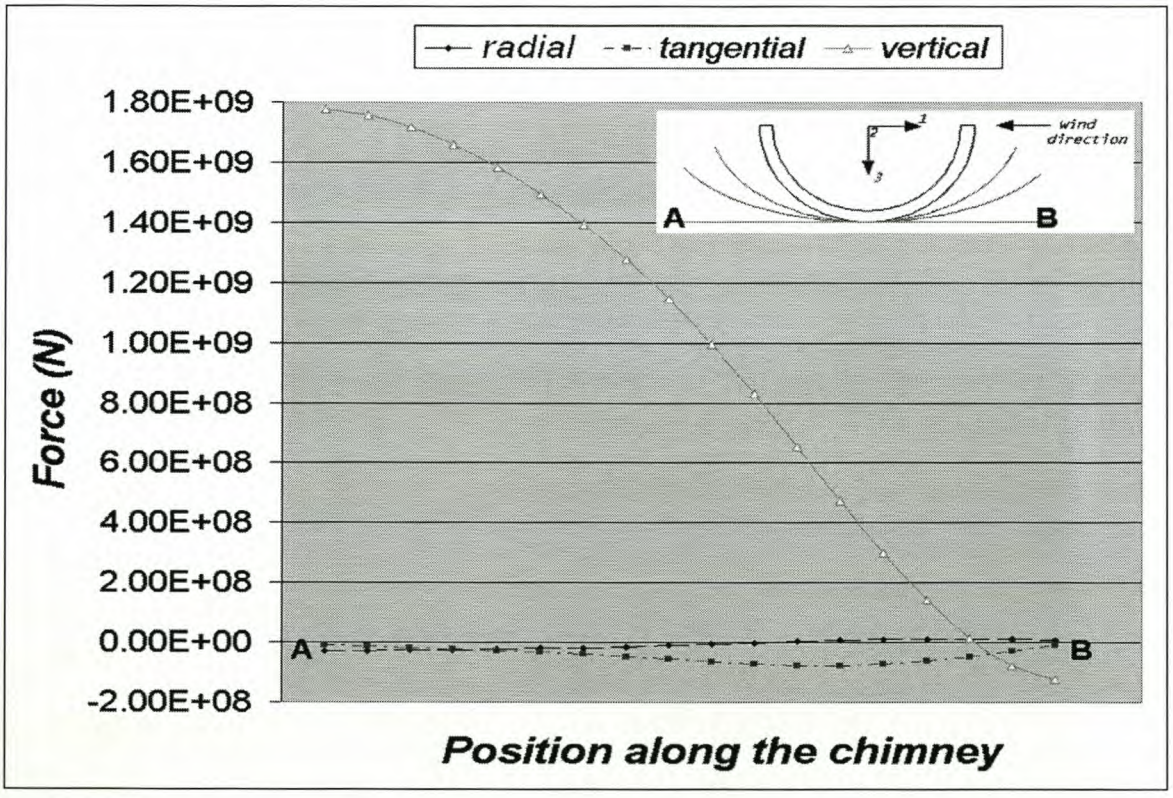

Figure 4-1. The reaction forces.

Three load cases are identified as critical, governing the IGV design, depending on its orientation with the wind direction. The positions of these forces are shown in *Figure 4-1* by the symbols A, B and C. At position A the vertical and radial loads are at their maximum values. The vertical force at A at $1.78*10^9$ N is the most critical force during the design process. At position B the vertical force is at its greatest negative value. This upward, tensile force must be accounted for by appropriate foundation

anchorage and tensile reinforcing steel in the IGV. Position C corresponds to the maximum tangential force. The exact values of the three load cases are given in *Table 4-1*.

These forces are re-interpreted as piecewise uniformly distributed forces, simplifying further application in the FE-package. The critical vertical load, rewritten as a pressure by considering the proposed 2.2-metre shell thickness at that chimney height (*Chapter 3 paragraph 3.2.3*), is $28.9*10^6$ N/m^2. *Appendix B* contains tables and figures displaying these reaction forces and moments. It also reports on the method of extraction and re-interpretation of these forces from nodal point reactions (data from FE model results), represented in the FE process by quadratic shape functions, to uniformly distributed forces.

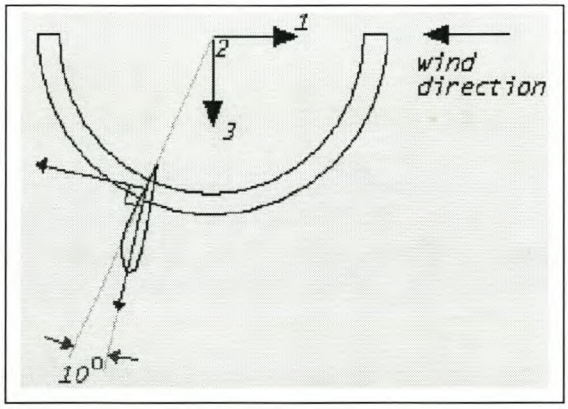

Figure 4-2. The local radial and tangential is defined for each IGV, rotated by 10°.

Load case	Direction of force	Magnitude (N)
1	**Vertical**	**-1.78E+9**
	Radial	**8E+6**
	Tangential	**2.98E+7**
2	**Vertical**	**-4.73E+8**
	Radial	**7.8E+7**
	Tangential	**-5.86E+6**
3	**Vertical**	**1.25E+8**
	Radial	**9.75E+6**
	Tangential	**-6.18E+6**

Table 4-1. The assimilated force data, as point reaction loads, introducing the load cases.

4.1.2 Air inflow

The air flowing radially inward from the perimeters of the glass roof collector reaches speeds of up to 50 km/h [32]. The IGV's re-direct this air; consequently pressure is exerted on them. *Figure 4-3* shows the re-direction of the air inflow.

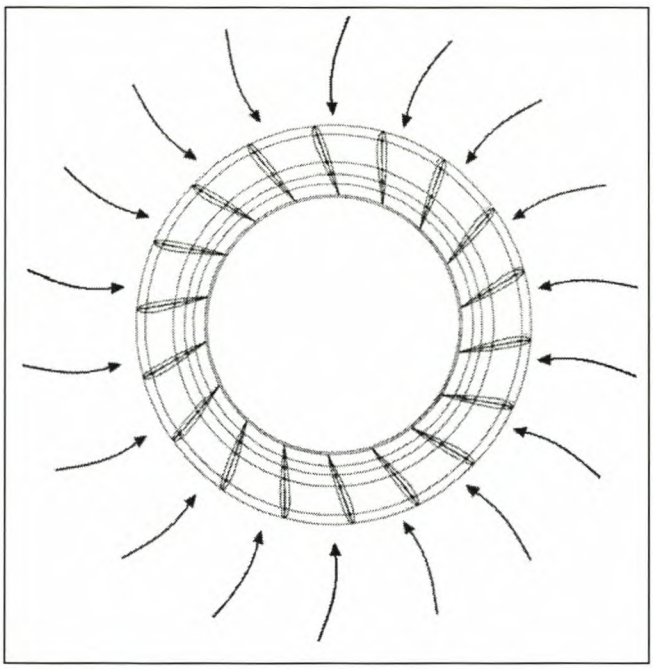

Figure 4-3. Portrayal of the airflow direction.

Apart from the direct pressure on the IGV's, the consequent force on each IGV blade exerts a shear force on the IGV, of which the maximum value occurs at IGV-base level. The greatest force is exerted on the leading edge of the IGV, it doing the most work in the re-direction of the air. The torsional action due the resulting asymmetric pressure distribution on the IGV blade adds to this shear force. The magnitude of these forces are currently the focus of research in the Department of Mechanical Engineering, University of Stellenbosch and, therefore, yet unpublished.

4.2 Local effects

The most distinct local effects on and around the IGV can be divided into four categories:

- compressive behaviour
- shear resistance

- moment-action caused by geometrical and concrete characteristics and
- arch phenomenon

This section aims at the studying of the behaviour and explaining the presence of these actions.

4.2.1 Compressive behaviour

Assuming each IGV to serve an $1/18^{th}$ of the chimney structure, and uniform axial stress, the compressive stress resistance in the chimney shell at the level above the IGV is well within normal (ULS criteria) concrete strengths. At the base of the IGV, with an area of 244.52 m^2, there is also no problem. However, the transference of the maximum vertical force from the shell to the IGV presents a problem – the evident area for transferral, at 9.9 m^2, is too small. (The calculations for and details of these findings are presented in *Appendix C*). Such an area would require a concrete that can resist a compressive stress (ULS criteria) of approximately 400 MPa to bear the load! Concrete with such high compressive strengths do not exist [30]. Designing for this problem asks for a transference structure transferring forces from the chimney shell to a big enough area on the IGV (refer to *Figure C-2* in *Appendix C*).

Later in this thesis a conceptual solution to this problem is proposed in which effective force transference is achieved through an anvil shaped structure, relying on the horizontal section of the structure to transfer loads exerted on it through compression. Another solution is proposed where not the compressive, but the shear resistant characteristic of reinforced concrete is utilised in the fin stiffener concept already mentioned in the previous chapter.

4.2.2 Shear resistance

Adjacent to columns

For the safe transfer of forces from one level to another it is important to check for necessary shear resistance in the structure. To simplify the problem, the chimney shell can be seen as a very deep beam supported on columns (the IGV's) – refer to *Chapter 2 paragraph 2.3.1.* Shear forces will be the highest directly next to the columns. The magnitude of the shear forces are in the order of $7.3*10^8$ N for the case where maximum compressive force and IGV transfer area width of 5 metres are used. The vertical section/area of the concrete and circumferential (hoop) steel must be sufficient to resist shear failure in order to transfer the load onto the columns.

Outward force vector

The distribution of vertical forces into radially outward regions (as seen in *Figure 4-4*) of the structurally active region of the IGV necessitates the presence of horizontal shear reaction. This has to be accounted for by a shear resistance mechanism. Minimum strength reinforced concrete should suffice in this role.

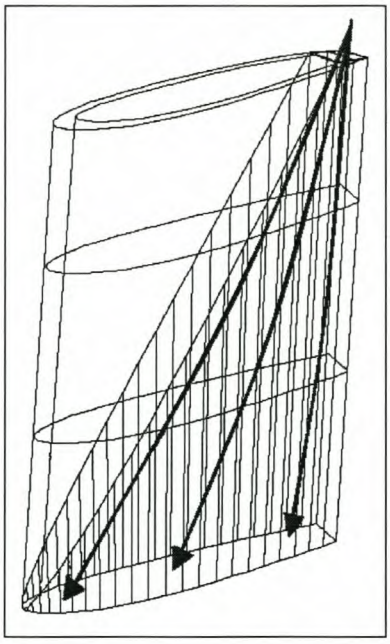

Figure 4-4. The IGV showing the vertical loads being distributed.

4.2.3 Moment action

Distinct moment-action can be predicted due to eccentric geometry of the IGV relative to the chimney structure, and concrete characteristics. These include moments due to eccentricity and concrete behaviour.

Eccentric moment

The eccentricity of the loads at the top of the IGV column to the centre of gravity of the IGV geometry causes moments around these centre-of-gravity points of the structure; see *Figure 4-5* for portrayal of the moments due to eccentricities in the structure under vertical load.

Another eccentric moment is identified and explained: force is automatically transferred toward stiffer parts of a structure. Deep beam theory [6], reported in *Chapter 2 paragraph 2.3.1*, shows that stress contour arches form, displaying this phenomenon. This force transfer in a non-vertical direction implies the existence of a lateral component, tangential to the circular chimney shell. The tangential

vector has an outward component (relative to the individual IGV). These outward forces form moments around the IGV. The arch phenomenon is investigated more closely later in the next section.

Concrete behaviour

Temperature gradients and expansion-effects cause the IGV's to have a clamping action on the chimney structure as the "free" sections of the chimney dilate outwards. Hygral effects in concrete have the same but opposite effect.

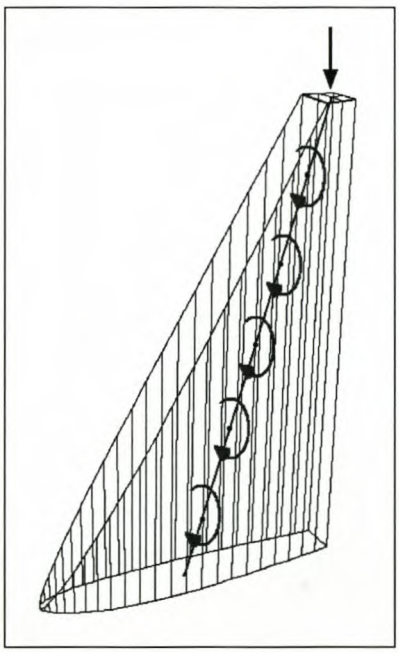

Figure 4-5. Moment (red arrows) forming due to an eccentric vertical load.

4.2.4 Arch forming

In a deep beam supported by columns, stress contours form in an arch shape, as mentioned in the previous section. The arched area, as seen in *Figure 4-6* is compression-free. There exists a contour under which the stresses in the region below it are tensile; the gravity force pulling the unsupported concrete downwards. Apart from the direct advantage of having a predominantly compressive structure transferring the forces from the beam to the column – the concrete under tensile stress does not have any function, it is purely dead weight – the presence of these tensile stressed arches have positive implications on the cost of the solar chimney: the inactive tensile concrete can be cut away – a form-finding application – and the geometry just upheld in the cheapest possible way to keep the system surrounding the chimney base airtight. Construction practicalities might limit the

implementation of such cutting away of material. Final design will govern the decision as to optimal geometry.

Concrete behaviour predicts the inclination angle, relative to the vertical direction, of the arch to be less than 45 degrees [2]. This angle determines the height of the arch. The lower the arch height is the bigger the magnitude of the horizontal force vector. These forces concentrate at the topmost point of the arch (or IGV transfer section), resulting in concentrated resultant forces.

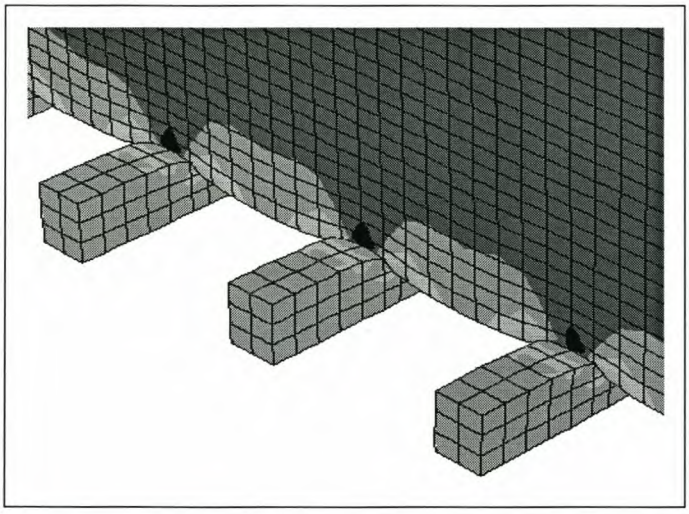

Figure 4-6. The "arch" phenomenon – low stressed regions between supports.

4.3 Concluding the chapter

The characteristics identified and briefly discussed in this chapter gives the conceptualist or designer insight into most of the behaviour patterns to be expected in the IGV. When results of analyses of the finite element models are studied he/she will be informed and critically equipped.

Critical load cases are isolated and design values for these forces determined. These are used in the further conceptualization process.

The global picture as to what the force distribution looks like is seen. Although the most critical design load is the load case having the maximum vertical force, the necessary steps for determining the forces at other positions along the circumference of the chimney base / IGV are taken.

CHAPTER 5: CONCEPTUALIZATION

Two concepts are investigated in this thesis; firstly the concept incorporating an anvil shaped transfer section, transferring forces through a compression resistant structure. The second concept relies on a structure with a shear resistant interface between the chimney and the IGV's to transfer forces. The conceptualization process commences with some initial calculations.

5.1 Initial calculations

Simple calculations and analyses performed at an early stage on a typical IGV provide direction in the design and later optimisation process. It also starts stimulating thought and insight into the behaviour of an IGV, aiming at eventually choosing a suitable section, volume, material and other considered main variables. Such calculations include

- Determination of inactive regions in IGV
- Determination of the critical load for an IGV
- Investigation of the decrease in dead load with increase in height

5.1.1 Determination of inactive regions

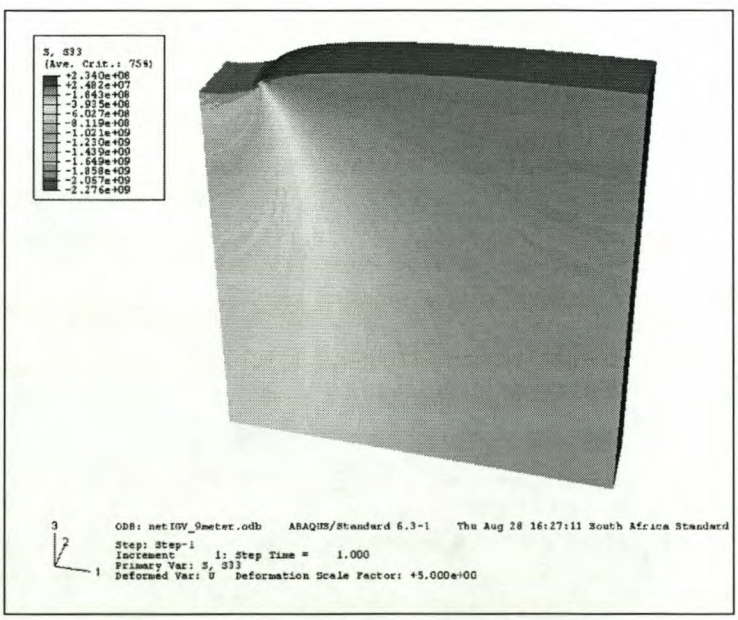

Figure 5-1. A distributed force is applied to an approximated IGV column.

Consider *Figure 5-1*. A distributed force equivalent to the maximum vertical force acting on an IGV is applied over an area of 9 metres (length) x 6 metres (width) of a simplified IGV geometry. The resultant compressive stress pattern can be seen in the figure. Note that the stresses in the red/orange (greyscale: darker regions on the right of the figure) regions are close to zero. Big volumes of the structure are inactive and can be cut away. *Appendix C* shows compressive stresses in some regions at the lower levels of the structure – after initial cutting away – to remain low, at 7.2 MPa (at base level, with the ULS factor applied), while a conventional strength concrete has a yielding stress of at least 30 MPa, (equivalent ULS strength = 13.5 MPa) and up to 95 MPa (equivalent ULS strength = 42.75 MPa) is viable. Therefore, further volume decrease is possible.

5.1.2 Determination of critical load

The critical load is a function of the elasticity modulus (material attribute), the inertia (volume/sectional attribute) and the effective height of the IGV, as seen in the Euler buckling expression for the critical axial load in a column:

$$P_{cr} = \frac{\pi^2 EI}{L_e^2} \tag{5-1}$$

For simplicity, the sectional area of the IGV is approximated with a 40 x 6 metre rectangle – refer to *Figure 5-2*. Thus the area used in the calculation of the inertia equals 240 m^2 as opposed to the actual area of 244.52 m^2.

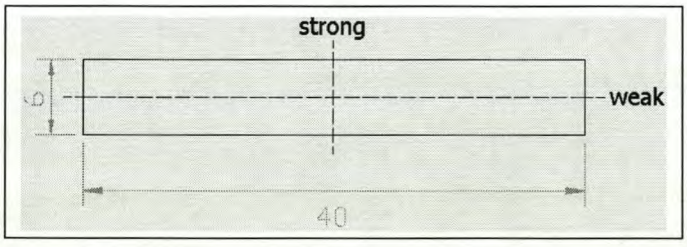

Figure 5-2. The IGV geometry as approximated during buckling analysis.

The formula yields P_{cr} = 1.48*10^{10} N and P_{cr} = 6.58*10^{11} N around the weak and strong axes (*Figure 5-2*), respectively,

with E = 30 GPa

I_{weak} = 1/12 * 40 * 6^3 = 720 m^4

I_{strong} = 1/12 * 6 * 40^3 = 32000 m^4

L_e = 2*60 m = 42 m (assuming the IGV to be a free-standing column)

The P_{cr} values are significantly larger than the maximum vertical load exerted on a single IGV. Therefore it is stated that the IGV's (as long as their plan-section remains the current dimensions) will fail in material failure before buckling locally.

5.1.3 Decrease in dead load with increase in height

The height at which the centroid of the chimney shell lies is determined to be at 382.50 metres – refer to *Appendix D* – showing that the gross volume of the chimney structure lies near foundational level. It is assumed that the additional vertical force in the lower regions of the chimney induced by the wind load is zero. The proposal: a significant decrease in the magnitude of the dead load at greater chimney heights implies that a section specifically for the force transfer from the thin shelled chimney to the IGV section is not needed. It can merely be accommodated by the gradual flow of the chimney into IGV's.

This concept is illustrated with a simple example: assume the forces due to dead and wind load at a 200-metre height to be small enough to be transferred through a structure with a sectional area of 8.145 m^2 (width x shell thickness at 200-metre height = 4.5 m * 1.81 m). A 200-metre tall fin stiffener type structure can transfer these forces to the foundation without the need of a shear resistant transference interface. The previously structurally active shell between these tall structures could just be filled in the most economical way, just upholding the aero dynamic geometry inside the chimney.

Result

Results in *Appendix D, Table D-1*, prove that the rate of decrease in dead load with increase in height is not enough to reach bearable compressive stress levels; hence this notion is not investigated further.

5.1.4 Implication of initial calculations

At this point it is necessary to interpret the above investigations.

- The compressive load calculation shows the stress in regions of the IGV to be very low, creating the possibility to significantly decrease the volume of the IGV using higher strength concrete. Alternatively, the concrete strength can be decreased while keeping the more voluminous geometry. The optimal design will depend on the stability of the structure, as

well as on the cost of material, construction (method and labour), transport and various other variables.

- From the local buckling calculations the smallest P_{cr} value for an individual IGV is approximately 8 times larger than the expected vertical load action on the IGV. Consequently, the vertical compressive load is the critical design load. Note that this calculation was done for an IGV with a section that is constant along the height. The proposed concepts later in this chapter have cross-sections varying with the height, and these approximate buckling calculations will not apply any longer.
- Elements of the investigation on the decrease of dead load with height increase are applied later when the "fin stiffener" concept is investigated.

These results also illuminate one of the main purposes of this thesis – the reduction and optimization of concrete volume, section (area, inertia and height of the transfer section – not the height of the IGV because it is determined by the air flow calculations as is seen in *Chapter 2 paragraph 2.1.2*) and material type (elasticity modulus and concrete type) of the IGV's, with the purpose of lowering overall capital expenditures.

5.2 Load transfer concepts

5.2.1 Concept 1: Transfer of forces from chimney to IGV through an "anvil" shaped structure

The concept

The axial (compressive) stress is critically high in the calculated small-area sections – *Table C-1* in *Appendix C* shows the axial stresses for variable areas. The areas purposed to transfer the forces onto the IGV's are too small. A method (structure) needs to be determined for the transfer of these forces to an adequate area of the IGV. An anvil shaped transfer structure is proposed. The anvil structure, see *Figure 5-3*, is located between the chimney shell and the IGV, and aims at maintaining an area capable of bearing the compressive forces exerted on it.

Geometry

Each IGV serves an $1/18^{th}$ of the chimney structure. The sectional area in the anvil is chosen to be large enough to bear the vertical force on it in compression.

The full blade shaped prism is minimised to a triangular shape cutting away structurally inactive volumes as was proposed in *paragraph 5.1.4* of this chapter. *Figure 5-3* portrays an alteration of the

proposed NACA blade geometry [1]. The aero dynamical shape is upheld by another structure (and is not investigated further in this thesis as lateral pressure force data is yet unpublished [29]). Further reduction in structure volume is realised by cutting away material that is inactive as discussed in *Chapter 2 paragraph 2.3.1*. The inactive trailing section of the IGV [1] is also cut away.

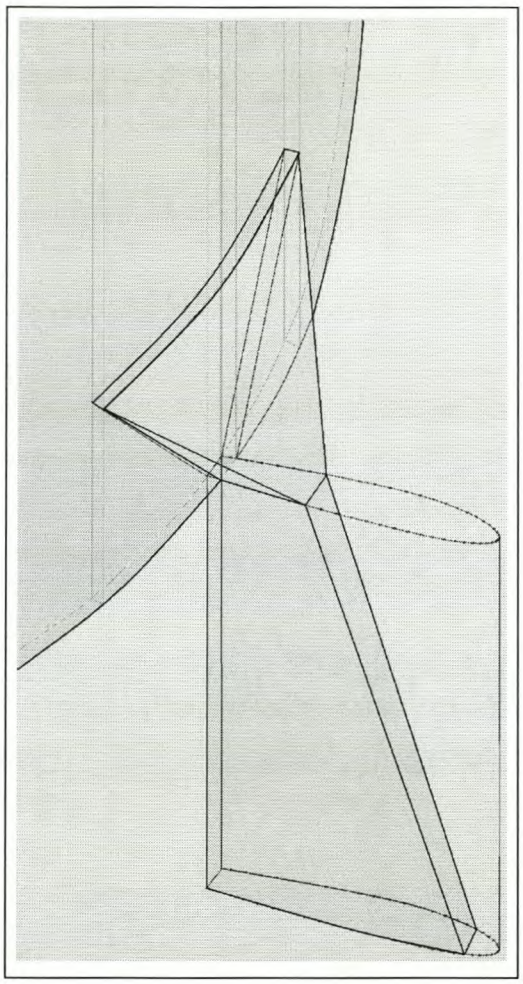

Figure 5-3. The IGV with the anvil shaped transfer section

Note that *Figure 5-3* displays the principle concept of the anvil shaped transfer section that contains irregular geometries likely to cause stress concentrations and discontinuities to form. In the final design the transition from chimney to anvil structure and from anvil structure to IGV will most probably be more continuous.

Model

A model is set up (*Figure 5-4a*) in the finite element package ABAQUS. The shell-piece geometry at the top of the model is realistically curved with an inner radius of 80 metres. The sides of the top section (hatched area in *Figure 5.4a*) are cut along lines proceeding radially from the centre of the

80-metre radius circle in order to set realistic boundary conditions corresponding to the action of adjacent IGV's on these surfaces. Translation in the local direction normal to this surface and the rotations around the vertical axis as well as the local tangential axis are constrained. The footing of the model is fixed against all translation and rotation. The rotation of the IGV's are modelled at zero degrees for simplicity (the global torsional action is not under investigation here justifying the zero degrees rotation assumption). Concrete with a Young's modulus of 28 GPa and Poisson's ratio of 0.2 is used as material.

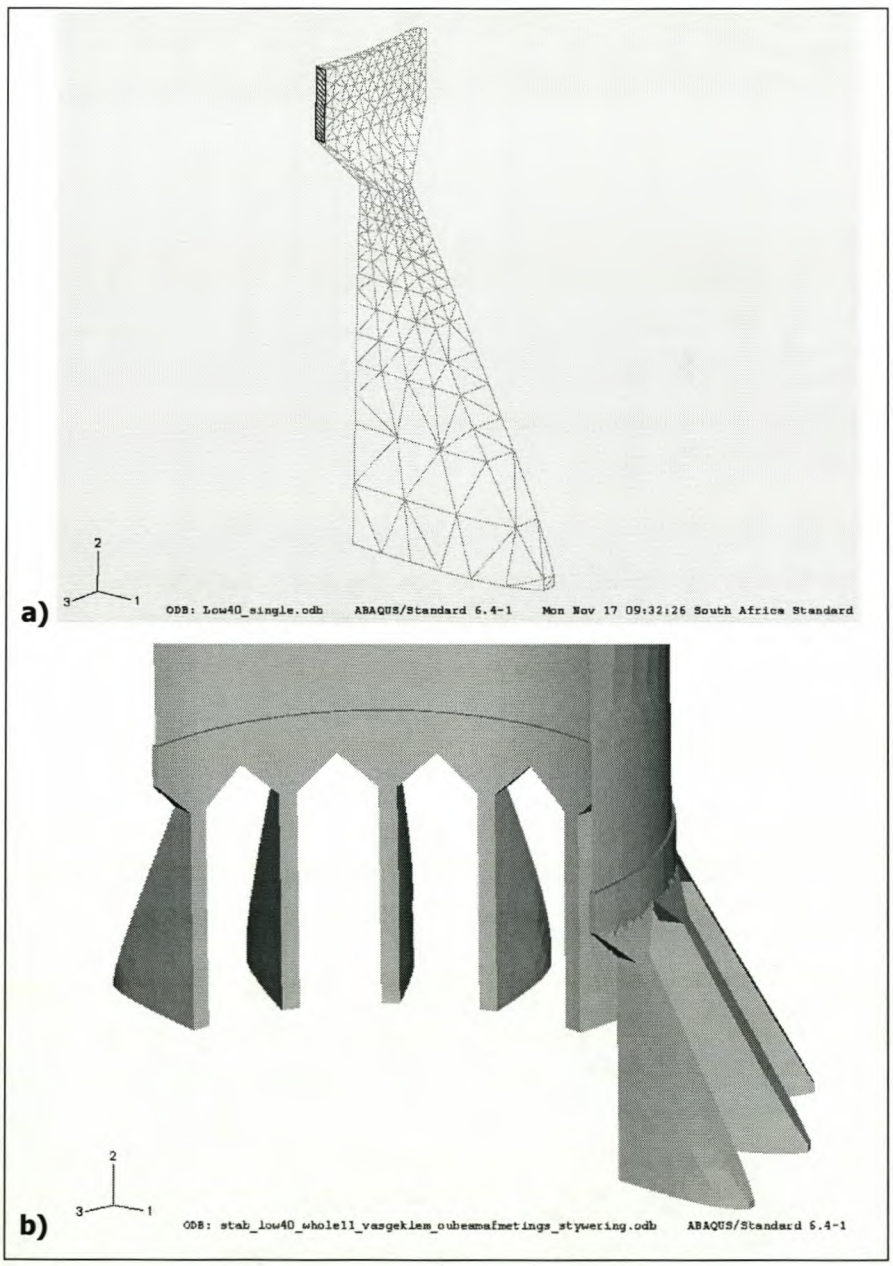

Figure 5-4. a) Typical model of Concept 1. The assembly of 9 IGV's into a symmetrical model are portrayed in b) with the arch shaped cutaways clearly visible.

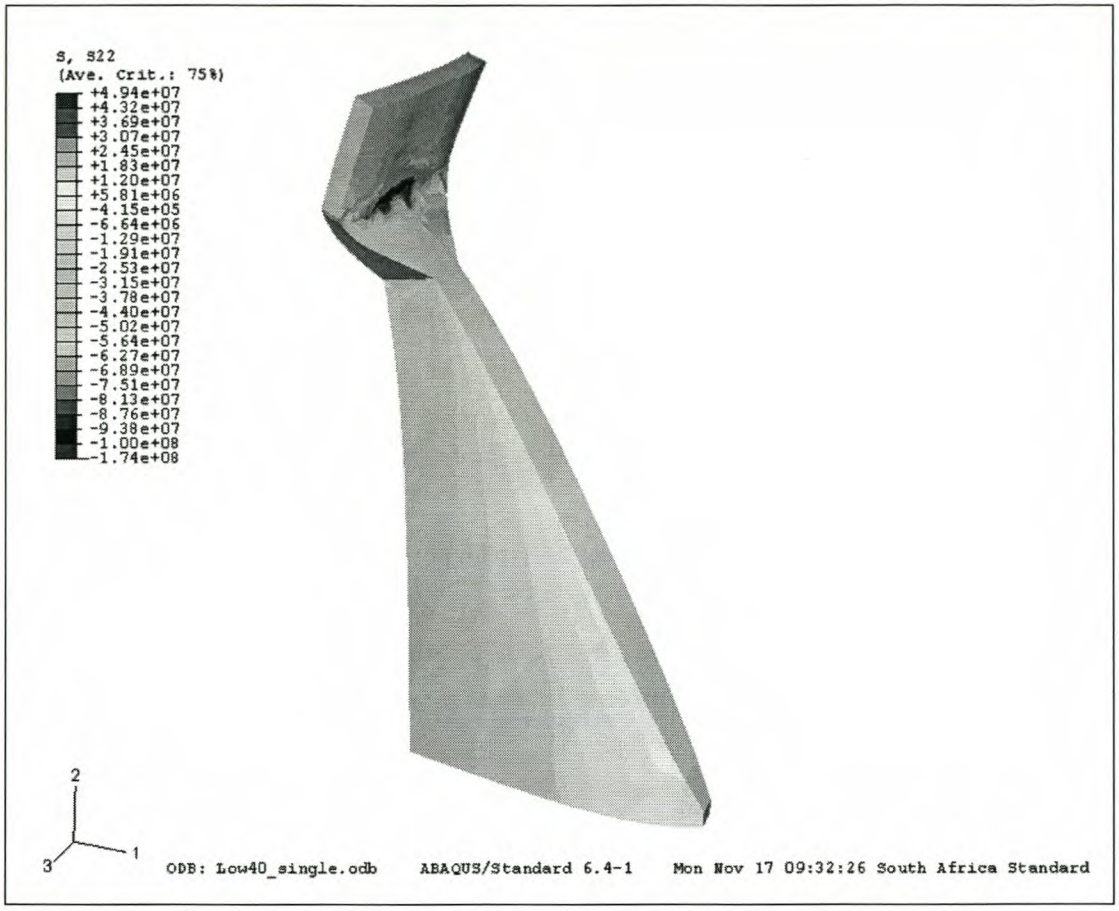

Figure 5-5. Axial stresses. Deformations are scaled up 50 times to show flexural behaviour.

Quadratic 10-node tetrahedral elements, C3D10M, are used to mesh the geometry. The mesh is refined near the regions of interest and where irregularities occur in the geometry. The vertical load is distributed uniformly over the top surface of the model; hence as a pressure force.

Discussion of stresses in individual IGV

The successful functioning of the anvil structure is the main focus of interest for judging the concept as an acceptable solution. *Figure 5-5* shows the resultant axial (with respect to vertical loading) stresses in the structure peaking at approximately 100 MPa. *Figure 5-6* shows some compressive stresses in the structure to concentrate at the discontinuous slope at the point of intersection between the anvil and the IGV. Maximum values of compressive stresses in this region are approximately 75 MPa.

Figure 5-7 displays, with blue (a) and orange (b) regions (greyscale: darker regions), high-localized axial stresses resulting in the top-centre of the anvil section. These stresses are not due to discontinuities or a small transfer area as is the case with the compressive stresses focussed on in

Figure 5-6 but rather due to flexural behaviour in the connection between the base of the chimney shell and the top of the anvil section. *Figure 5-7* shows these stresses to be significant – up to 100 MPa in compression and 35 MPa in tension. A few solutions are possible for counteracting this behaviour by stiffening the region, amongst others the employment of high strength concrete and reinforcement steel and the thickening of the section.

Compression stresses of the magnitude as seen here are well outside the boundaries of safety, as determined by ultimate limit state criteria for collapse. Stresses from 0.45 times the maximum feasible concrete strength of 95 MPa – refer to *Appendix C* – that is, from 42.75 MPa, are judged excessive.

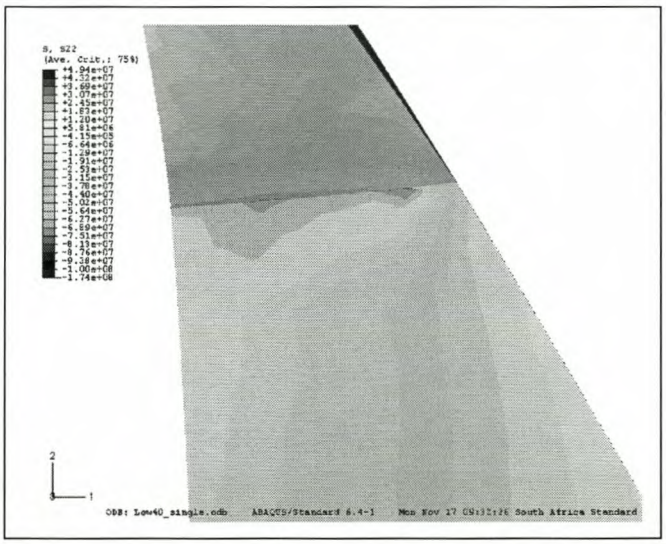

Figure 5-6. Compressive stress displayed focussing in on the discontinuity.

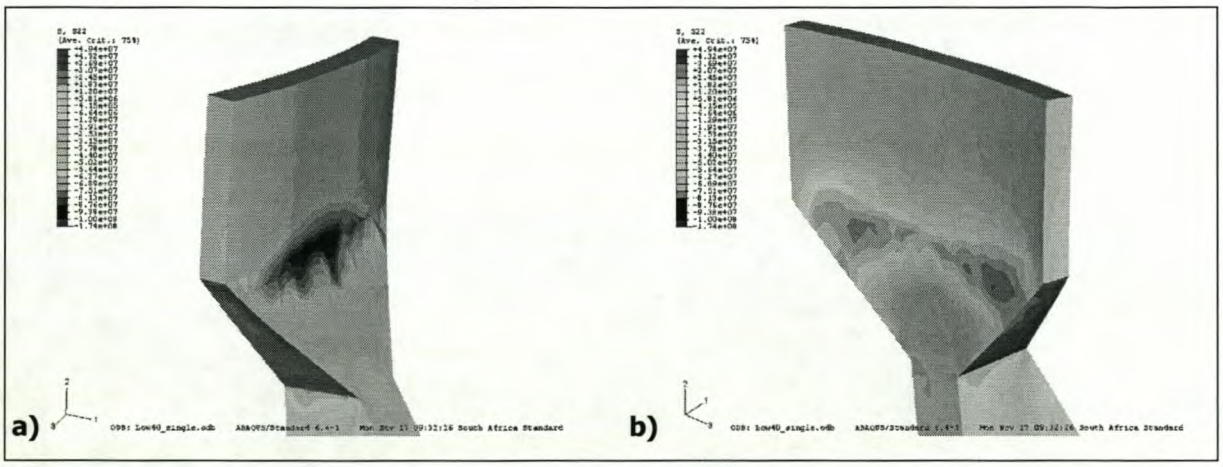

Figure 5-7. Axial stresses due to flexural behaviour with b) the position of maximum compressive stress and c) maximum tensile stress.

There are great volumes of the IGV that are only under slight, if any, compression. In *Figure 5-5* these regions are clear – the yellowish regions (greyscale: lighter regions). (Remember that regions judged to be structurally inactive have already been cut away.) These inactive regions may also be cut away further during the optimization process, with the stability of the particular geometry posing as the limiting criterion.

Studies on the assembly

A model of the chimney, symmetrical with regards to the vertical plane (because the wind pressure distribution around the circumference of the shell will be symmetric), with the ring stiffeners and an assembly of IGV's is created and was shown in *Figure 5-4b*. The full wind and gravity load is applied. The purpose of setting up this model is multi-faceted:

- The full distribution of forces through the whole model can be seen – only the extreme load case (maximum compressive force) was considered during the conceptualization phase. The tensile and moment behaviour in the IGV's can also be studied.
- Global behaviour and interaction between the full assembly of IGV's and the chimney can be studied.
- The stability of the whole structure, and the influence of the IGV's on it, can be studied.
- Whereas the stability of an individual IGV must be ensured, it is not the minimal structure from which the global stability can be derived. Overall natural frequencies of the tower are of importance for studying aerodynamic effects. It is imperative that the influence on the global dynamic behaviour of the IGV design and the transfer to the chimney be studied.
- This model also serves as a waypoint – comparing the single IGV model's deformation with that of the IGV's in the assembled model – to verify the assumptions with regards to load cases considered and to investigate the effectivity of the concept of the individual IGV in the global system.

Note that for modelling simplicity the flaring characteristic of the chimney [13] mentioned in *Chapter 1 paragraph 1.2.3* is not implemented in this symmetrical model. The chimney shell is modelled with quadratic 8-node S8R shell elements. The chimney height is 1500 metres and the inner diameter is 160 metres. Six ring stiffener assemblies consisting of 36 stiffener beams each are implemented, spaced 220 meters apart ending at the top of the chimney. They are modelled with 3 noded (quadratic) beam elements and all degrees of freedom of the nodes coinciding with the chimney shell are coupled. The stiffener beams are modelled with the typical material characteristics of steel – a Young's modulus of 210 GPa and a Poisson's ratio of 0.3. Nine of the Concept 1 structures are assembled and the interaction between the shell (chimney) and solid (transfer section) elements established with a "shell-to-solid" interaction tool in the software used. The rotation of the shell

nodes (incompatible to the solid elements' degrees of freedom) is hereby transferred to the solid nodes by rigid constraining of the movement of the solid nodes that lie within a set tolerated distance to the shell nodes. Finally, linear elastic behaviour is assumed.

The distribution of the stresses

The distribution of forces and resulting stress action through the IGV's can be seen in *Figure 5-8*. The first two figures show the localised axial stresses, a) compressive in blue (greyscale: dark grey) and b) tensile in orange (greyscale: darker greys), forming in the IGV's due to flexural action.

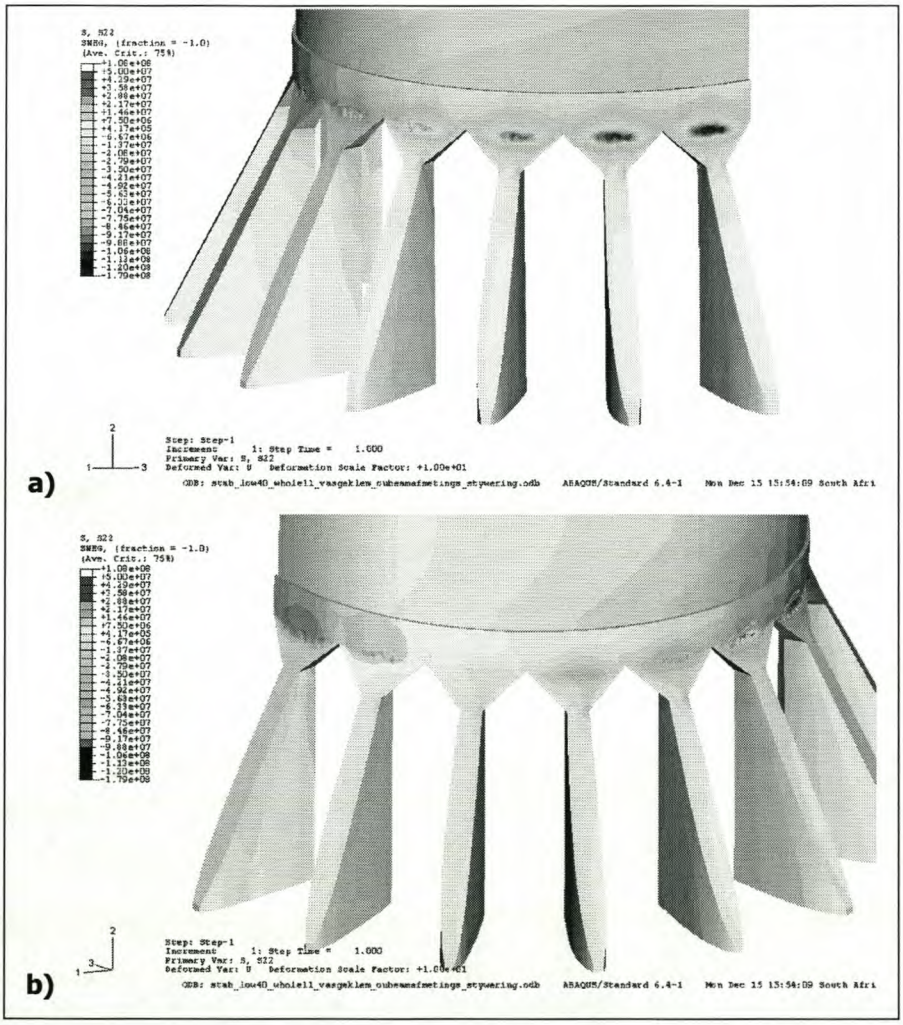

Figure 5-8. Axial stresses in the assembly model.

From the figures it is clear that the chimney and IGV structure acts like a cantilever beam, with compressive stresses forming on the trailing side of the assembly and tensile stresses on the side facing the wind. The "neutral axis" of the "cantilever" is present in the IGV's in between the leading

and the trailing side, where the stress levels relatively neutral and never near compressive stress limits.

The assumptions with regards to the isolation of load cases applied on the individual IGV are verified by the similar stress magnitudes and deformations in the assembled structure.

Frequency

Two models of the chimney structure are studied for the free vibration characteristics, one with and one without IGV's. The latter model ignores the required transition from cylindrical shell to discrete supports, thus assuming the cylinder to continue to ground level. The boundary conditions at ground level are fixed, meaning that all translational and rotational degrees of freedom are suppressed. These frequency analyses are conducted to see the effect the IGV's have on the dynamic characteristics of the global structure.

As reported in previous research [14] the frequency analysis yields many low frequency modes in which deformation is localized to individual ring stiffener beams or to sets of ring stiffeners. These modes are ignored in order to proceed to the first global mode, in order to compare the lowest structural frequency with and without the IGV's. This is done to ensure that the IGV-support system is not detrimental to the global stability. For a fair comparison, it is ensured that, apart from the difference in the IGV region, both models are exactly the same. In this regard especially the ring stiffener characteristics must be similar, because they play a governing role in the global behaviour, both statically and dynamically.

Results of frequency analyses

The first global mode of the model with IGV's coincides with a frequency of 0.09 Hz, corresponding to a period of 10.89 seconds. For the model without IGV's the first global mode has a frequency of 0.10 Hz, corresponding to a period of 10.00 seconds. This result is consistent with the frequency found in literature [9] – refer to *Chapter 2 paragraph 2.5.2*. For the chimney structure the wind velocity exciting the first global mode [9] is, from *Equation 2-14*, with the 160-metre chimney diameter and Strouhal number of 0.2 applied,

$$V = 800N \tag{5-2}$$

where N is the natural frequency in Hertz. For the found modes velocities which may induce resonant lateral vibration are 73.54 m/s and 79.18 m/s, respectively. The first mode of an individual IGV occurs at 3.80 Hz – much higher due to the relatively stiff structure. The visual results of these analyses are documented in *Appendix E* (*Figure E-1 and E-2*).

An in-depth discussion of the frequency analyses results is reported in *Chapter 6 paragraph 6.4* of this thesis after the optimization process and hence will not be treated here.

Advantages of Concept 1

- The volume of material used in the solar chimney is decreased. Big volumes of concrete had already been cut away in this first iteration model through the omitting of the structurally inactive parts of the aero dynamic section of the structure and the arch shaped tensile stress regions. The estimated cost of this concept is R 9 783 110.
- Shear forces are kept to a minimum through the transference of force through direct compression and those resulting can easily be resisted. The literature study on deep beams (*Chapter 2 paragraph 2.3.1*) provided information on the role arches play in transference of forces by generating a mainly compressive system with shear resisted by the reinforced concrete.
- To the author's judgement this concept is aesthetically pleasing. Public favour is a vital asset especially in contentious projects such as the solar chimney, and an unattractive structure will only be detrimental to this cause.

Disadvantages of Concept 1

- The axial stresses are very high.
- The low natural frequency remains to be addressed. This is inherent to the slender cylindrical shape, as a solid tower, without air flow cut-outs in the IGV region, has a frequency of a mere seven percent higher.
- This concept affects only the lower 60-100 m of the chimney, not adding to the stability of the global structure.
- The irregular section (the volume reducing cut-out, as well as the anvil section) of this concept will need special construction methods. Conventional slipform construction cannot be used directly. Also keep in mind the size of the IGV column and the chimney. Nevertheless, financial considerations may justify the implementation of such a special construction method at this scale.

The concept has to undergo improvements and optimization before it can be deemed a solution.

5.2.2 Concept 2: Transfer of forces from chimney to IGV at a great height – fin stiffeners

The concept

In this concept the transferral of the vertical force takes place through both compressive and shear resistant interfaces. If an area of a transfer structure is in full contact with a part of the chimney

shell, vertical force can be transferred through that contact interface if the necessary shear resistance is present. Such an interface can be utilised together with the compressive capabilities of concrete to transfer all forces from the chimney to foundation level.

The resulting geometry of this concept reminds of that of the "fin stiffeners" [22] where the transfer of forces from the chimney starts at a great height. *Figure 5-9* displays the stiffeners.

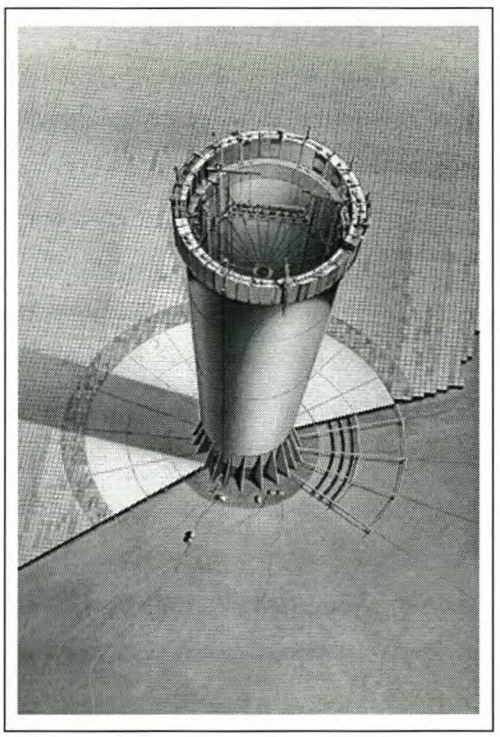

Figure 5-9. An artists' impression of the solar chimney under construction with the fin stiffeners present at the base [22].

Geometry

The simple calculation of compressive stress reduction due to self-weight reduction along the chimney height, as discussed in *paragraph 5.1.3* of this chapter and detailed in *Appendix D*, shows that the decrease in dead load does not bring about a significant change in the dead weight in a variation along height. The compressive transfer area of the support (IGV / fin stiffener) is never, even at great heights, big enough to transfer the vertical force.

Consider *Figure 5-10*. The fin stiffener will only be efficient as a force transfer structure if the vertical forces are sufficiently distributed throughout the structure. An adequately reinforced interface would be able to fulfil this function. The face must resist the great shear forces acting upon it in order to transfer the vertical forces in the chimney through the vertical face of contact to the fin structure.

The area that was too small to transfer the vertical force on it previously because compressive stresses were too high (red area – greyscale: black) is also considered in order to minimize the vertical contact area needed.

As was the case with Concept 1, the fin stiffener does not incorporate the proposed full NACA blade-shaped geometry of the IGV. Basic material minimization is already applied.

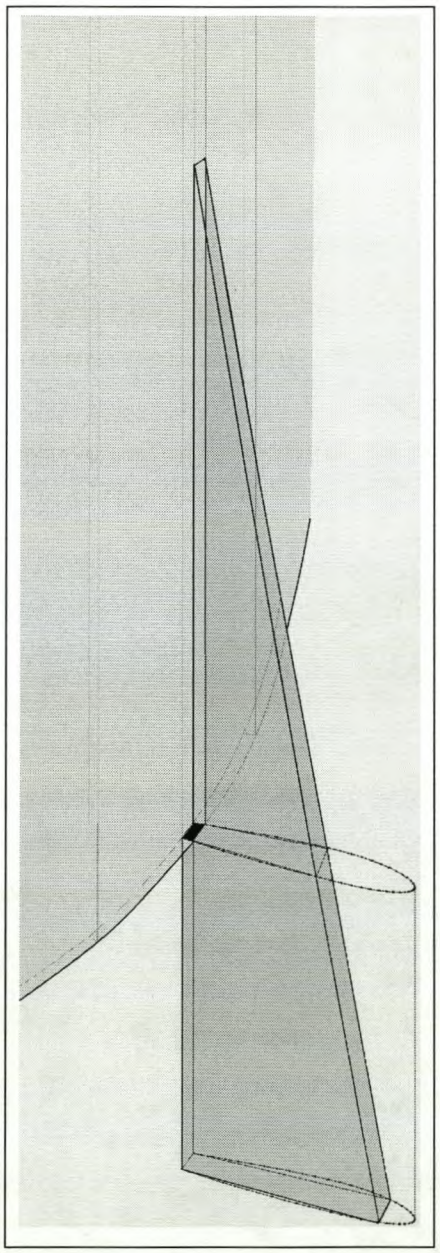

Figure 5-10. An approximation of a single fin stiffener.

The height of the transfer section

The maximum vertical load to be transferred by a fin stiffener is $1.78*10^9$ N. (In reality, there is an slight decrease in this force because of the decrease in dead weight of the shell with increase in height – refer to *paragraph 5.1.4.*)

The 9.9 m^2 face (red area in *Figure 5-10* – greyscale: black) can transfer $4.23*10^8$ N at a concrete stress level of 95 MPa. The remaining vertical force, to be transferred by the contact interface, is $1.357*10^9$ N. Assume the maximum allowable shear stress of concrete to be 0.5 MPa and the area of the full contact interface to be of dimensions 5 metres x *h* metres. The height, *h*, needed to transfer the vertical force is calculated to be 542.8 metres.

Model

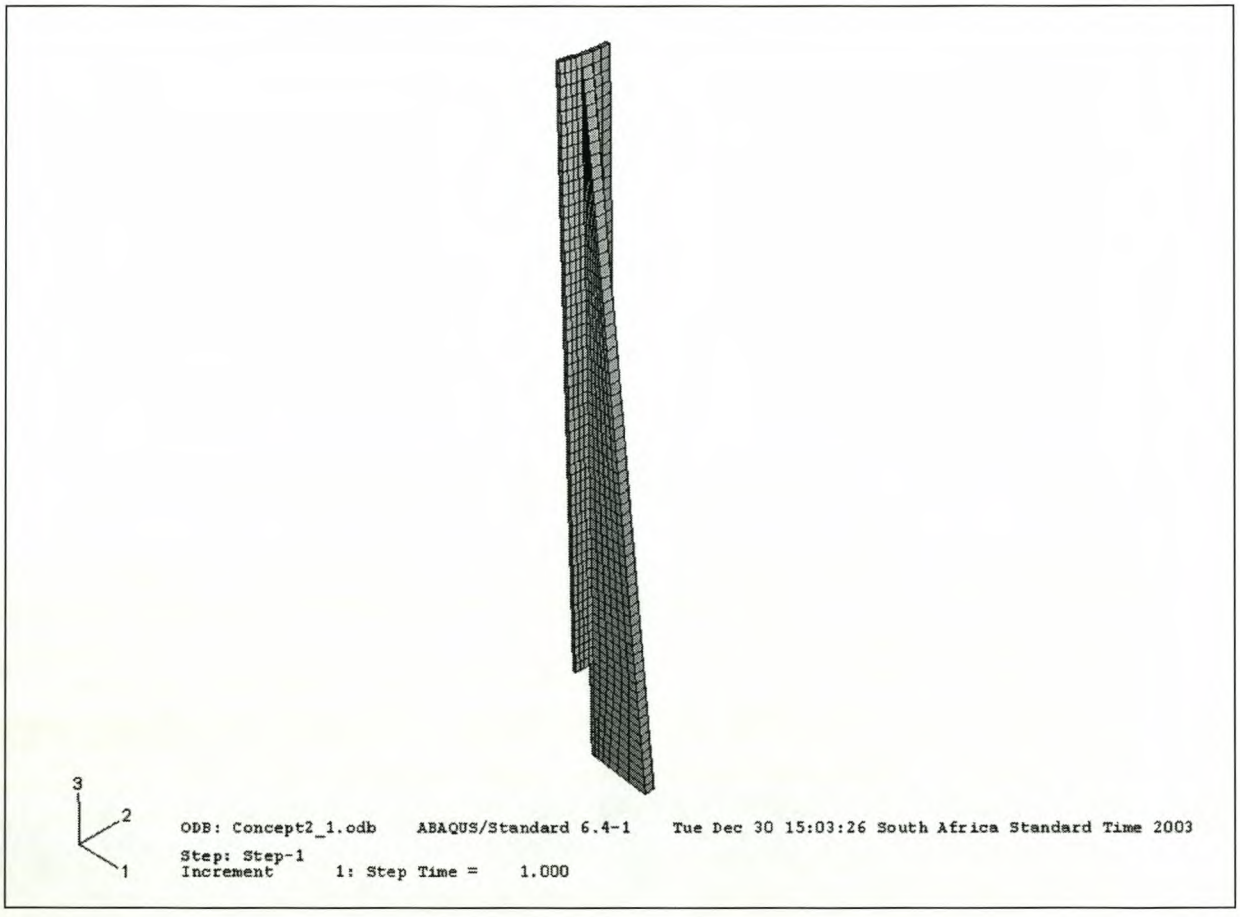

Figure 5-11. Typical model of Concept 2.

A model is set up in the FE-package ABAQUS [17]. To commence the iteration process the fin stiffener reaches up to a height of 300 metres (chimney height, not model height). Note that, for simplicity, the expected tensile stress regions for this model (arches) are not cut away. Also, the

thickness of the shell in between adjacent fin stiffeners up to the height of 300 meters along the chimney is constantly 2.2 metres; it is not decreased along the tower height according to the proposed shell thickness variation.

Quadratic solid elements are used. The footing of the structure is fixed against all degrees of freedom. The boundary conditions against lateral movement are set up as for Concept 1 to resemble the effect of adjacent shell parts and fin stiffener structures. *Figure 5-11* depicts a typical model that is used during the conceptualization and optimization process. Only the maximum vertical load (*Chapter 4 paragraph 4.1.1*) is applied on the horizontal surface at the top of the model. A static load analysis is performed on the model.

Results and discussion

Figure 5-12 shows the resultant axial (with respect to vertical loading) stresses in the structure.

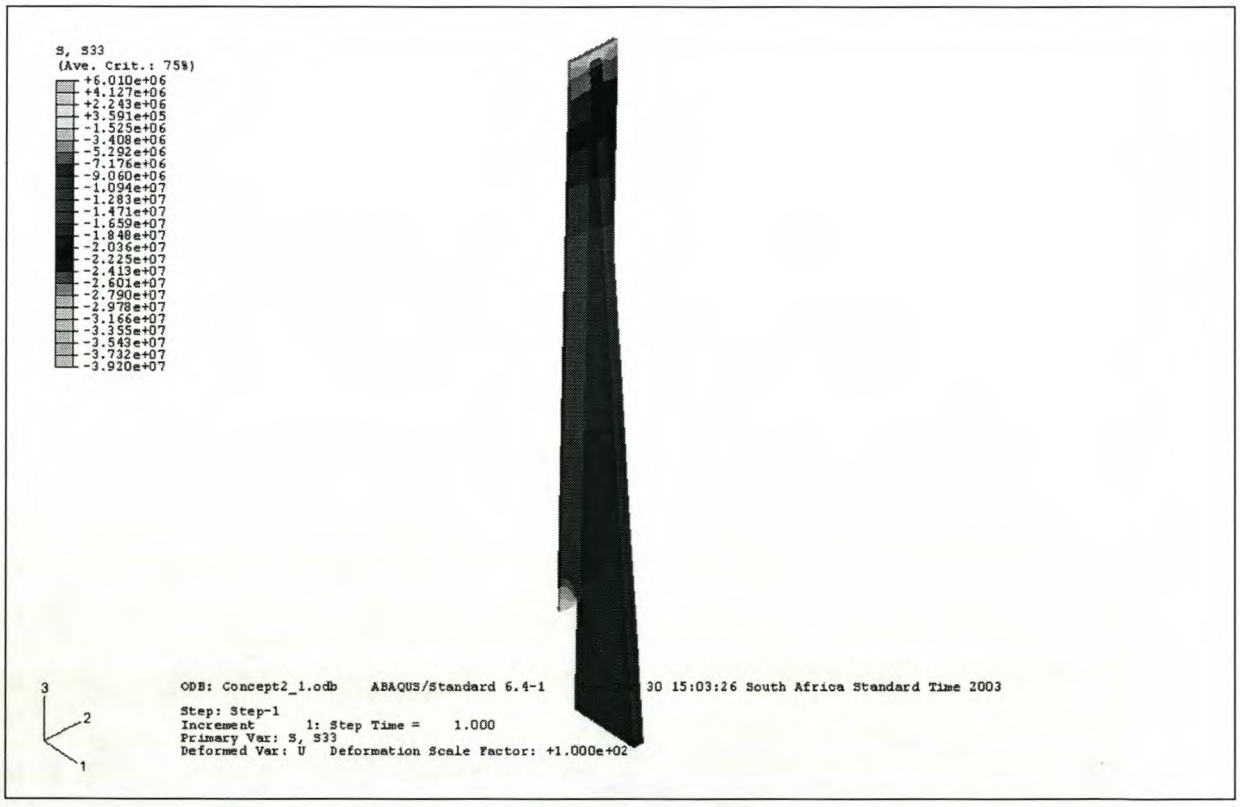

Figure 5-12. Axial stresses distribution.

The concept successfully transfers the vertical force through the shear mechanism into the IGV's. Resultant compressive stresses are low with the maximum, at a value of approximately 35 MPa, occurring in the chimney shell at the upper tip of the fin stiffener – see *Figure 5-12*. *Figure 5-13* shows the compressive stresses as the much localized blue areas (greyscale: darkest regions) in the

region where the chimney shell meets the IGV part of the fin stiffener. Here, the stresses peak at approximately 24 MPa. Note the arch shaped tensile stress depicted in the yellow/orange areas (greyscale: lighter areas) in *Figure 5-13*.

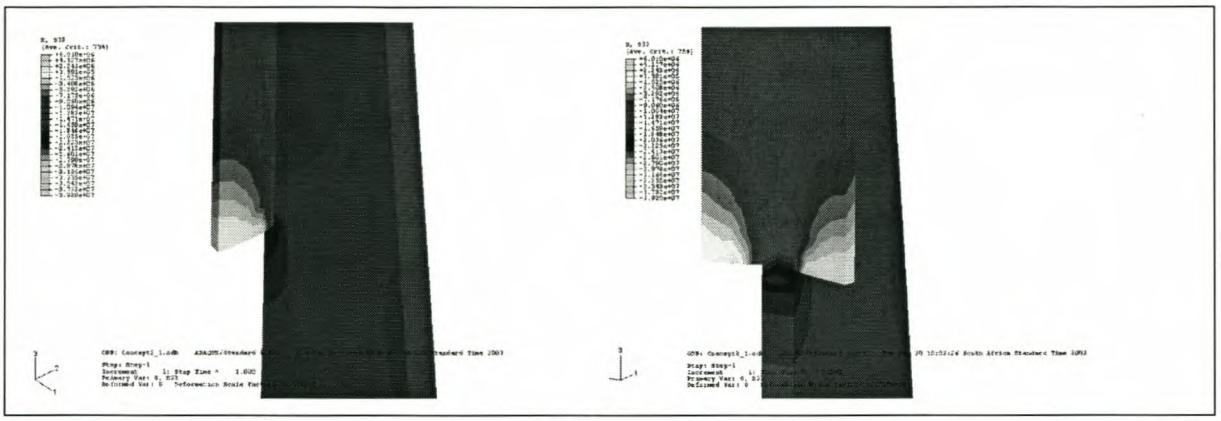

Figure 5-13. Localized compressive stress in the region where chimney shell joins the IGV.

Frequency analysis and result

A frequency analysis is conducted on the assembled fin stiffener model. The model, with the correct wall thickness distribution, was setup in the FE software FEMAS2090 [33]. The first global mode of the model with fin stiffeners is higher than 0.1 Hz, at 0.12 Hz.

Advantages of Concept 2

- The resultant compressive stresses in this concept are always within the ULS criteria for collapse.
- Simple construction: there are no drastically varying sections in this concept; the fin section decreases linearly. Construction methods such as slipform can be implemented.
- The stiffness of the global structure proves to be higher than that of the assembled Concept 1 model.

Disadvantages of Concept 2

- The fins are voluminous, adding further material costs to the already costly project. The estimated cost is R 31 096 580 which is more than 3 times higher than the cost of Concept 1.

5.3 Concluding the chapter

Concept 2 proves to be the optimal solution satisfying the static load cases isolated in *Chapter 4* with the disadvantage of being more costly. The low eigenfrequencies of the global structure for the chimney structure remain a cardinal topic for further research. A feasible solution may imply changes in the overall concept, which will in turn have implications on the IGV / force transferral concepts investigated here.

The investigated concepts are currently not of optimal geometry – many improvements are possible in order to lower the compressive stresses and project cost, and stiffen the structure– to fulfil the requirements for an IGV, set out earlier in this thesis. The next chapter investigates the prospect of optimization, both geometrically and financially.

CHAPTER 6: GEOMETRY AND COST OPTIMIZATION

Many improvements can be made to the two concepts proposed in *Chapter* 5. These can be approached from two design criteria, namely those pertaining to geometrical optimization and those of financial benefit. This chapter investigates the possibility of accomplishing such improvements.

Rough cost estimation is done for each parameter change made on the original concepts. The cost estimations are then compared and discussed. Finally, a summary of improvisations to be investigated toward the stiffening of the chimney structure, increasing the eigenfrequencies, are reported.

The geometrical/financial factors under investigation are

- Volume decrease through the cutting away of structurally inactive regions.
- Investigations toward the optimization of the specific geometries of the concepts proposed in *Chapter 5*.
- IGV rotation.
- Number of IGV's.
- Cost decrease through the application of appropriate material.
- Means for improving the stiffness of the global structure.

6.1 Optimization

6.1.1 Structurally inactive regions

The IGV geometry proposed by [1] used directly in structural analysis proves to be structurally over-designed as proved in *Chapter 5 paragraph 5.1.1* and the main inactive regions have already been cut away in the first iteration concept geometries. Further optimization is done through the implementation of the column interaction diagrams, studied in *Chapter 2 paragraph 2.3.2* for purpose of it aiding the design of the geometrical dimensions. The formulas shaping the column interaction diagrams contain parameters describing the concrete volume and strength, as well as the amount of reinforcement steel. Boundary limits for these parameters can be determined through these diagrams. Refer to *Appendix F* for the comprehensive design tables used in the determination of the first iteration geometry of Concept 1.

Arches

The first conceptual solution investigated in *Chapter 5 paragraph 5.2.1* exploited the presence of tensile arches by the approximate cutting away of the tensile volumes (refer to *Figure 5-4b)*. These regions were merely approximated; hence the linear increase in anvil width with height. A more realistic (optimized) design will have the traditional parabolic arch shaped cutaways, as is also proposed by the shape of the tensile stress contours in *Figures 4-6* and *5-13*.

6.1.2 Optimization of Concept 1

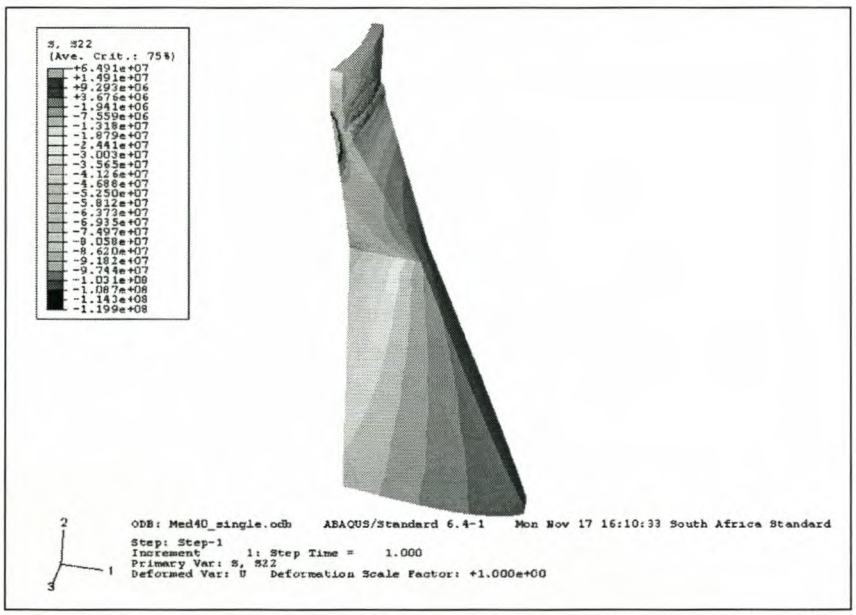

Figure 6-1. Axial stress distribution in the adapted geometry.

The geometry of the concepts investigated in *Chapter 5 paragraph 5.2.1* were chosen with the knowledge and foundation acquired through the literature study and the tests performed as reported earlier in this thesis. This section reports the investigation into optimization of Concept 1. Consequently, *paragraph 6.1.3* reports optimization prospects of Concept 2.

The first iteration geometry of Concept 1 yielded large compressive stress resultants. One of the aims in this section is to lower these stresses and consequently the height of the transfer section is investigated. The prospect of further volume decrease is also attended to.

Height of transfer section

The optimal height of the transfer section is investigated. Another model, with transfer height of 30 metres (opposed to the 10-metre high transfer section with 45 degree arch inclination used

previously) is created and tested. *Figure 6-1* shows the resultant axial (with regards to vertical loading) stresses.

An overall decrease in compressive stresses due to the heightening of the transfer section is evident. Where the original concept yields axial force compressive stresses of up to 75 MPa the adapted concept yields stresses of approximately 55 MPa – a decrease of 27 % on the maximum compressive stress. The estimated cost of this optimized model is R 11 130 766 which is only 1.14 times more than the original concept. An eigenfrequency analysis on this individual structure yielded a first eigenmode corresponding to a frequency of 2.18 Hz which is significantly lower than that resulting from the original concept geometry (3.80 Hz – refer to *Chapter 5 paragraph 5.2.1*) predicting a less stiff global structure, if modelled with this more slender IGV / force transfer section.

Length of IGV

The compressive stresses in the lower regions of the original Concept 1 are very low. A model is proposed where the section of these lower regions is decreased – the length of the IGV is decreased from 40 metres to 32 metres. *Figure 6-2* shows the compressive stresses in the adapted model (the 30-metre transfer section is adapted).

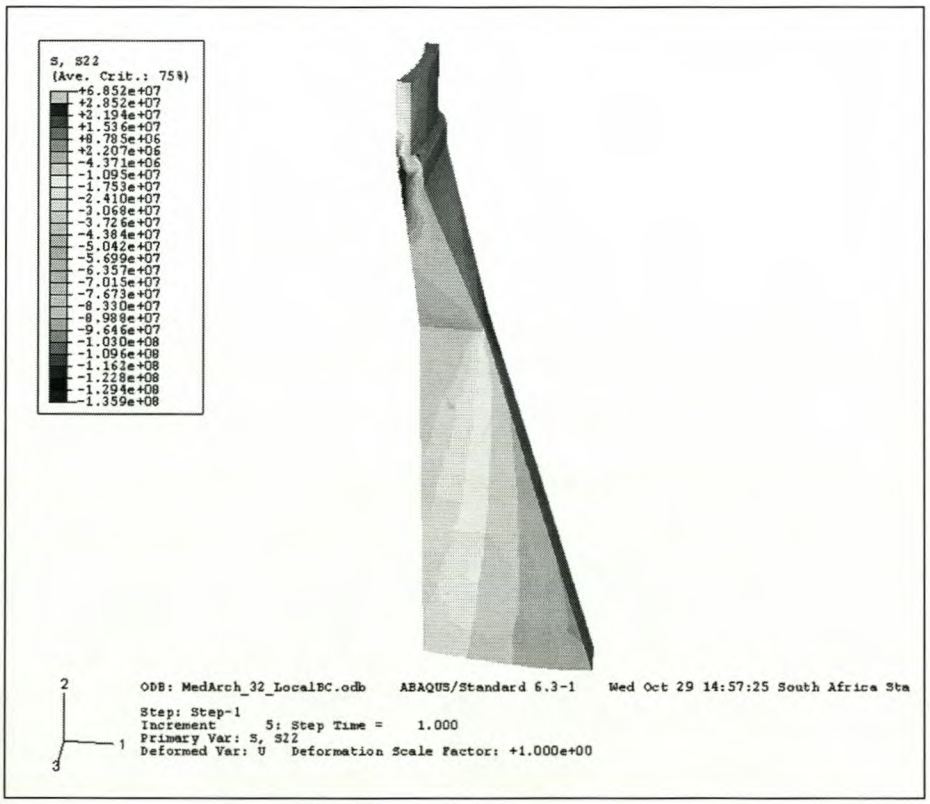

Figure 6-2. Transfer structure with a decrease in sectional area.

As expected, the compressive stresses are higher in the smaller sectioned structure – the 55 MPa in the previous paragraph increases to approximately 70 MPa. The estimated cost of this optimization of Concept 1 is R 8 078 581 which is 0.83 times the cost of the original concept.

6.1.3 Optimization of Concept 2

The first iteration geometry of Concept 2 yielded a voluminous structure with a relatively great cost. An aim in this section is to lower this cost while remaining within ULS criteria boundaries for compressive stresses in concrete. The obvious variable to investigate is the height of the fin stiffener.

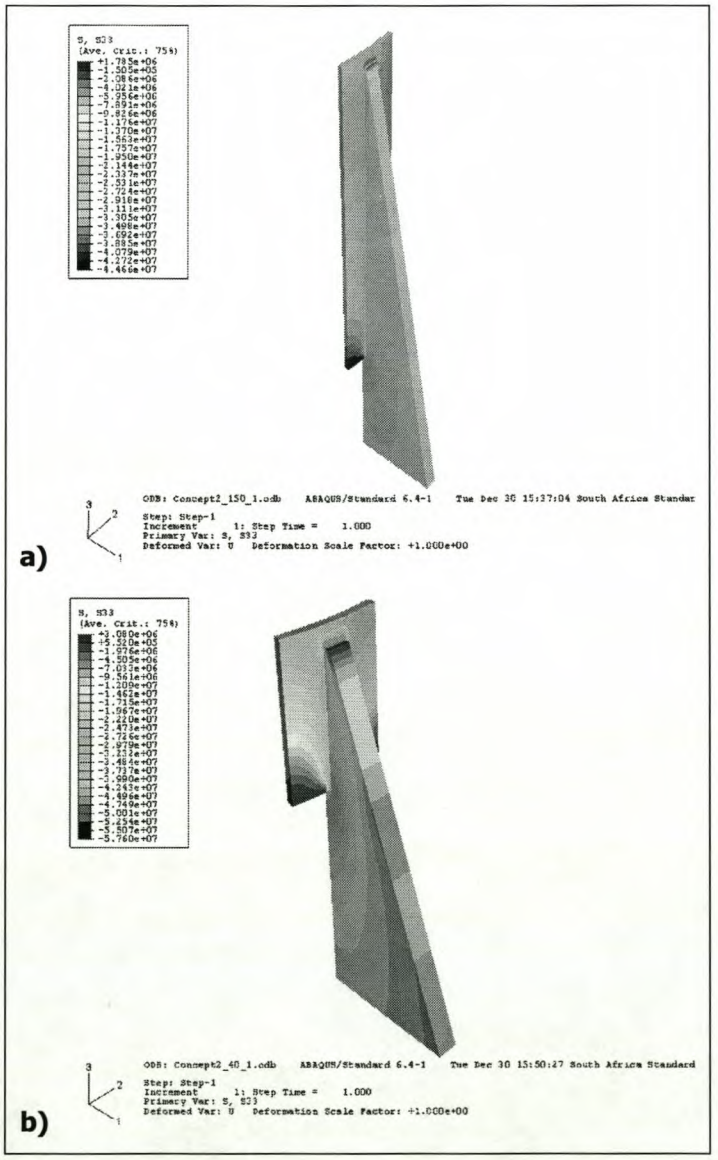

Figure 6-3. Adaptations to Concept 2: a) 150 and b) 40-metre high transfer section.

Height of shear resistant interface

The compressive stresses in the fin stiffener structures reported in *Chapter 5 paragraph 5.2.2* are relatively low. The decrease of the area transferring the vertical load through shear resistance and compression (that is, the fin stiffener height) is investigated. *Figure 6-3* shows analysis results for models with transfer heights 150 metres and 40 metres.

The maximum compressive stress in the model with 150-metre high transfer section increases from 35 MPa in the original concept to approximately 40 MPa. Its estimated cost is R 15 672 392 which is approximately half the cost of the original Concept 2 model. The model with 40-metre high transfer section shows an increase in compressive stress – up to approximately 55 MPa. Its estimated cost is R 7 992 493 which is less than the cost of the original Concept 1 model!

6.1.4 IGV rotation

In his research on the turbine performance Dr. Gannon [1] proposes the IGV's to be rotated with a maximum angle of 22.5 degrees. To see whether this rotation improves structural behaviour, a simplified model resting on rotated columns were created. The rotation was found not to increase the eigenfrequency (Table 6-1).

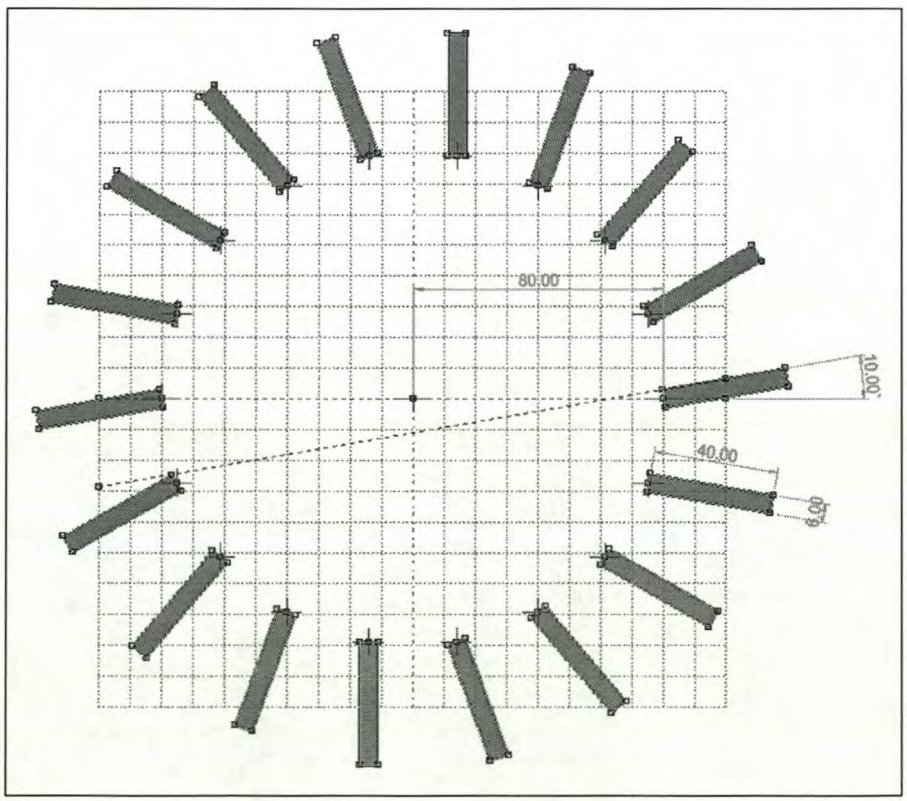

Figure 6-4. Approximated section of rotated IGV model.

Three models, with approximated IGV's rotated with 0, 10 and 20 degrees (*Figure 6-4* depicts the 10 degree case), are set up. The FE-models are simplified by not considering the ring stiffeners, by assuming the shell thickness to be constant (500 millimetres) throughout the chimney height and by the approximation of the IGV's with the prismatic rectangular section used earlier in this thesis with the first order buckling analysis – refer to *Chapter 5 paragraph 5.1.2*. Eigenmodes of each model are calculated and the results are tabulated in *Table 6-1*.

Rotation angle [degrees]	Frequency at 1st mode [Hz]	Corresponding period [s]	Percentage improved [%]
0	0.10	9.91	0
10	0.10	9.91	0.01
20	0.10	9.90	0.09

Table 6-1. Frequency and period corresponding to models with varying IGV rotation angle.

The increase in frequency is not significant and can be considered as negligible. The increase in frequency with an increased IGV rotation of from 20 degrees is only 0.1 %.

6.1.5 Number of IGV's

Optimizing by decreasing the number of IGV's

Eighteen IGV's are proposed and used in this research. The possibility exists to decrease this number while increasing the structural properties of the remaining IGV's. This can only be investigated by repeating the stress analyses procedures performed in *Chapter 5*. The question of the optimal number of IGV's, however, remains a case of optimal design, considering both aerodynamic and structural aspects.

Optimizing while using the same number of IGV's

Literature study proposes all 18 IGV structures to be used as column structures. However, not all IGV's have to fulfil a column function – alternate IGV's can be installed with a transfer section or fin stiffener sufficient to uphold the force exerted on it. The remaining IGV's can be constructed using a structure with optimal cost only able to resist the pressure forces exerted on it by the airflow. This concept could result in a further decrease in project costs.

6.1.6 Cost decrease through the application of appropriate material

The compressive stress contours seen throughout *Figures 6-1* to *6-3*, describe the magnitude of the compressive stresses present in the material of IGV structures. The concrete strength can be varied to fit the requirements for the regions indicated by these contours. Regions exist where the stresses are very low. A 30 MPa concrete will be sufficient in these regions with consequential lowering of capital expenditures of the project.

Another advantage of using low strength concrete is that stress concentrations are less likely to occur. Early crack forming lowers the elasticity modulus of a region of concrete subject to a great load which is then transferred to adjacent regions. Also, the lower density of the low strength concrete, implying the presence of more air in the material, isolates the structure against sudden and great temperature changes and result in the lowering and less localization of stresses in the regions loaded with a great temperature gradient.

Inversely, the lowering of the characteristic concrete strength will lower the elasticity modulus and hence the global stiffness and eigenfrequencies of the structure.

6.2 A brief look at cost optimization

It is complicated to fix a cost to a structure because of varying material, transport and construction costs. A parameter study was conducted, weighing a few concepts against each other. Material costs as is current for the Western Cape region of South Africa are used in this approximation. Transport and construction costs are not considered.

Rough cost estimation for the original and optimized concepts was done and reported at the relevant paragraphs. The costs can now be compared and discussed.

6.2.1 Models under investigation

Table 6-2 displays the estimated costs for six investigated models, incorporating appropriate material strength distribution. Refer to *Appendix G* for the full cost estimation tables.

Note: for the sake of simplifying calculations all reinforcement steel quantities were chosen as the prescribed minimum, at 0.15 %. ULS criteria for the compressive stresses are applied.

Model	Estimated cost	Cost – as a fraction of Model 1
1. Concept 1 with 40-metre length and cut away sections	R 9 783 110	1.00
2. Concept 1 as above but adapted with a 30-metre high transfer section – 40 metres in length	R 11 130 766	1.14
3. Concept 1 as above but 32 metres in length	R 8 078 581	0.83
4. Fin stiffener height 300 metres	R 31 096 580	3.18
5. Fin stiffener height 150 metres	R 15 672 392	1.60
6. Fin stiffener height 40 metres	R 7 992 493	0.82

Table 6-2. Estimated cost of concepts.

Discussion

The compressive stresses in the model with 300-metre high rising fin stiffeners (Model 4 in *Table 6-2*) are relatively low. Its cost, on the other side, is relatively high. If the stability added by this structure is not significant, which could have brought about a decrease in the shell thickness in the lower regions of the chimney as well, this option is not optimal. Model 6, where the compressive stresses peak at 55 MPa, proves to be fairly efficient in distributing the stress and is the cheapest structure of all those evaluated making it the most feasible solution. Models 1 and 2 are relatively cheap.

It is difficult to judge these structures with regard to structural and cost efficiency. The many variables surrounding the physical construction of a structure of such magnitude in a far off region as the Northern Cape in South Africa complicate preliminary cost estimations. Material availability and cost, transport costs, construction methods and corresponding costs and labour costs are amongst these variables. Each region and country has its own unique complications. For instance, added live loads may be induced on the structures due to extreme meteorological or geological conditions such as subzero temperatures, causing ice to form in critical regions, hail or earthquakes. The final decision as to the optimal geometry and detailing of the design lies with the local consultant engineer. Nevertheless, *Table 6-2* serves to initiate cost estimations and aid future conceptual design decisions.

The vexing point of the inadequate global stiffness of the structure calls for further investigation into increasing this characteristic. Only once a satisfactory solution is found can the cost estimations be fixed. The stiffness of the chimney structure will be discussed later in this chapter.

6.2.2 Further cost optimization

The column interaction diagrams prove to be a useful design tool, as seen earlier in *paragraph 6.1.1* of this chapter. The real worth of it lies in performing detailed optimization, where various factors like volume, material cost and the reinforcement volume ratios are taken into account. The same strength resistance can, for instance, be accomplished through various configurations of concrete and reinforcement steel with regard to material volume and strength. As an example, a column of constant section with dimensions 16 x 6 metres can resist given axial force–moment combinations with a factorised concrete strength of 35 MPa and reinforcement steel area factor of 0.014. Decreasing the concrete strength to 25 MPa while doubling the area of reinforcement steel still yields a solution resistant to all load cases. Only after the determination of the values of the many relevant variables one option will be isolated as the most economical choice.

6.3 Overview of optimization

Each investigated optimization strategy implemented on the original concepts delivered positive results. The decrease in the length of the IGV in Concept 1, as well as the decrease in the height of the fin stiffener structure, resulted in a decrease in cost while the compressive stresses due to the vertical load remained approximately in the same region. The increase in the height of the transfer section of Concept 1 resulted in a decrease in compressive stresses but an increase in cost.

All the optimization strategies applied will probably – it have not been specifically investigated – result in a lowering of global stiffness of the chimney structure. This aspect is discussed in the next section but it can be stated here that the stiffness of the individual optimized structures is less than for their original geometry (refer to *paragraphs 6.1.2* and *6.1.3*).

6.4 Comparing and discussing stiffness

In this section the many aspects surrounding the optimization of the IGV's and the global chimney structure with regards to its stiffness, is discussed.

Models studied

Setting up FE-models for frequency analyses is a challenging task. The actual analysis also takes a lot of time, especially since the first global mode occurs only around the overall 210^{th} eigenmode due the presence of all the mentioned local modes due to excitation of individual or sets of ring stiffeners.

Consequently only two models were created for eigenfrequency analyses on the assemblies of the concept models, namely the anvil concept model and the fin stiffener concept model. *Table 6-3* recaps on the results and shows the corresponding wind velocities that will generate these frequencies.

Model	***Frequency [Hz]***	***Wind velocity [m/s]***
Chimney – without IGV / transfer section	*0.10 Hz*	79.18
Chimney – Concept 1 assembly added	*0.09 Hz*	73.54
Chimney – Concept 2 assembly added	*0.12 Hz*	96.25

Table 6-3. Comparing the frequency analyses results.

For the Concept 1 assembly the eigenfrequency without IGV's is higher than for the model with IGV's. This implies that the IGV's make the global structure more flexible. This can be expected since the space generating IGV's bring an abrupt break in the continuity of the prismatic-cylindrical chimney shell, creating the channels for the through flow of air. The addition of IGV's brings the frequency corresponding to the first global mode down by 7%. The assembly applying the fin stiffener concept shows a 20 % improvement in the frequency of the global structure.

The eigenfrequencies corresponding to the first eigenmode of both global structures investigated is very low and therefore prone to resonance under the assumed wind load. This is still a matter of great concern in the conceptualization of a feasible chimney structure. Cooling tower design (the reader is referred back to *Chapter 2 paragraph 2.5.2*) aims to reach a stiffness corresponding to first eigenfrequencies of more than 0.7 Hz [5] in order to fall outside the wind excitation frequencies. Research conducted by [9] aimed at increasing the eigenfrequency of the chimney structure by implementing cooling tower geometry concepts to the base of the chimney. Despite these attempts, the frequencies remained relatively low, in the region of 0.1 Hz. The eigenfrequencies found in this current research also yields the same relatively low values. The stiffness of the solar chimney must be increased to reach a realistic global mode eigenfrequencies for this structure.

Increasing the global chimney stiffness

A possibility for increasing the eigenfrequency of the chimney is to lower the centre of gravity by replacing mass to lower regions. However, the upper shell regions, only 0.25 metres thick, are already extremely thin. The increase of the diameter of the lower part of the chimney to resemble a cooling tower structure, with the added stabilising effect of the parabolic hyperboloid, as was investigated by [9], did not have a significant effect on the frequency of the structure.

A few prospects toward the aim of decreasing the material volume of the structure have implications on its stiffness. Such are:

- Optimization of shell thickness: the effective application of appropriate shell thickness and concrete strength in higher stressed regions will improve the global stiffness and performance of the chimney. Research by Lumby [4] initiated the process of the shell thickness optimization.
- The outward flanging of the IGV's/force transfer structures increases the stiffness of the chimney (although the discontinuity they create in the constantly prismatic chimney shell decreases the material present to stiffen the chimney). The longer chord length of the IGV blade, extending radially away from the chimney structure, will bring about such an outward flanging.
- The outward flanging of the fin stiffeners (Concept 2) from a significant height increases the moment of inertia of the lower regions of the chimney shell and the IGV's.
- Larger, heavier transfer structures and IGV's could serve the purpose of increasing the stiffness of the chimney – a function the thick lower shell regions fulfilled previously.

The implementation of stabilising cable guys and vertical pre-stressing of the chimney shell should be investigated as it could add to the stiffness of the structure.

Damping

As an alternative to increasing the frequency, or complimentary to it, the vibrational amplitude can be reduced by damping mechanisms, as implemented against resonance in ultra tall structures and ships.

Ring stiffeners

At this stage it must be mentioned that the ring stiffeners, the structures proposed to uphold the circular structure of the chimney shell to prevent ovalling and global buckling, are not functioning realistically. Large deformations are characteristic of the current "solutions" even to an extent where geometric non-linear dynamic analyses are impossible. A lowering of the own weight of the six ring stiffeners and their increased effectivity could result in an increase in the eigenfrequencies. The ring stiffener beams also display large deformations due to excitation at loading corresponding to very low wind velocities. The first (local) mode in the chimney structure occurred in a single ring stiffener corresponding to a frequency of 0.06 Hz (refer to *Appendix E, Figure E-4* for the visualization)! Research on the realisation of these structures must therefore be performed.

Development of realistic wind models

In addition to optimizing the structure, the wind excitation characteristics should be modelled for this hyper-structure. As mentioned in *Chapter 2 paragraph 2.2*, the used wind load models are conservative: the other wind extrapolation models used in previous research [14] yielded peak velocities of 82 m/s and 56 m/s at the top of the chimney (a height of 1500 metres) that are respectively just outside the border and well within the resonance-corresponding velocities found in the frequency analyses (the velocity used in this research is 108 m/s – *Chapter 2 paragraph 2.2*. Also note that ULS factors for wind loading are not considered). A more realistic wind model could verify the safety of a structure with such low stiffness. The lower total static wind load may be the result of such a research effort, but it remains to be seen if such a study will deduce a lower frequency band within which the wind load occurs.

Concluding the discussion

The facts, ideas, and methods mentioned in this section touch on the more global aspects of the solar chimney. The optimization of shell thickness, for instance, although closely related to the problem addressed in this thesis, is a topic requiring individual attention, as is the global stiffness.

CHAPTER 7: CONCLUSION

The aim of this research was to engage a previously unexplored topic of the solar chimney, namely the transfer of forces from the solar chimney tower shell to its foundation. The utilisation of the inlet guide vane structures to form part of such a transfer structure were investigated. Forces acting at the foundation level of the chimney were studied and internal local behaviour was investigated. Consequently, two concepts were proposed as solutions to the force transfer problem. Concluding the research effort the possibility of the optimization of these concepts was investigated.

7.1 Summarising the findings

7.1.1 Forces

The vertical force resulting from the own weight of the structure combined with the wind force on the chimney shell was found to be the most critical design parameter. The magnitude of this force is $1.78*10^9$ N (load per IGV). The other forces were found to be insignificant relative to this immense force, and it governs the conceptualisation process, with the only further load to point out being the tensile (negative) vertical load of $1.25*10^8$ N, which will have to be provided for by foundation anchoring.

The most noteworthy internal reaction to these forces is the excessive compressive stresses forming in the small sectioned regions that are to transfer the vertical forces. Necessary attention must be given to the various shear and moment actions resulting locally. Design accommodating the moment action due to the eccentricity of the vertical load relative to the IGV is particularly crucial. *Chapter 5* showed high stresses caused by the flexure in some parts of the transference structure. Such accommodating measures may include the thickening of the transfer section and the adequate placement of steel reinforcement in the critical regions. The arch forming phenomenon opened up the possibility for volume reduction. Vertical shear stresses in the interface between the chimney shell and the IGV's / force transfer structure must be accommodated by the placement of reinforcement steel.

7.1.2 Concepts

Two main concepts were isolated and each investigated individually and in assembly, in order to determine typical behaviour of such a massive concrete structure supporting a structure of such immense dimensions.

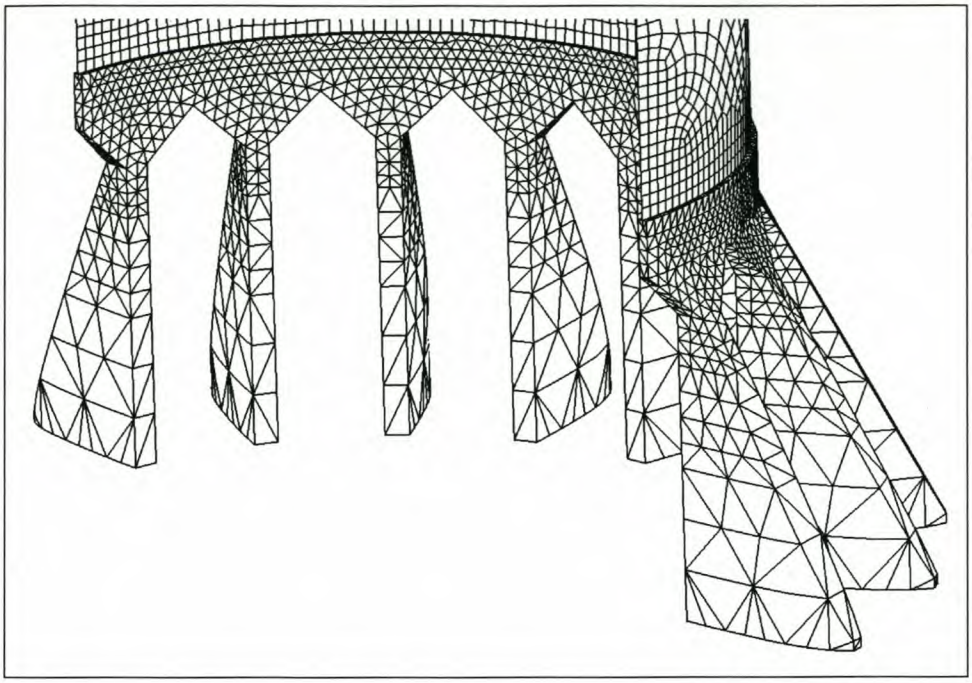

Figure 7-1. Assembled model of the anvil shaped transfer section structures.

An anvil shaped transfer section (*Figure 7-1*) was investigated, aiming at the axial transference of the vertical forces with the least lateral forces that could result in shear. The arch forming phenomenon aids this aim in that it, per definition, transfers force in compression as far as possible.

Compressive stresses in this concept were found to be up to 100 MPa which exceeds the ULS for concrete under compression. Compression stresses of up to 75 MPa concentrate around the irregular geometry of the region where the IGV blade geometry widens into the anvil structure. The significant flexural action in the upper section of the anvil causing compressive stresses of up to 100 MPa and tensile stresses of up to 35 MPa was a point of concern. The greatest shortcoming of this concept is its inadequacy in stiffening the global structure in order for its eigenfrequencies to fall within safe boundaries. The eigenfrequency of the assembled structure corresponding to the first eigenmode was 0.09 Hz. This is very close to the frequencies of the wind load so that it may excite lateral vibration resonance in prevailing wind speeds at the chimney top, as it equates by empirical formulation to a critical wind speed of as low as 73.54 m/s.

Advantages of this concept are its low cost, low shear stresses and its aesthetic appeal. Disadvantages are that no increase in the stiffness of the chimney structure results due to the small volume of material and the discontinuity of the regular chimney geometry, as well as the construction difficulties to be encountered with such a complicated geometry.

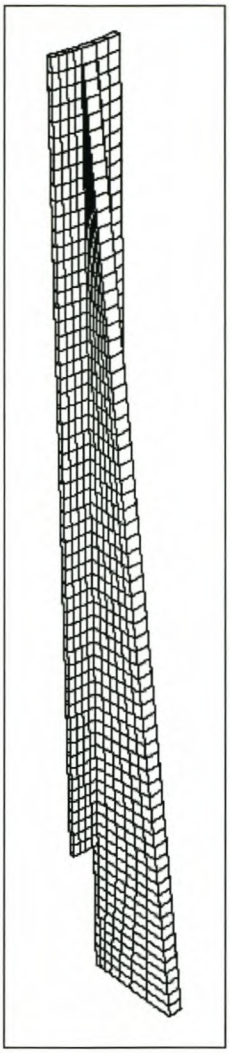

Figure 7-2. Meshed FE model of the fin stiffener concept.

The fin stiffener concept (*Figure 7-2*) aimed at transferring vertical forces with shear resistant interfaces. This concept would not require a widening section such as the anvil shaped structure proposed in the first concept, resulting in a simpler structure that is easier to construct.

Compressive stresses resulting from the application of the vertical load on this concept were lower than with the previous concept, peaking at approximately 35 MPa in the 300 meter tall model.

Unfortunately the resulting stiffness of this, the second, concept investigated was also inadequate, still falling close to the range of the wind excitation frequencies.

Advantages of this concept are the low compressive stresses and simple construction as there are no discontinuous sections in the geometry. A disadvantage is the increase in overall project cost because of the magnitude of these structures.

7.1.3 Optimization

The concepts isolated during the conceptualization process were optimised with regards to the dimensions that could have the greatest effect on the lowering of compressive stresses, increase of stiffness and stability of the chimney structure, as well as on project cost minimization.

It was proved that variations of the fin stiffener concept would suffice in fulfilling the stress resistance requirements with the full vertical force exerted on them. The height of the transfer sections in Concept 1 and 2 as well as the length of the IGV were varied improving resultant compressive stress values and lowering project costs. The assembly with fin stiffeners yielded a slight increase in the eigenfrequencies of the global structure.

Detailed optimization to determine the most stable, stiff, cost efficient structure becomes a problem to be solved by the design engineer resident in the proposed region for the project execution. To, at this stage, fix the optimal geometry and material distribution would be nonsensical as the cost parameters are bound to change significantly.

Structurally inactive regions were cut away. Such regions include parts of the full aerodynamic section of the IGV blade as well as the tensile stressed material forming arch shaped tensile stress areas in the shell between adjacent IGV's.

Optimal utilisation and optimization of the concrete and steel reinforcement material yielding strength in appropriate regions would lower project costs. As this research effort did not accommodate for non-linear material behaviour, a more detailed optimization of material placement remains to be performed in future research.

7.1.4 Overall

The looming problem of the low stiffness of the global chimney structure has two possible separate areas where combined improvisation could resolve the inadequately low eigenfrequencies of the chimney structure. Firstly, the structural stiffness of the chimney has to be increased. Such an increase could be achieved through, for instance, the innovation and implementation of a more effective ring stiffener assembly, and also with optimal choice of the shell thickness distribution and consequent added weight in the lower regions of the chimney. The second prospect is the lowering of the intensity and frequency range of the wind load through mathematical and probabilistic interpretation of wind gust data, ranging from the intensity, the range and the duration of such loads.

7.2 Topics for further research

Throughout the research performed on the realisation of the inlet guide vanes and force transfer structures, several areas for further and more focussed research were identified. The conceptual nature of the research reported in this thesis leaves room for detailing to be performed in the future.

- Nonlinear material and geometrical models have to be applied to the global solar chimney. Crack forming, material behaviour like shrinkage and creep (hygral effects) and temperature gradients and fluctuation must be studied and brought into consideration.
- The stiffness of the chimney structure has to be increased to avoid resonance of the structure under wind excitation. The vague hope for the wind characterisation to decrease the lower limit for the stiffness of the structure exists. Measures to alter vortex shedding frequencies can also be investigated.
- The current ring stiffener geometry is, as a whole, unsatisfying. Local deformations in the stiffeners are caused by own weight, while large stress concentrations and gradients result at the points of fastening to the chimney shell. Furthermore, complications during nonlinear geometry analyses are experienced due to low buckling loads of the stiffener elements.
- Geotechnical study of the foundation – FE modelling of the foundation to determine the effect on the stiffness of the chimney structure.
- Further, more detailed, optimisation with regard to the various design parameters of the IGV's, amongst others the determination of the optimal amount of structurally active IGV's in the global system, may be performed.
- The publishing of Carl Kirstein's research [29] on the optimal IGV height and angle of rotation will fix some more variables surrounding the IGV geometry. Subsequently, more focussed research can be conducted on the effect of these lateral forces on the IGV's.

7.3 Value of the research performed

The solar chimney, as a concept, has now been in existence for more than two decades. Much research had been performed on various aspects, although mostly non structural. Little detailed information of the structural behaviour and even the dimensions of the chimney and the glass roof collector is available today. The aspect of the transfer of the great forces acting on the chimney shell to the foundation has been unpublished or nonexistent. This study reporting on the prospect of utilising the inlet guide vanes towards the transferring purpose is therefore ground breaking. It serves as a basis study on structural aspects of the foundation of the chimney, its stabilisation and

overall realisation. It proposes two conceptual solutions for the force transfer and isolates the shortcomings of the current solar chimney concept for further research and detailing.

This report also provides valuable insight into the forces present in massive concrete structures.

Designers of the solar chimney can use this groundwork as a starting point from which to establish some of the many variables still lacking before the blueprint for the first solar chimney can be rolled open on the table, ready to be constructed, ready to lift the standard of life for the many who still lack this basic necessity for modern everyday life – energy.

REFERENCES

Publications

1. Gannon, A. J. (2002). *Solar chimney turbine performance*. Dissertation presented for the Degree of Doctor of Philosophy at the University of Stellenbosch
2. Kong, F.K. and Evans, R.H. (1993). *Reinforced and Prestressed Concrete*, 3rd edition. Chapman & Hall
3. Kröger, D.G. and Buys, J. (2001). *Performance evaluation of a solar chimney power plant. Proc. ISES*, Adelaide
4. Lumby, M. (2003). *Solar chimney turbine performance*. Paper presented as partial fulfilment of the requirements for the degree of Bachelor at the University of Stellenbosch
5. Montag, U., Andres, M., Harte, R., Krätzig, W.B. (2002). *World's largest natural draft cooling tower shell made of high performance concrete*. In: G. König, F. Dehn, T. Faust (Hrsg.), Proceedings of the 6th nternational Symposium on Utilization of High Strength / High Performance Concrete, 16.-20.06.2002, Leipzig, 725-738.
6. Park, R. and Paulay, T. (1975). *Reinforced Concrete Structures*. John Wiley & Sons
7. Popov, Egor P. (1999). *Engineering mechanics of solids Third edition*. Prentice-Hall, New Jersey
8. Sachs, P. (1978) *Wind forces in engineering*, Second edition. Biddles Ltd
9. Schindelin, H. (2002). *Entwurf eines 1500 m hohen Turms eines Solar-Aufwindkraftwerkes – Parameteruntersuchung zur Geometrieoptimierung*. Diplomarbeit, Bergische Universität Wuppertal.
10. Schlaich, J. (1995). *The Solar Chimney: Electricity from the Sun*. Edition Axel Menges
11. Schlaich, J. (1995). *Tension Structures for Solar Electricity Generation. Engineering Structures, Vol. 21,* pp. 658-668
12. South African Bureau of Standards 0160:1989, Loading code, p.39-65
13. Stinnes, W.-W., (1997). "*On a 200MW Solar Power station in the Northern Cape Province, Republic of South Africa*". Report of Pre-feasibility Study, commissioned by Ministry of Sport, Recreation, Science, Technology and Transport, Kimberley, Northern Cape Province, South Africa
14. Van Dyk, C. and Van Zijl, G.P.A.G. (2002). *A large scale solar chimney structure, Proc. Int. IASS Symp. on lightweight structures in Civil Engineering* (ed. JB Obrebski). pp. 144-150
15. Von Backström T.W. (2003). *Calculation of pressure and density in solar power plant chimneys*. Accepted for publication in *ASME Journal of Solar Energy Engineering*, February 2003 issue

16. Von Backström, TW and Gannon, A.J. (2000). *Compressible flow through solar power plant chimneys*. Accepted for publication in *ASME Journal of Solar Energy Engineering, February 2000 issue*

Internet resources

17. ABAQUS superior finite element analysis solutions – http://www.hks.com/, 2003
18. Clean Dry Air Incorporate – http://www.cleandryair.com/the_inlet_guide_vane.htm, 2003
19. Enviromission Ltd. – http://www.enviromission.com.au, 2003
20. Ingersoll-Rand Air Solutions – http://www.irairsolutions.co.uk/IGV.htm, 2003
21. Oil rig photo gallery – www.cleddau.com/oilrigphotogallery.html, 2004
22. Schlaich Bergermann und partner – http://www.sbp.de/en/fla/projects/solar/aufwind/index.htm, 2003
23. Solar Millenium AG – http://www.solarmillennium.de, 2003
24. Striking images photo gallery – www.strikingimages.com/light.htm, 2004
25. Turbo Technology Service Corporation – http://www.turbotechservices.com/igv.html, 2003
26. United Nations Department of Economic and Social Affairs, Division for Sustainable Development – www.un.org/esa/sustdev/documents/agenda21, 2004
27. Waoline.com – www.waoline.com/science/NewEnergy/HydroEnergy/OceanPower.htm, 2004
28. Wind turbine photo gallery, Danish wind turbines – www.afm.dtu.dk/wind/turbines/gallery.htm, 2004

Personal correspondence

29. Kirstein, C.: Personal correspondence during joint research forming part of the completion of his Masters-degree in Mechanical Engineering at the University of Stellenbosch, 2002-2003. His thesis should be published in 2004
30. The Lafarge Group, correspondence with Dave Miles, Product Manager of Lafarge South Africa (PTY) Ltd, 2003

Others

31. Article on a breakthrough in solar panel production taken from *Die Burger*, a South African newspaper – www.news24.com/Die_burger/nuus/forum/0,,4-75-1424_1467381,00.html, 2004
32. Videoclip from Schlaich Bergermann und Partner and Solar Millenium AG, 2003
33. *FEMAS 2000 Finite Element Moduls Of Arbitrary Structures*
    - Beem, H., Könke, C., Montag, U., Zahlten, W. (1996). *FEMAS 2000 – Finite Element Moduls Of Arbitrary Structures* – User's Manual. Institut für Statik und Dynamik, Rurh-Universität Bochum

APPENDIX A: LITERATURE STUDY – WIND FORCES

The wind velocities were found using the formula most often used in the extrapolation of wind speeds to that at great heights (*Table A-1 column 2*). The coefficients are found in SABS0160-1989 [10]. The force per meter height is determined.

	Wind speed at height z	Free stream velocity pressure		Force per meter
Height (m)	V_z	q_z (N/m^2)	q_z (kN/m^2)	F (kN/meter)
	$\left(\frac{V_z}{V_{10} \times k_r}\right) = \left(\frac{z}{10}\right)^{\alpha}$	$q_z = k_p \times V_z^2$		$F = C_f \times q_z \times A_e$
	alpha = 0.19 k_r = 1.04	k_p = 0.518		$C_f * A$ = 95.672 m^2
10	41.6	896.4	0.896	85.763
50	56.48	1652.4	1.652	158.092
100	64.431	2150.4	2.15	205.732
150	69.591	2508.6	2.509	240.003
200	73.5	2798.4	2.798	267.727
250	76.684	3046	3.046	291.419
300	79.386	3264.5	3.265	312.325
350	81.746	3461.5	3.461	331.167
400	83.846	3641.7	3.642	348.405
450	85.744	3808.4	3.808	364.353
500	87.478	3963.9	3.964	379.236
550	89.076	4110.1	4.11	393.223
600	90.561	4248.3	4.248	406.442
650	91.949	4379.5	4.379	418.995
700	93.253	4504.6	4.505	430.962
750	94.483	4624.2	4.624	442.41
800	95.649	4739	4.739	453.394
850	96.757	4849.5	4.849	463.96
900	97.814	4956	4.956	474.147
950	98.824	5058.8	5.059	483.99
1000	99.791	5158.4	5.158	493.516
1050	100.721	5254.9	5.255	502.751
1100	101.615	5348.7	5.349	511.718
1150	102.477	5439.8	5.44	520.435
1200	103.309	5528.5	5.528	528.92
1250	104.113	5614.9	5.615	537.189
1300	104.892	5699.2	5.699	545.255
1350	105.647	5781.5	5.782	553.131
1400	106.379	5862	5.862	560.828
1450	107.091	5940.7	5.941	568.357
1500	107.783	6017.7	6.018	575.726
1550	108.457	6093.2	6.093	582.945
1600	109.113	6167.1	6.167	590.02

Table A-1. Wind extrapolation, free stream velocity pressure calculation and the calculation of the force per unit meter height.

Table A-2 gives the force coefficients corresponding to a position on the circumference of a circular structure. *Figure A-1* shows the pressure distribution pattern.

Position on periphery – theta (degrees)	0	10	20	30	40	50	60	70	80	90	100	120	140	160	180
C_f	1	0.9	0.7	0.35	0	-0.7	-1.2	-1.4	-1.5	-1.4	-1.1	-0.6	-0.4	-0.4	-0.4

Table A-2. Force coefficients.

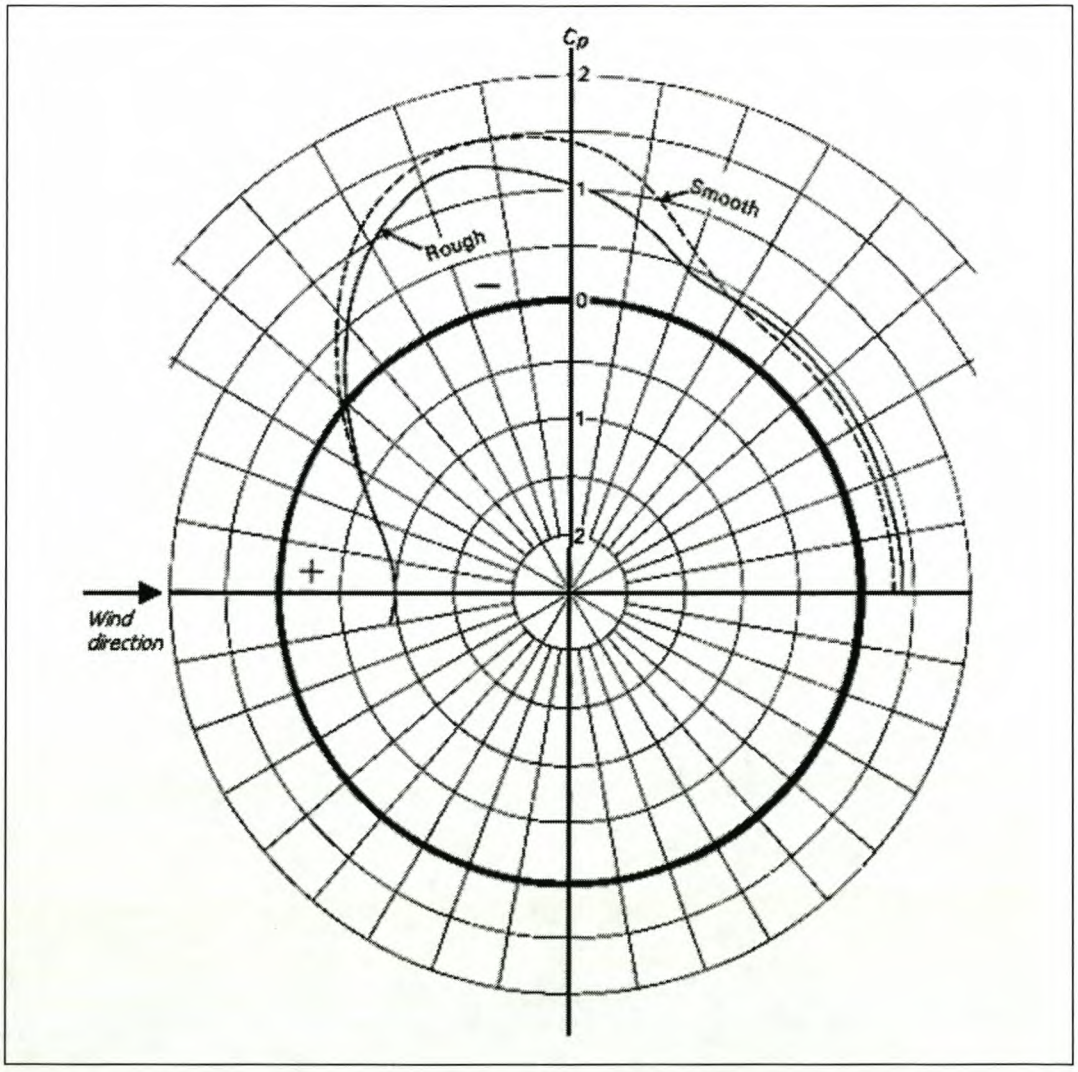

Figure A-1. The pressure distribution around a cylinder due to wind from the direction as shown. The curve gives the values of the pressure coefficient, C_p, at positions around the cylinder.

The force for each area under investigation can now be determined by multiplying the pressure coefficients (last column in *Table A-1*) with the force.

APPENDIX B: REACTION FORCES and METHOD OF EXTRACTION OF FORCES

B.1 Reaction forces

Table B-1 and *Figure B-1* give the overall forces while *Table B-2* and *Figure B-2* show the moments that are channelled into the IGV's. In the tables the extreme (absolute maximum) values are highlighted in red and the adjacent values in orange. The two columns on the right, "Ratio", show the ratio of the vertical to the lateral forces, pointing out the excessive magnitude of the vertical force relative to the radial and tangential force.

The column on the left of the tables displays the position of the forces relative to the wind direction.

	Reaction forces [N]				
				Ratio	
Force direction	Vertical	Radial	Tangential	Vertical/Radial	Vertical/Tangential
Wind leading side	**1.78E+09**	**-2.98E+07**	-8.00E+06	59.59	**222.21**
	1.76E+09	-2.86E+07	-1.32E+07	61.42	133.15
	1.72E+09	-2.71E+07	-1.82E+07	63.38	94.27
	1.66E+09	-2.53E+07	-2.31E+07	65.61	71.71
	1.58E+09	-2.32E+07	-2.82E+07	68.30	56.11
	1.50E+09	-2.08E+07	-3.39E+07	71.98	44.13
	1.39E+09	-1.80E+07	-4.05E+07	77.62	34.43
	1.28E+09	-1.46E+07	-4.82E+07	87.45	26.53
	1.15E+09	-1.08E+07	-5.67E+07	106.27	20.20
	9.97E+08	-6.51E+06	-6.54E+07	153.08	15.26
	8.32E+08	-2.08E+06	-7.28E+07	**399.74**	11.43
	6.55E+08	2.18E+06	-7.75E+07	300.83	8.45
	4.73E+08	5.86E+06	**-7.80E+07**	80.76	6.07
	2.98E+08	8.60E+06	-7.32E+07	34.65	4.07
	1.41E+08	1.00E+07	-6.32E+07	14.05	2.23
	1.21E+07	1.01E+07	-4.84E+07	1.20	0.25
	-7.86E+07	8.79E+06	-3.02E+07	8.94	2.61
Wind trailing side	-1.25E+08	6.18E+06	-9.75E+06	20.30	12.87

Table B-1. Reaction forces.

Three load cases are chosen consider during the conceptualization process. The positions of these forces are shown in *Figure B-1* by the symbols A, B and C. At position A the vertical and radial loads are at their maximum values. Position C corresponds to the maximum tangential force. At position B the vertical force is at its greatest negative value.

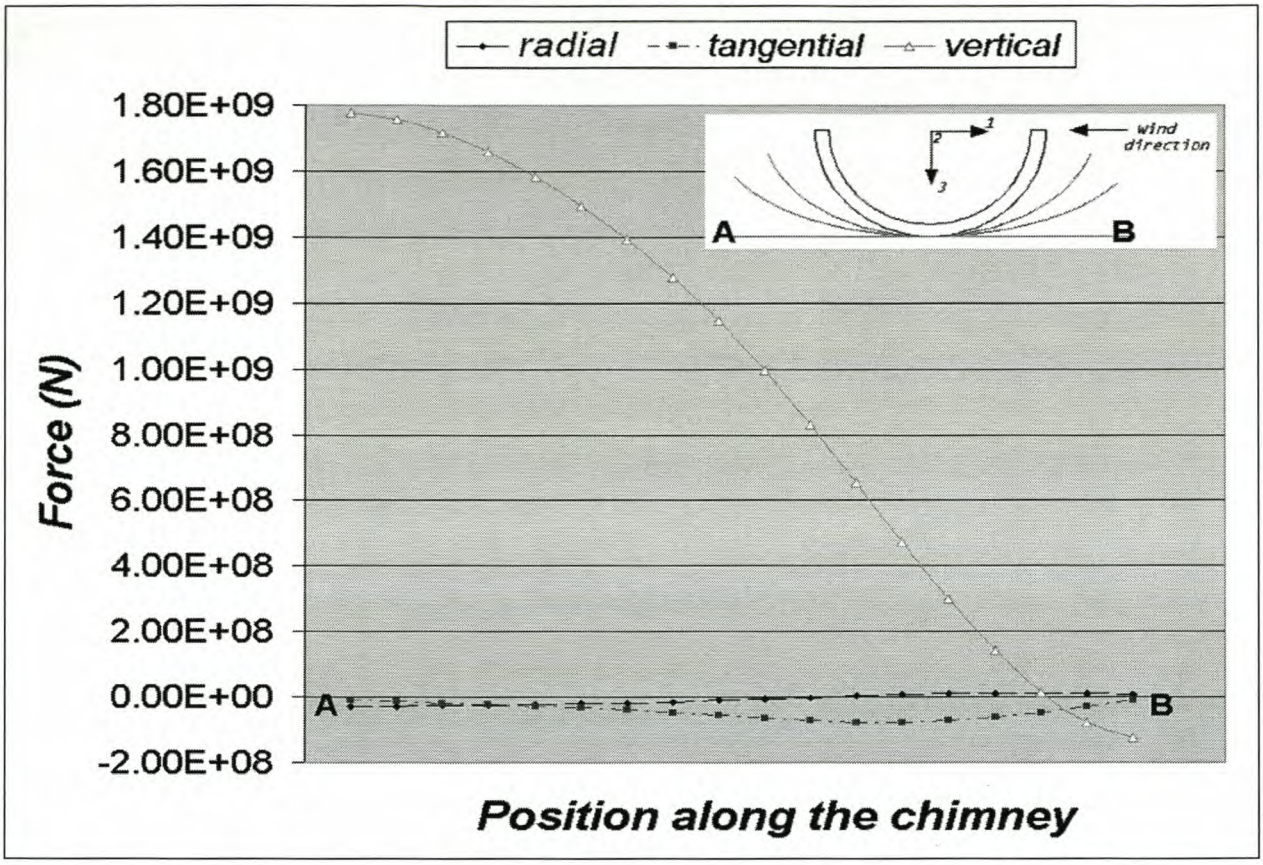

Figure B-1. Reaction forces.

	Reaction moments [N.m]		
	Around the ... axis		
Force direction	Vertical	Radial	Tangential
Wind leading side	3.24E+04	**-3.45E+07**	**1.96E+08**
	-3.66E+03	-3.41E+07	1.93E+08
	-2.92E+04	-3.33E+07	1.88E+08
	-1.34E+05	-3.21E+07	1.81E+08
	-1.75E+05	-3.08E+07	1.74E+08
	-2.45E+05	-2.94E+07	1.65E+08
	-4.22E+05	-2.79E+07	1.57E+08
	-5.48E+05	-2.61E+07	1.46E+08
	-5.90E+05	-2.40E+07	1.34E+08
	-5.70E+05	-2.12E+07	1.18E+08
	-5.91E+05	-1.77E+07	9.76E+07
	-4.70E+05	-1.35E+07	7.35E+07
	-3.24E+05	-8.69E+06	4.62E+07
	-3.47E+05	-3.74E+06	1.83E+07
	-4.40E+05	7.05E+05	-6.57E+06
	-3.91E+05	4.40E+06	-2.69E+07
	-2.60E+05	7.04E+06	-4.12E+07
Wind trailing side	-8.87E+04	8.48E+06	-4.85E+07

Table B-2. Reaction moments.

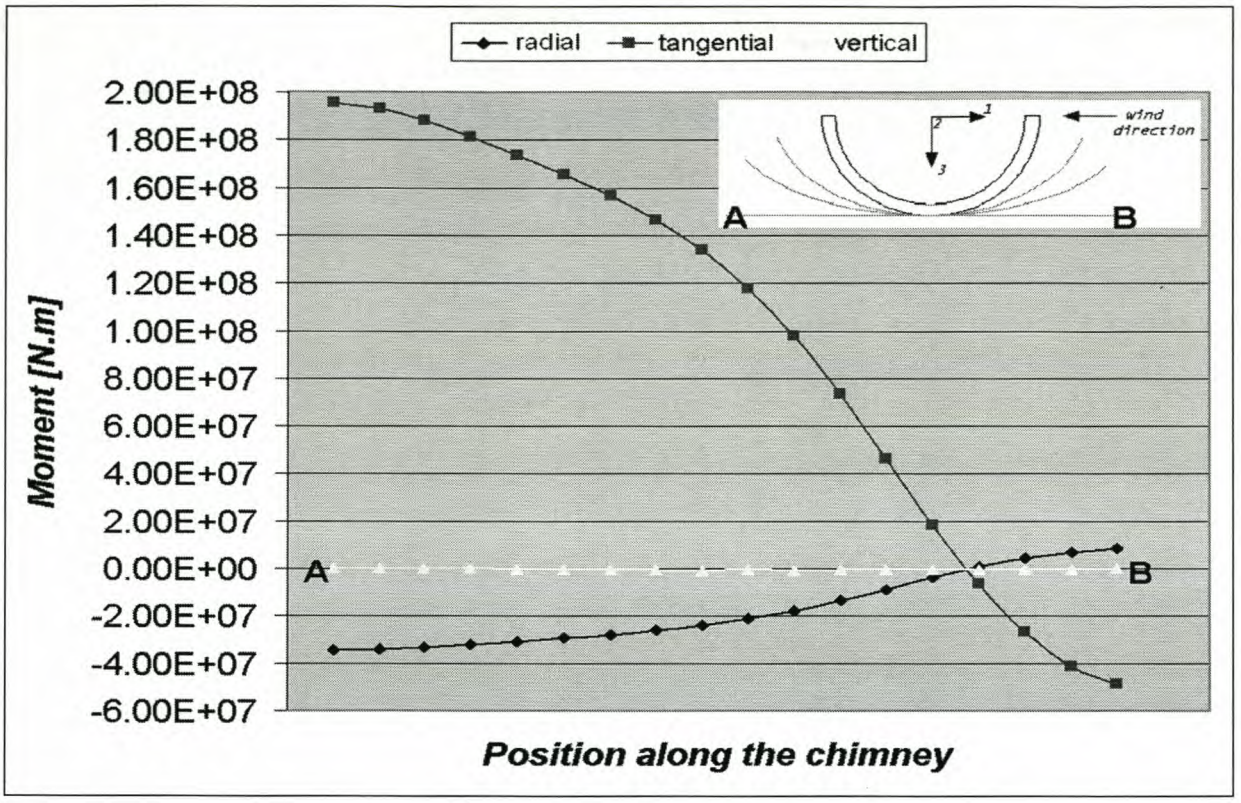

Figure B-2. Reaction moments.

B.2 Method of extraction

B.2.1 Processing the output data

In order to determine the maximum load case(s) for an IGV, for use in further research, the reactions, given in global coordinates, are processed to local coordinates

- radial (minus 10 degrees, remembering the IGV's are not radially positioned but turned with an maximum angle – 10 degrees anticlockwise [1]) and
- tangent (minus 10 degrees) to the chimney shell

as can be seen in *Figure B-3*.

Consequently each midside node has force vectors radial-horizontal-minus-10° to the shell and tangential-horizontal-minus-10° to the shell. The results are calculated and shown after the next phenomenon is considered.

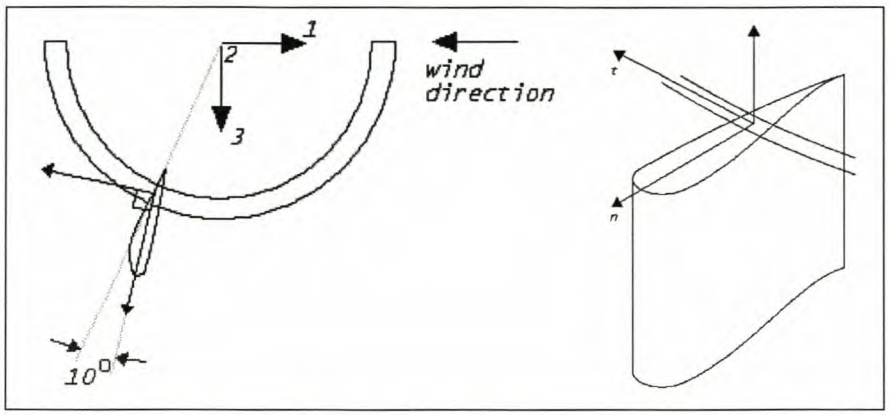

Figure B-3. The position of local coordinates (blue) with regards to global coordinates (black, numbered).

B.2.2 Interpretation of the cyclic pattern seen in reaction force (ABAQUS output data) graph

From the ABAQUS results in the output-file "onderweg2_swaarring300Gpa.dat" the nodal reaction forces was found to be as shown in *Figure B-4*.

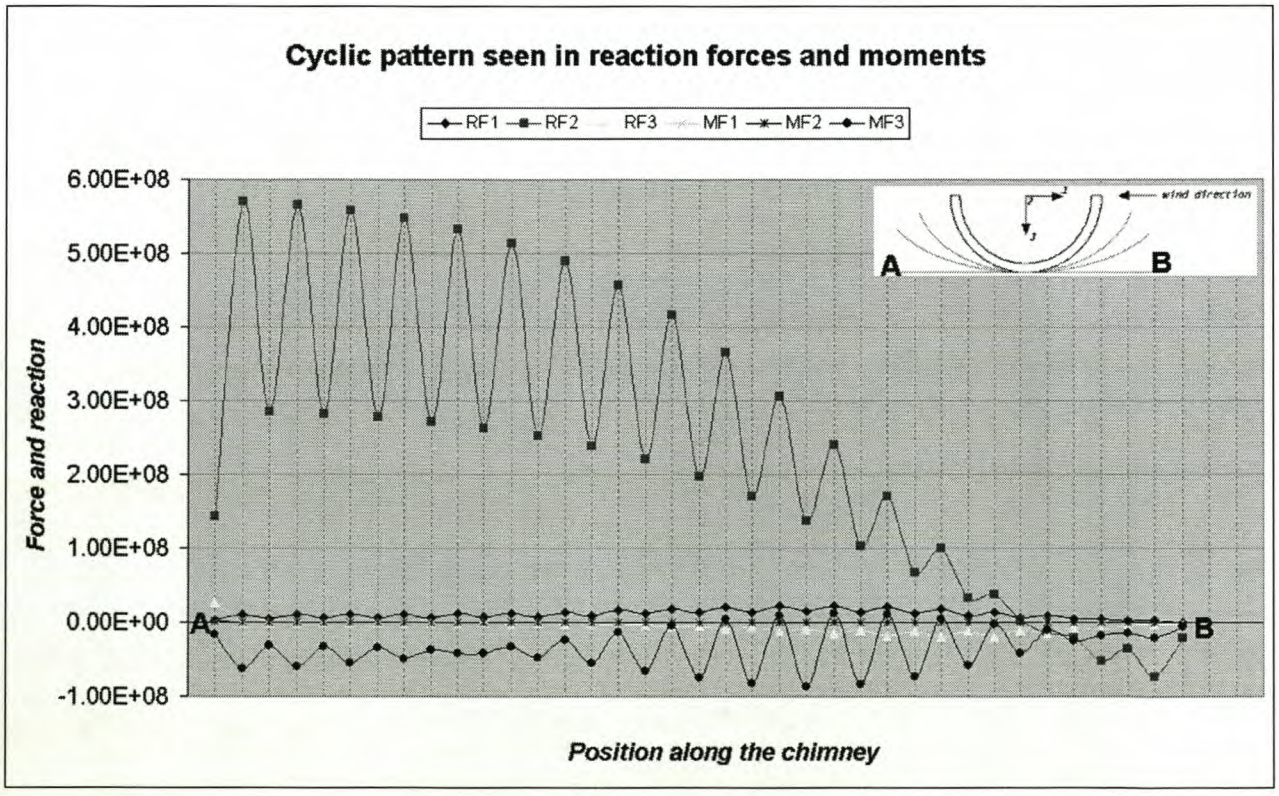

Figure B-4. The cyclic phenomenon in the output from the ABAQUS data file.

The pattern

Upon post-processing the reaction force data as seen in the previous paragraph a cyclic phenomenon is observed where the forces acting on the vertex nodes of the quadratic shell elements are approximately half (keep in mind the increase/decrease of the forces, moving around the circumference of the chimney) that of the reaction force on the midside node of the element – see *Figure B-5*.

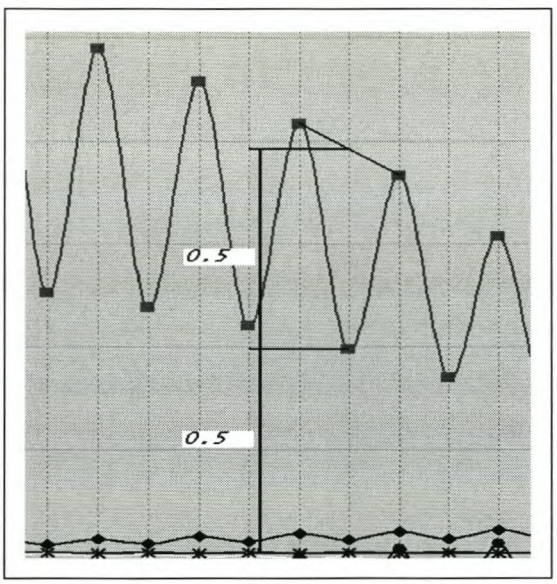

Figure B-5. Zooming in on the phenomenon.

The interpretation

The shape functions used on the quadratic shell element can be portrayed as seen in *Figure B-6*.

Now consider a distributed force on in the plane of one of these quadratic shell elements. The shape functions are:

$$SF1 = \frac{(x_2 - x)(x_3 - x)}{(x_2 - x_1)(x_3 - x_1)}$$

$$SF2 = \frac{(x_1 - x)(x_3 - x)}{(x_1 - x_2)(x_3 - x_2)}$$

$$SF3 = \frac{(x_1 - x)(x_2 - x)}{(x_1 - x_3)(x_2 - x_3)}$$

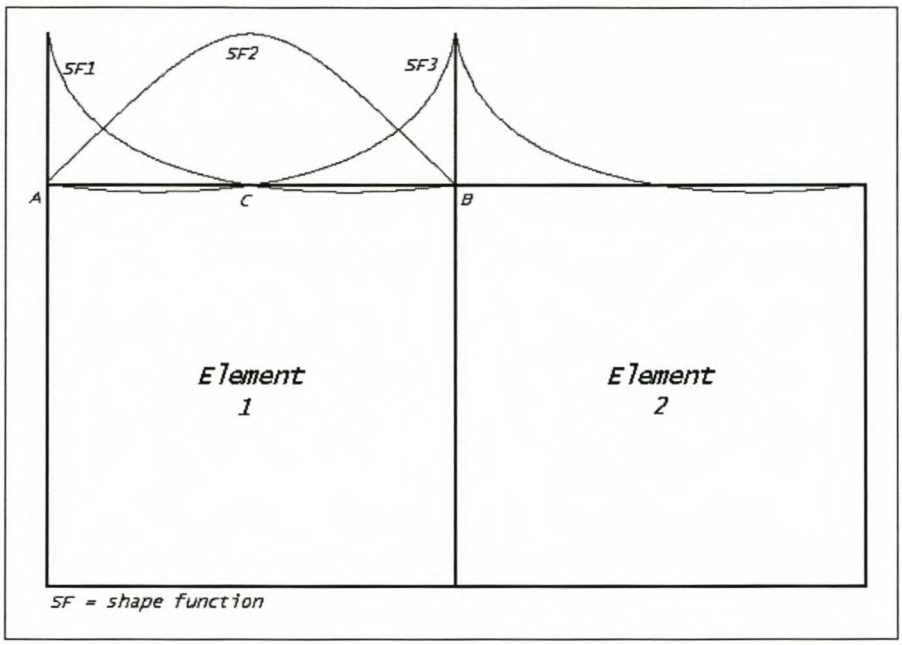

Figure B-6. Shape functions for a quadratic element.

Hence, for Element 1 in the *Figure B-6*, with the origin at C and the x-values at A = -1 and B = 1, the shape functions become:

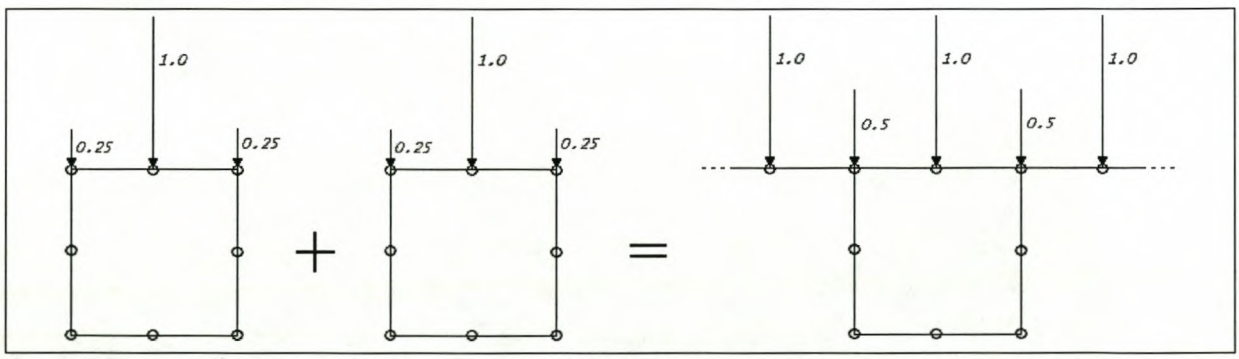

Figure B-7. Weight carried after assembly process.

$$SF1 = \frac{1}{2}(x^2 - x)$$

$$SF2 = 1 - x^2$$

$$SF3 = \frac{1}{2}(x^2 + x)$$

Integrating these shape functions over the domain $x \in [-1,1]$ yields the measure with which each shape function carries a distributed load. Performing the integration yields SF2 to carry 4 times the

weight that SF1 and SF3, respectively, does. *Figure B-7* illustrates the phenomenon, shows the assembly process and gives the result – midside nodes carry double the load of the respective vertex nodes.

Efficiently extracting loads, keeping in mind the above phenomena.

Reversing this method, the distributed force can be calculated:

1. In any quadratic element with the quadratic shape functions as set up earlier, the node C (*Figure B-6*) carries 4 times the weight that the vertex node carries. Hence the total distributed load over the whole length is carried by the three nodes, A:B:C in the relation 1:1:4.
2. The distributed reaction load can be calculated using only the reaction force at the midside node or the vertex node.
3. Assume the distributed load to be uniform over an element, yielding an overall piecewise linear distribution.
4. There are 18 quadratic elements describing the circumferential geometry of half the chimney at foundation level. Therefore each element represents a 10-degree difference in the angle of the tangential of the vertex nodes (nodes A and C in *Figure B-8*). The reaction force values are taken from the midside nodes, assuming it to be the average of the values at the vertex nodes. This might be seen as a risky assumption in the case where the reaction values between adjacent nodes vary significantly, but this is not the case in the nodes where the greatest forces act (*Figure A-1*), making it a safe assumption.
5. Note that the forces considered up to this stage are the vertical forces only.

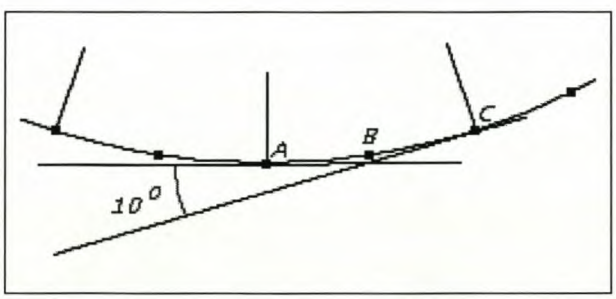

Figure B-8. Difference in angle between tangents of vertex nodes of an element.

Node B in *Figure B-8* carries four times the force that node A does. Therefore

if W = x Newton/meter over a length equal to 14.15 meters (length of one element in FE-model)

then the total load over an element = x * 14.15 Newton = $6*F_A$

but $F_B = 4*F_A$

so that $x * 14.15 = 1.5 * F_B$

$x = 0.106 * F_B$

And maximum $F_B = 6.0*10^8$ N

so that $W = 6.36*10^7$ Newton/meter

where W = distributed load to be calculated

F_A = vertical load at vertex-node – from ABAQUS data file

F_B = vertical load at midside-node – from ABAQUS data file

B.2.3 Calculation of radial and tangential forces:

With the above algorithm applied on each midside node the actual reactions at these positions are determined – note that all the reaction forces are now considered, not only the vertical (z-axis) forces. *Table B-1* and *B-2* and *Figure B-1* and *B-2* in the first section of this Appendix reports these forces multiplied with the area over which they act (28 x 2.2 metres – the width of the section supported by one IGV x shell thickness at base level). *Figure B-9* displays the local vectors of the radial and tangential reaction forces. Note their gradual change in sign and magnitude.

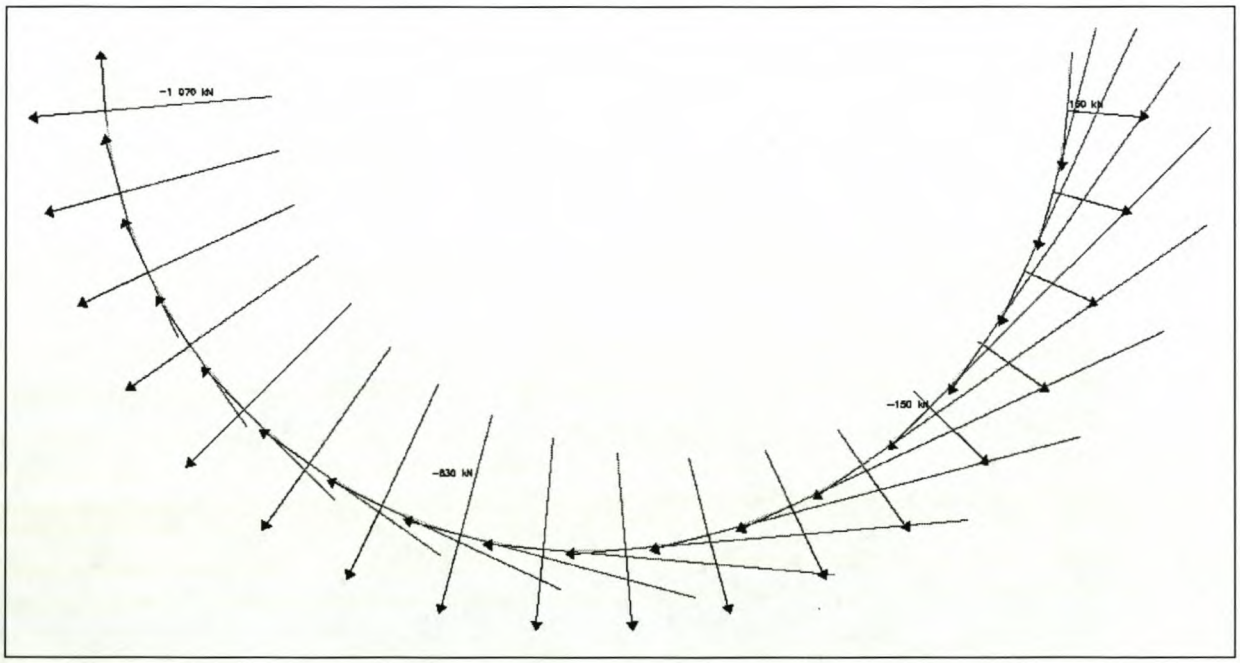

Figure B-9. Radial and tangential reaction forces (red lines) at each midside node. The blue coordinate systems show the local coordinates for each midside node. The positive wind direction is from the right.

APPENDIX C: AXIAL STRESS CALCULATION

A calculation is done to determine the magnitude of the axial stresses ($\sigma_v = \frac{F_v}{A}$) forming with the worst-case axial force, F_v, distributed through variably sized areas of the IGV. F_v is calculated using the biggest vertical reaction force, excited at the base of the chimney due to gravitational and wind action. The maximum value for F_v follows from *Chapter 4.1.1.* ULS safety design criteria are applied in these calculations, multiplying the stress values with a factor of 0.45.

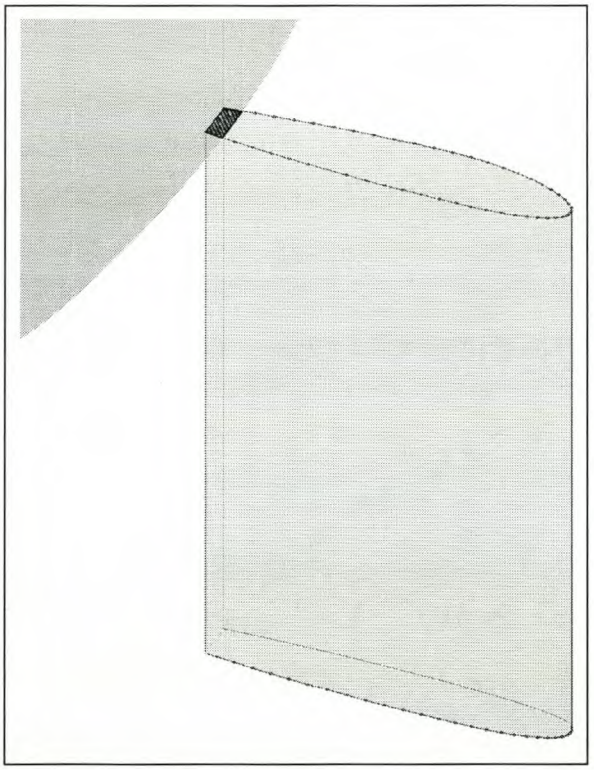

Figure C-1. The chimney shell (2.2 metres thick at base level) rests on the IGV. The area of prospective contact is highlighted in blue.

The blue (hatched, for greyscale copies) area of prospected contact, shown in *Figures C-1* and *C-2* (length = 2.2 metres), proves to be too small to transfer the axial force (1.78e+9 N force assumed to act vertically on the IGV) exerted on it. Consequently, this area must be increased. *Figure C-2* and *Table C-1* below reports the axial stress values for several larger areas.

The axial stress value with the insufficient transfer area section, at an offset of 2.2 metres from the inner radius position (x=0 in the key provided in *Table C-1*), and assuming infinite strength concrete (linear behaviour at high axial load), is approximately 180 MPa. For the offset at 4 metres,

corresponding to a force transfer area of 18.66 m^2, the stress reaches 95.4 MPa. Concrete will fail under such high stress values.

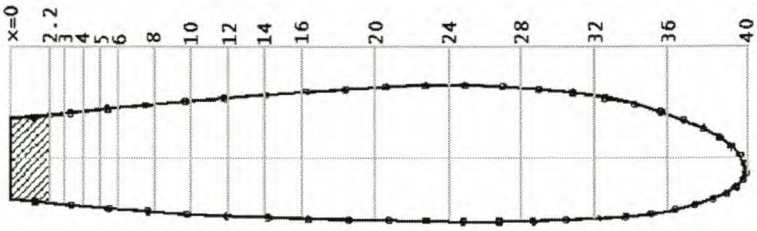

$$\sigma = \frac{F}{A}$$

Axial Force: 1.78e+9 N

Distance from x=0	Area(m^2)	Axial Stress (Pa)
2.2	9.9	1.80E+08
3	13.75	1.29E+08
4	18.66	9.54E+07
5	23.92	7.44E+07
6	29.28	6.08E+07
8	40.53	4.39E+07
10	52.42	3.40E+07
12	65.21	2.73E+07
14	77.59	2.29E+07
16	91.26	1.95E+07
20	119.4	1.49E+07
24	148.58	1.20E+07
28	177.54	1.00E+07
32	205.68	8.65E+06
36	229.33	7.76E+06
40	244.52	7.28E+06

Table C-1. Axial stress calculated for variable areas.

(Concrete with a compressive stress yielding point of up to 185 MPa is commercially available in South Africa but only at grave costs. Concrete with a compressive yielding stress of 95 MPa is commercially available at R1189.09 / m^3, excluding transport costs [28]. This strength of concrete is assumed to be the strength upper limit within economical feasibility.)

Conclusion

The axial (compressive) stress is critically high in the calculated small-area sections. The rows highlighted in *Table C-1* show these stresses. The areas purposed to transfer the forces on the IGV's are too small. A method (structure) needs to be determined for the transfer of these forces from the thin chimney shell to a capable area of the IGV (*Figure C-2*).

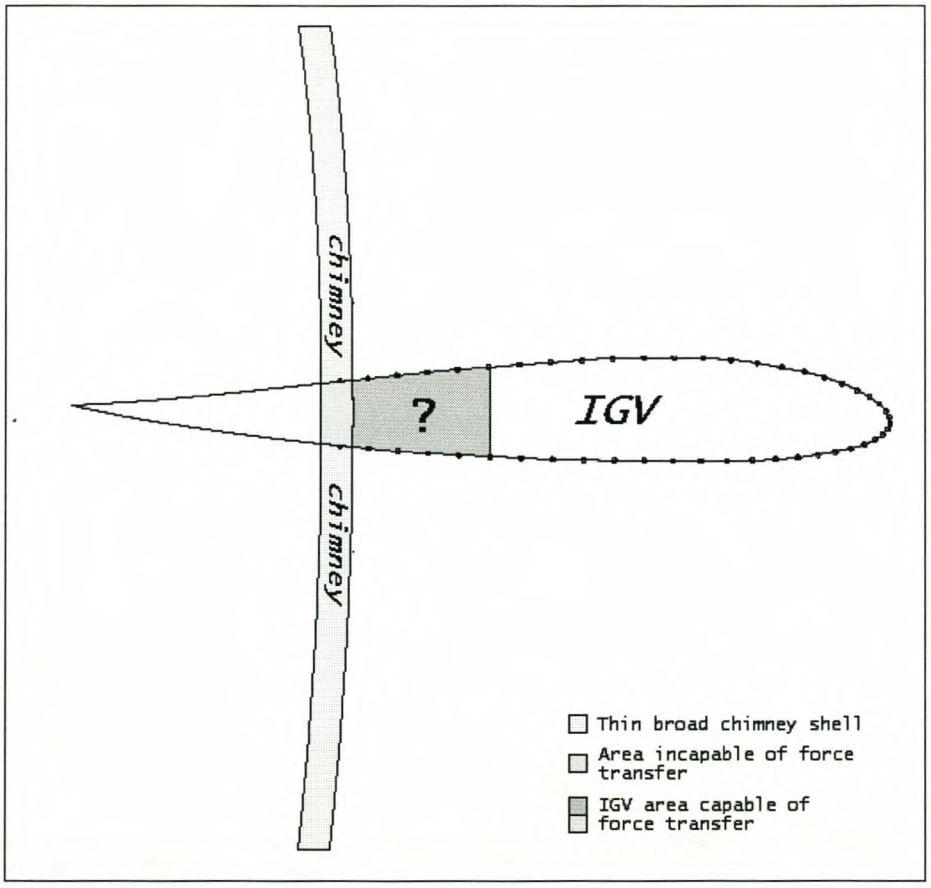

Figure C-2. Plan view showing the thin broad area of the chimney shell placed on the IGV section, and the irresolute area of the transfer section.

APPENDIX D: CALCULATIONS FOR CONCEPTUALIZATIONS

D.1 Decrease in dead load

Figure D-1 shows the chimney shell thickness against the height. The thickness decreases linearly from the base up to the level of 1000 metres and then remains constant for the remaining 500 metres.

The height at which the volume of material below it equals the volume of material above it is found to be approximately 382.5 metres; hence it is stated that the great volumes of concrete are situated below 382.5 metres. The immense amount of dead load stabilises the chimney structure.

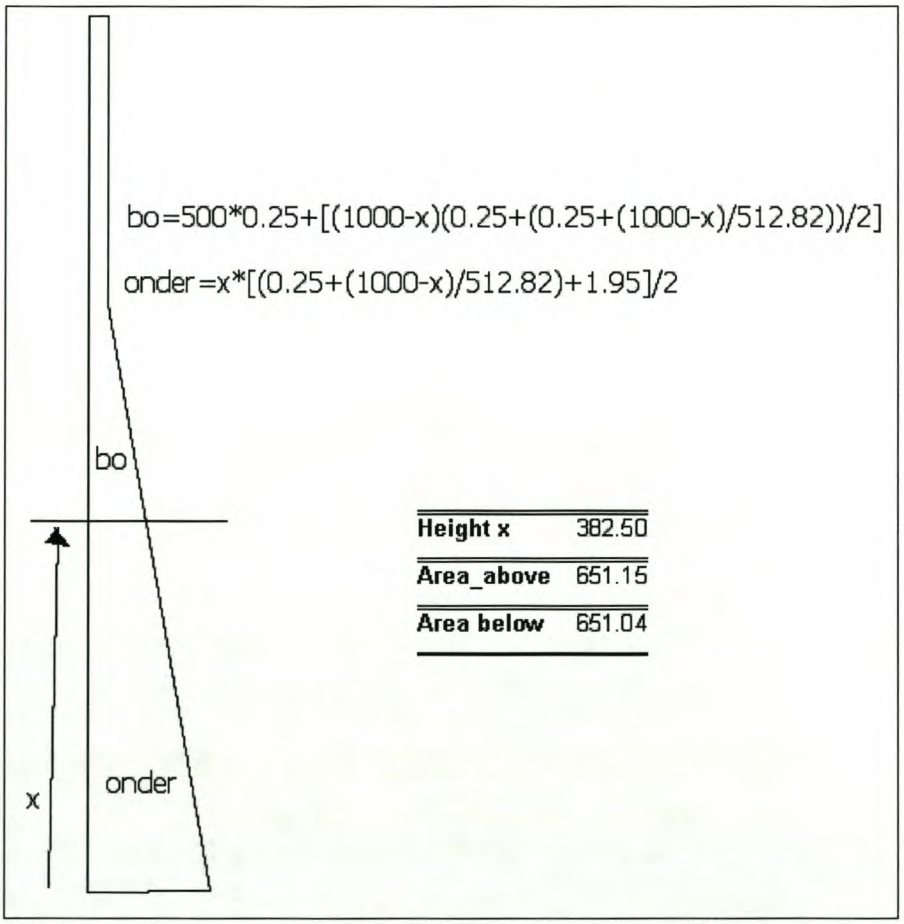

Figure D-1. Centroid (in the vertical direction) of chimney shell.

(Note: the assumption is made that the additional vertical force in the lower regions of the chimney induced by the wind load is zero. The conversion of wind load to vertical force in the chimney is therefore assumed to have happened in the chimney region above these "investigated heights".)

A question is asked: if such a large amount of material is situated so low down in the chimney structure, is it possible to have the transfer mechanism start at a great height, where the dead load is significantly smaller?

The fact that the gross volume of the chimney structure lies around foundational level is utilised in this calculation. The magnitude of the vertical force at various heights along the chimney is investigated, aiming to find a height at which the minimum transfer area (9.9 m^2) found to be insufficient previously would suffice. If the magnitude of the vertical force decreases significantly the presence of a transfer section for the transfer of forces from the broad but thin shell to the IGV section might not be necessary but can be accommodated wholly by the gradual flow of the chimney into IGV's. Remember, however, that the shell thickness (the width dimension of the transfer area) also decreases with height, making the transfer area smaller. Hence the object is to investigate whether the volume at greater heights decreases sufficiently (that is, a decrease in the dead load) to result in a bearable stress in the transfer section at that height.

Table D-1 on the next page displays some calculations made to answer this question.

Conclusion

The compressive stress in the support/transfer area does not get smaller due to decrease in dead load, the reason being that although the dead load decreases the sectional area also decreases at a relatively faster rate resulting in the increase in compressive stress – refer to the last column in *Table D-1*.

Decrease of distributed load as calculated at base of the chimney, as height increases

Distributed load due to gravity and wind: 63600000

N/m

Note that only gravity load decreases...no adaptation to windload... thus not very conservative...

Height considered [m]	Wall thickness [m]	Volume per m width [m^3]	Difference kN/m less	cumulative kN/m less	Resulting load at that height [kN/m]	corresponding load channeled into IGV [N]	Area [m^2]	Stress [Pa]
0	2.2	22	517.968	517.97	63600.00	1.78E+09	11	1.62E+08
10	2.143	21.43	504.54792	1022.52	63082.03	1.77E+09	10.715	1.65E+08
20	2.086	20.86	491.12784	1513.64	62577.48	1.75E+09	10.43	1.68E+08
30	2.029	20.29	477.70776	1991.35	62086.36	1.74E+09	10.145	1.71E+08
40	1.972	19.72	464.28768	2455.64	61608.65	1.73E+09	9.86	1.75E+08
50	1.915	19.15	450.8676	2906.51	61144.36	1.71E+09	9.575	1.79E+08
60	1.858	18.58	437.44752	3343.95	60693.49	1.70E+09	9.29	1.83E+08
70	1.801	18.01	424.02744	3767.98	60256.05	1.69E+09	9.005	1.87E+08
80	1.744	17.44	410.60736	4178.59	59832.02	1.68E+09	8.72	1.92E+08
90	1.687	16.87	397.18728	4575.78	59421.41	1.66E+09	8.435	1.97E+08
100	1.63	32.6	767.5344	5343.31	59024.22	1.65E+09	8.15	2.03E+08
120	1.573	31.46	740.69424	6084.01	58256.69	1.63E+09	7.865	2.07E+08
140	1.516	30.32	713.85408	6797.86	57515.99	1.61E+09	7.58	2.12E+08
160	1.459	29.18	687.01392	7484.87	56802.14	1.59E+09	7.295	2.18E+08
180	1.402	28.04	660.17376	8145.05	56115.13	1.57E+09	7.01	2.24E+08
200	1.345	40.35	950.0004	9095.05	55454.95	1.55E+09	6.725	2.31E+08
230	1.288	38.64	909.74016	10004.79	54504.95	1.53E+09	6.44	2.37E+08
260	1.231	36.93	869.47992	10874.27	53595.21	1.50E+09	6.155	2.44E+08
290	1.174	35.22	829.21968	11703.49	52725.73	1.48E+09	5.87	2.52E+08
320	1.117	33.51	788.95944	12492.45	51896.51	1.45E+09	5.585	2.60E+08
350	1.06	31.8	748.6992	13241.15	51107.55	1.43E+09	5.3	2.70E+08
380	1.003	30.09	708.43896	13949.58	50358.85	1.41E+09	5.015	2.81E+08
410	0.946	28.38	668.17872	14617.76	49650.42	1.39E+09	4.73	2.94E+08
440	0.889	26.67	627.91848	15245.68	48982.24	1.37E+09	4.445	3.09E+08
470	0.832	24.96	587.65824	15833.34	48354.32	1.35E+09	4.16	3.25E+08
500								

Table D-1. Decrease of dead weight with height.

APPENDIX E: FREQUENCY ANALYSIS RESULTS

E.1 Global modes

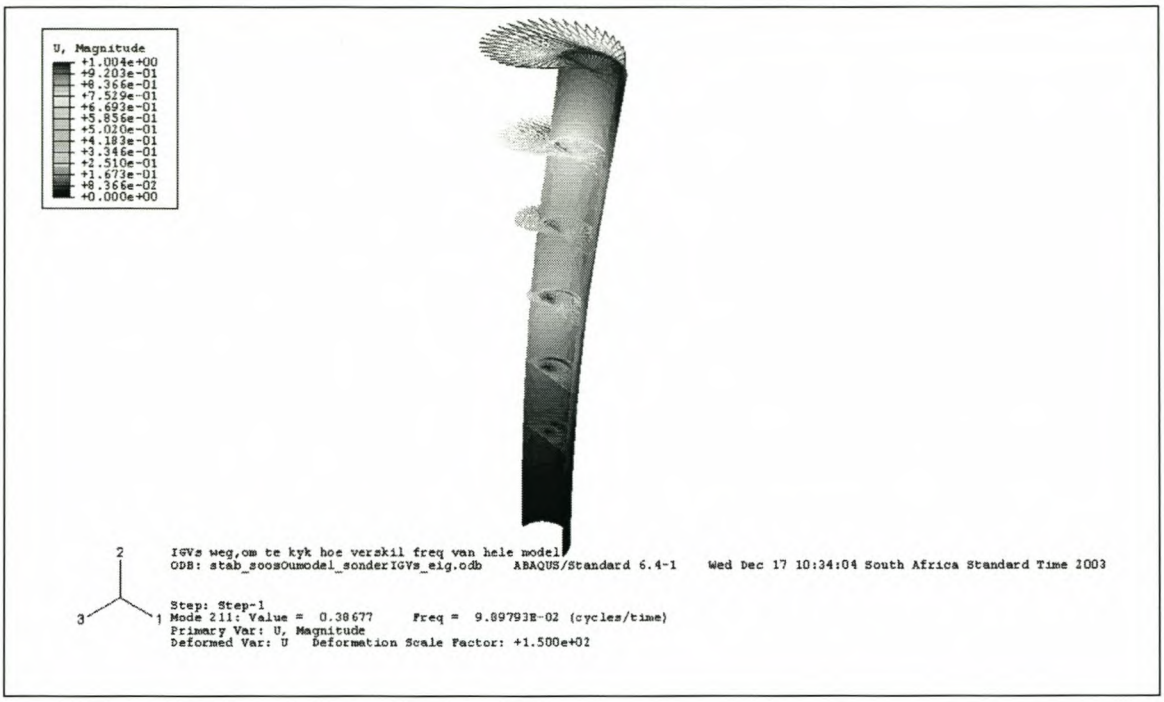

Figure E-1. The global structure without IGV's: frequency (f) = 0.0990 Hz.

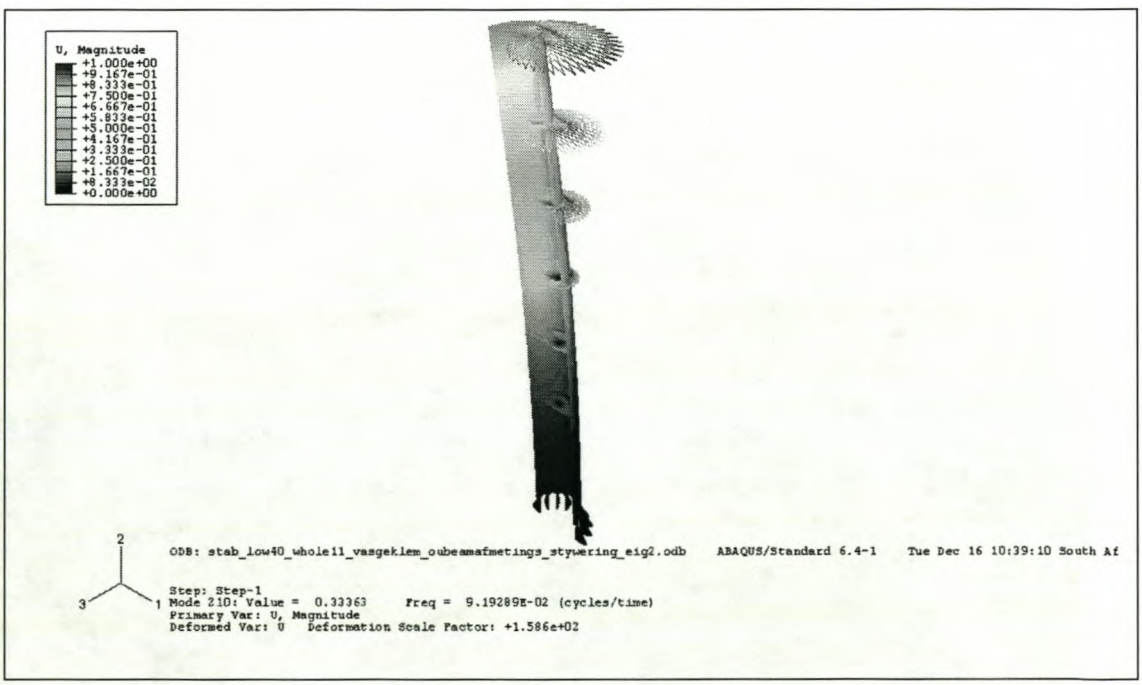

Figure E-2. The global structure with IGV's: frequency (f) = 0.0920 Hz.

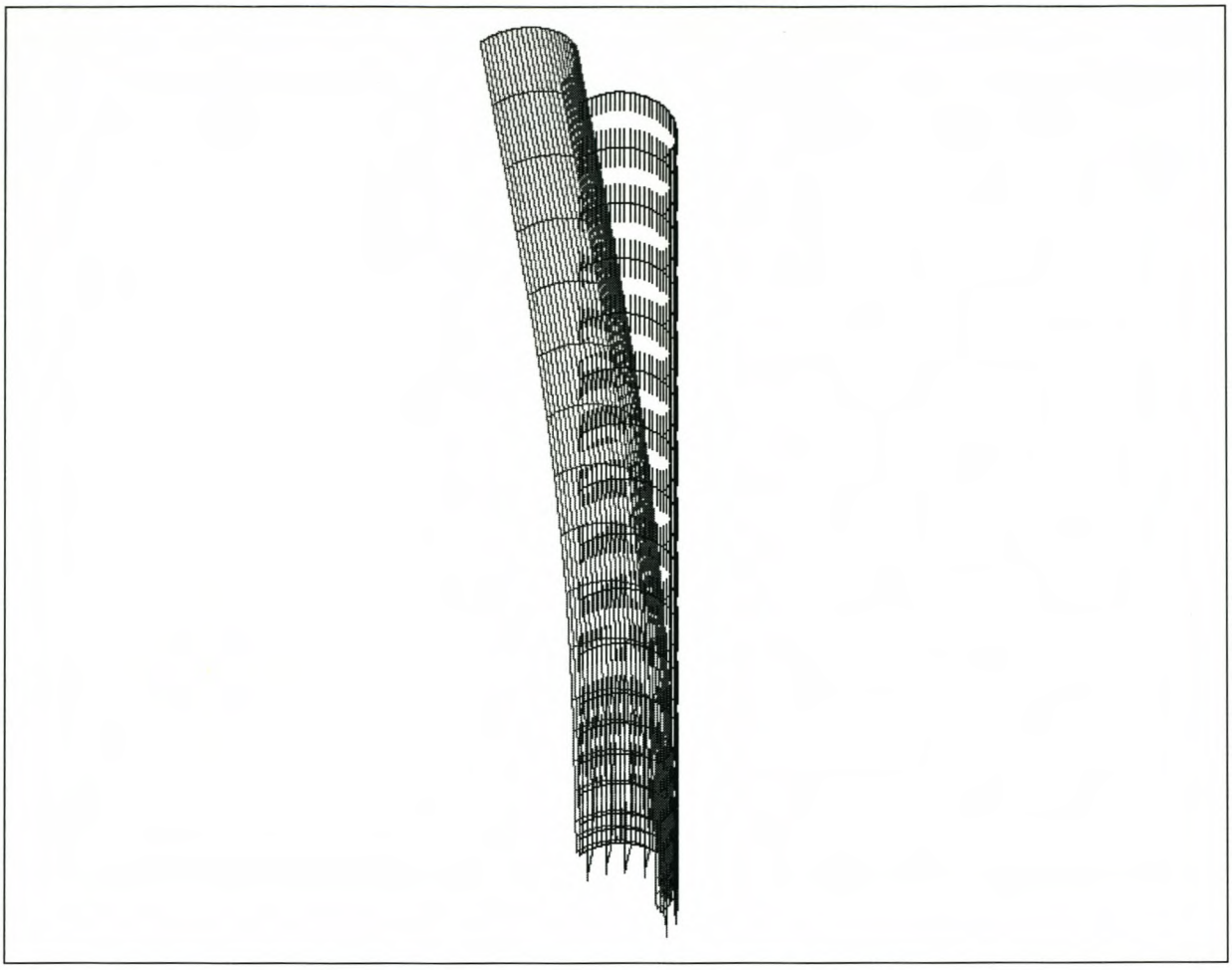

Figure E-3. The global structure with fin stiffeners: frequency (f) = 0.120.

E.2 Local excitation modes

As reported in previous research reports [11] the frequency analysis yields many modes in which deformation is localized to individual ring stiffener beams, or to sets of ring stiffeners. The figures below display the first and second mode for the assembled chimney. These spurious local modes are a great source of concern and their behaviour needs to be stabilized before the prospect of the solar chimney can become a reality.

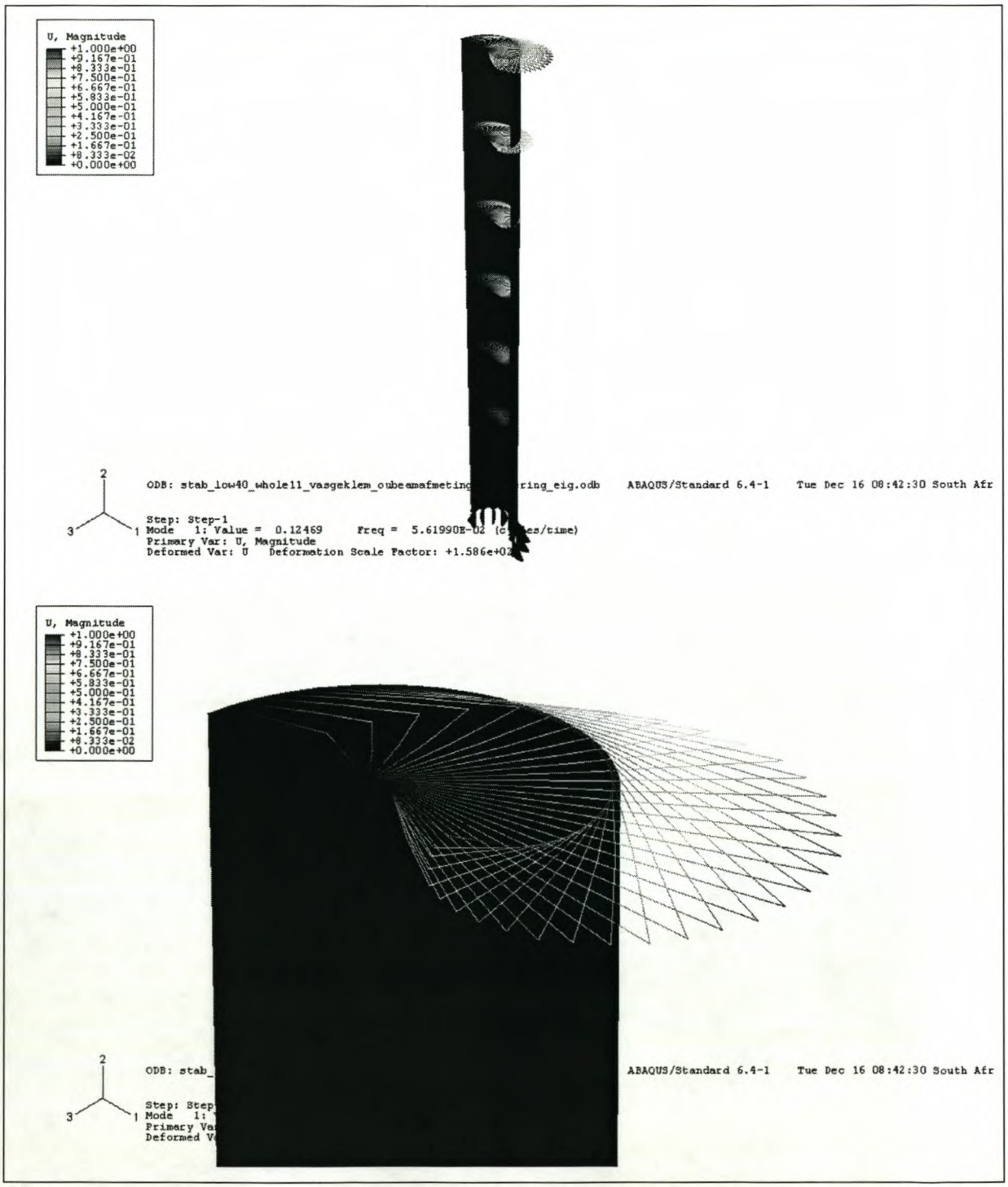

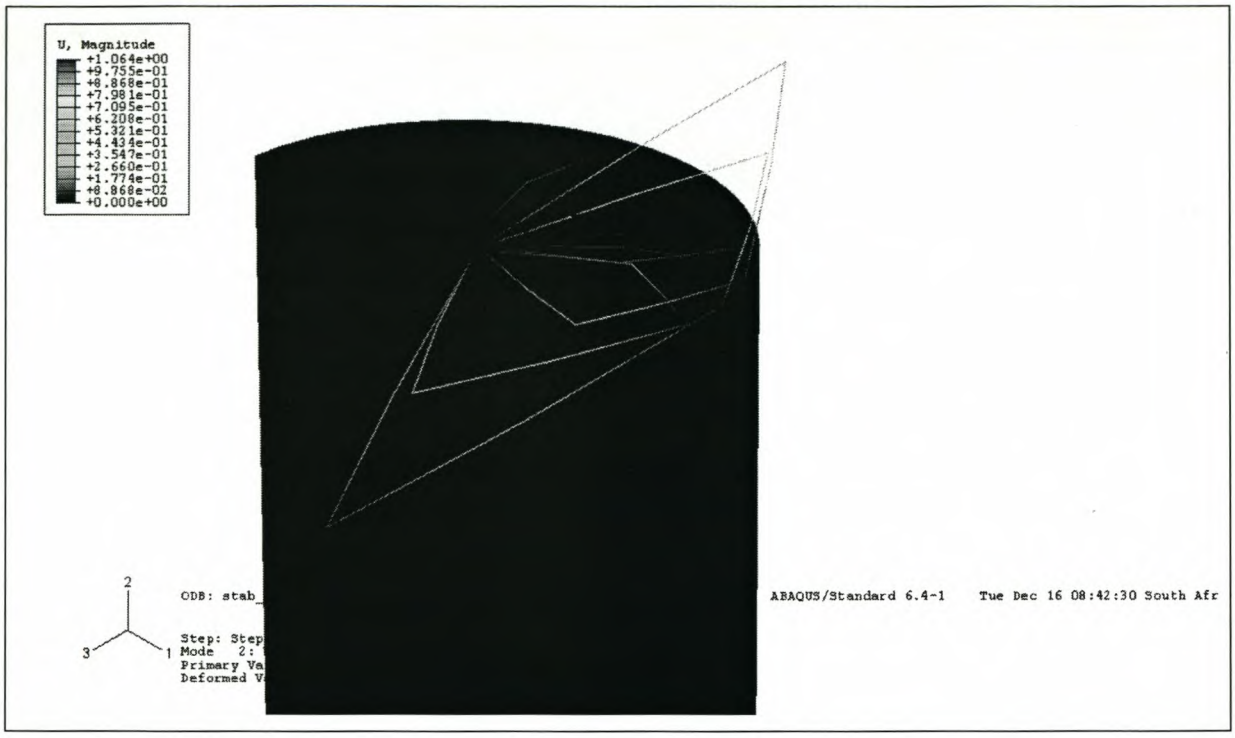

Figure E-4. Local modes.

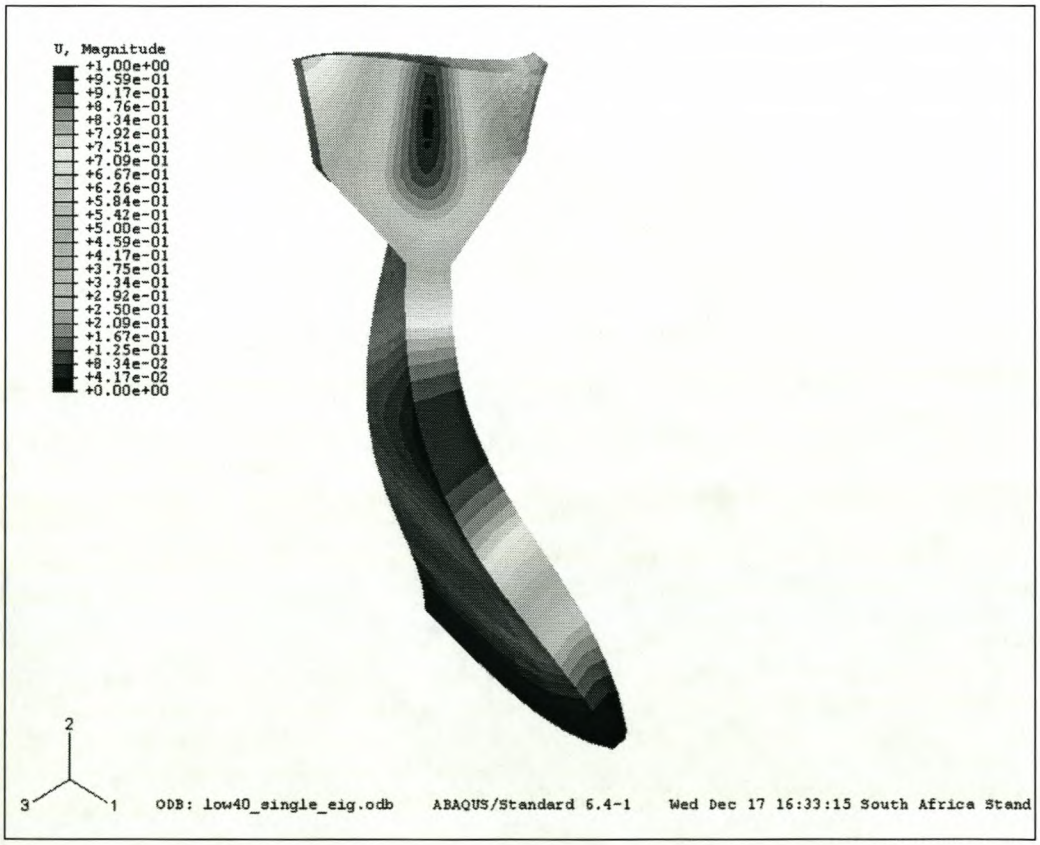

Figure E-5. The first mode of the individual IGV occurs at f = 3.798 Hz.

APPENDIX F: COLUMN INTERACTION DIAGRAMS

The forces and moments acting on the IGV's are shown in *Table F-1*. These values are used to set up the design combinations (axial and moment force) to be resisted when setting up the column interaction diagrams.

Assume IGV to be turned 10 degrees anticlockwise

Radial	Tangential	Vertical	M_radial	M_tangential	M1	abs val	M2	abs val
-2.98E+07	-8.00E+06	**1.78E+09**	-3.45E+07	1.96E+08	-4.80E+08	4.80E+08	-5.15E+08	5.15E+08
-2.86E+07	-1.32E+07	1.76E+09	-3.41E+07	1.93E+08	-7.92E+08	7.92E+08	-8.26E+08	8.26E+08
-2.71E+07	-1.82E+07	1.72E+09	-3.33E+07	1.88E+08	-1.09E+09	1.09E+09	-1.13E+09	1.13E+09
-2.53E+07	-2.31E+07	1.66E+09	-3.21E+07	1.81E+08	-1.39E+09	1.39E+09	-1.42E+09	1.42E+09
-2.32E+07	-2.82E+07	1.58E+09	-3.08E+07	1.74E+08	-1.69E+09	1.69E+09	-1.72E+09	1.72E+09
-2.08E+07	-3.39E+07	1.50E+09	-2.94E+07	1.65E+08	-2.03E+09	2.03E+09	-2.06E+09	2.06E+09
-1.80E+07	-4.05E+07	1.39E+09	-2.79E+07	1.57E+08	-2.43E+09	2.43E+09	-2.46E+09	2.46E+09
-1.46E+07	-4.82E+07	1.28E+09	-2.61E+07	1.46E+08	-2.89E+09	2.89E+09	-2.92E+09	2.92E+09
-1.08E+07	-5.67E+07	1.15E+09	-2.40E+07	1.34E+08	-3.40E+09	3.40E+09	-3.43E+09	3.43E+09
-6.51E+06	-6.54E+07	9.97E+08	-2.12E+07	1.18E+08	-3.92E+09	3.92E+09	-3.94E+09	3.94E+09
-2.08E+06	-7.28E+07	8.32E+08	-1.77E+07	9.76E+07	-4.37E+09	4.37E+09	-4.38E+09	4.38E+09
2.18E+06	-7.75E+07	6.55E+08	-1.35E+07	7.35E+07	-4.65E+09	4.65E+09	-4.66E+09	4.66E+09
5.86E+06	**-7.80E+07**	4.73E+08	-8.69E+06	4.62E+07	-4.68E+09	4.68E+09	-4.69E+09	4.69E+09
8.60E+06	-7.32E+07	2.98E+08	-3.74E+06	1.83E+07	-4.39E+09	4.39E+09	-4.40E+09	4.40E+09
1.00E+07	-6.32E+07	1.41E+08	7.05E+05	-6.57E+06	-3.79E+09	3.79E+09	-3.79E+09	3.79E+09
1.01E+07	-4.84E+07	1.21E+07	4.40E+06	-2.69E+07	-2.91E+09	2.91E+09	-2.90E+09	2.90E+09
8.79E+06	-3.02E+07	-7.86E+07	7.04E+06	-4.12E+07	-1.81E+09	1.81E+09	-1.80E+09	1.80E+09
6.18E+06	-9.75E+06	-1.25E+08	8.48E+06	-4.85E+07	-5.85E+08	5.85E+08	-5.76E+08	5.76E+08

M1 = F-tangential * lever arm M2 = F-tangential * lever arm + M-radial

Table F-1. Reaction forces and moments in the chimney at foundational level.

The following tables display column interaction procedures for several heights along an IGV/transfer section of medium height (the second investigated concept in *Section 6.2*). The triangular prism shape is approximated at this stage; hence the column section under investigation in each table decreases linearly. In the graphs below the tables the column interaction diagrams are shown. From the last table it is clear that the section, with a length of 2.2 metres – the chimney shell thickness at base level is too small to resist the forces acting upon it. The second last table gives a solution to this problem, increasing the length to 4.1 metres. Note that the ULS criteria for safety are included in the principles formulas from which the dimensionless parameters where derived (refer to *Chapter 2.3.2*).

for found-ational-level									Sign convention					Sonder staal	
fcu	h	b	x	fs1	%As1	As1	d'	fs2	%As2	As2	d	N	M	N	M
2.00E+07	40	6	0	4.50E+08	**0.0015**	0.36	6	4.50E+08	**-0.0015**	-0.36	6	0.00E+00	4.54E+09	0.00E+00	0.00E+00
2.00E+07	40	6	2	4.50E+08	**0.0015**	0.36	6	4.50E+08	**-0.0015**	-0.36	6	9.72E+07	6.40E+09	9.72E+07	1.86E+09
2.00E+07	40	6	4	4.50E+08	**0.0015**	0.36	6	4.50E+08	**-0.0015**	-0.36	6	1.94E+08	8.08E+09	1.94E+08	3.55E+09
2.00E+07	40	6	6	4.50E+08	**0.0015**	0.36	6	4.50E+08	**-0.0015**	-0.36	6	2.92E+08	9.59E+09	2.92E+08	5.06E+09
2.00E+07	40	6	8	4.50E+08	**0.0015**	0.36	6	4.50E+08	**-0.0015**	-0.36	6	3.89E+08	1.09E+10	3.89E+08	6.39E+09
2.00E+07	40	6	10	4.50E+08	**0.0015**	0.36	6	4.50E+08	**-0.0015**	-0.36	6	4.86E+08	1.21E+10	4.86E+08	7.55E+09
2.00E+07	40	6	12	4.50E+08	**0.0015**	0.36	6	4.50E+08	**-0.0015**	-0.36	6	5.83E+08	1.31E+10	5.83E+08	8.54E+09
2.00E+07	40	6	14	4.50E+08	**0.0015**	0.36	6	4.50E+08	**-0.0015**	-0.36	6	6.80E+08	1.39E+10	6.80E+08	9.34E+09
2.00E+07	40	6	16	4.50E+08	**0.0015**	0.36	6	4.50E+08	**-0.0015**	-0.36	6	7.78E+08	1.45E+10	7.78E+08	9.98E+09
2.00E+07	40	6	18	4.50E+08	**0.0015**	0.36	6	4.50E+08	**-0.0015**	-0.36	6	8.75E+08	1.50E+10	8.75E+08	1.04E+10
2.00E+07	40	6	20	4.50E+08	**0.0015**	0.36	6	4.50E+08	**-0.0015**	-0.36	6	9.72E+08	1.53E+10	9.72E+08	1.07E+10
2.00E+07	40	6	22	4.50E+08	**0.0015**	0.36	6	4.50E+08	**-0.0015**	-0.36	6	1.07E+09	1.54E+10	1.07E+09	1.08E+10
2.00E+07	40	6	24	4.50E+08	**0.0015**	0.36	6	4.50E+08	**-0.0015**	-0.36	6	1.17E+09	1.53E+10	1.17E+09	1.08E+10
2.00E+07	40	6	26	4.50E+08	**0.0015**	0.36	6	4.50E+08	**-0.0015**	-0.36	6	1.26E+09	1.50E+10	1.26E+09	1.05E+10
2.00E+07	40	6	28	4.50E+08	**0.0015**	0.36	6	4.50E+08	**-0.0015**	-0.36	6	1.36E+09	1.46E+10	1.36E+09	1.01E+10
2.00E+07	40	6	30	4.50E+08	**0.0015**	0.36	6	4.50E+08	**-0.0015**	-0.36	6	1.46E+09	1.40E+10	1.46E+09	9.50E+09
2.00E+07	40	6	32	4.50E+08	**0.0015**	0.36	6	4.50E+08	**-0.0015**	-0.36	6	1.56E+09	1.33E+10	1.56E+09	8.73E+09
2.00E+07	40	6	34	4.50E+08	**0.0015**	0.36	6	4.50E+08	**-0.0015**	-0.36	6	1.65E+09	1.23E+10	1.65E+09	7.79E+09
2.00E+07	40	6	36	4.50E+08	**0.0015**	0.36	6	4.50E+08	**-0.0015**	-0.36	6	1.75E+09	1.12E+10	1.75E+09	6.66E+09
2.00E+07	40	6	38	4.50E+08	**0.0015**	0.36	6	4.50E+08	**-0.0015**	-0.36	6	1.85E+09	9.90E+09	1.85E+09	5.37E+09
2.00E+07	40	6	40	4.50E+08	**0.0015**	0.36	6	4.50E+08	**-0.0015**	-0.36	6	1.94E+09	8.43E+09	1.94E+09	3.90E+09

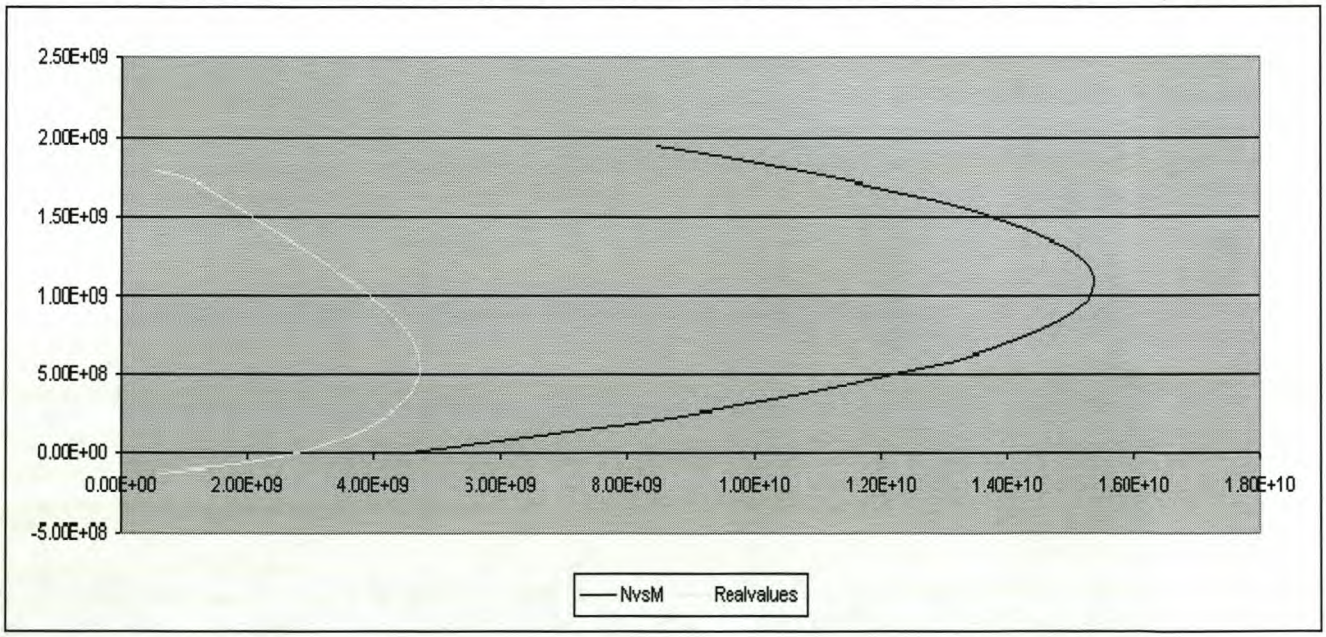

for 10m-level									Sign convention					Sonder staal	
fcu	h	b	x	fs1	%As1	As1	d'	fs2	%As2	As2	d	N	M	N	M
2.00E+07	36	6	2.4	4.50E+08	**0.0015**	0.324	5.4	4.50E+08	**-0.0015**	-0.324	5.4	1.17E+08	5.65E+09	1.17E+08	1.98E+09
2.00E+07	36	6	4.8	4.50E+08	**0.0015**	0.324	5.4	4.50E+08	**-0.0015**	-0.324	5.4	2.33E+08	7.38E+09	2.33E+08	3.70E+09
2.00E+07	36	6	7.2	4.50E+08	**0.0015**	0.324	5.4	4.50E+08	**-0.0015**	-0.324	5.4	3.50E+08	8.85E+09	3.50E+08	5.18E+09
2.00E+07	36	6	9.6	4.50E+08	**0.0015**	0.324	5.4	4.50E+08	**-0.0015**	-0.324	5.4	4.67E+08	1.01E+10	4.67E+08	6.40E+09
2.00E+07	36	6	12	4.50E+08	**0.0015**	0.324	5.4	4.50E+08	**-0.0015**	-0.324	5.4	5.83E+08	1.10E+10	5.83E+08	7.37E+09
2.00E+07	36	6	14.4	4.50E+08	**0.0015**	0.324	5.4	4.50E+08	**-0.0015**	-0.324	5.4	7.00E+08	1.18E+10	7.00E+08	8.08E+09
2.00E+07	36	6	16.8	4.50E+08	**0.0015**	0.324	5.4	4.50E+08	**-0.0015**	-0.324	5.4	8.16E+08	1.22E+10	8.16E+08	8.55E+09
2.00E+07	36	6	19.2	4.50E+08	**0.0015**	0.324	5.4	4.50E+08	**-0.0015**	-0.324	5.4	9.33E+08	1.24E+10	9.33E+08	8.76E+09
2.00E+07	36	6	21.6	4.50E+08	**0.0015**	0.324	5.4	4.50E+08	**-0.0015**	-0.324	5.4	1.05E+09	1.24E+10	1.05E+09	8.71E+09
2.00E+07	36	6	24	4.50E+08	**0.0015**	0.324	5.4	4.50E+08	**-0.0015**	-0.324	5.4	1.17E+09	1.21E+10	1.17E+09	8.42E+09
2.00E+07	36	6	26.4	4.50E+08	**0.0015**	0.324	5.4	4.50E+08	**-0.0015**	-0.324	5.4	1.28E+09	1.15E+10	1.28E+09	7.87E+09
2.00E+07	36	6	28.8	4.50E+08	**0.0015**	0.324	5.4	4.50E+08	**-0.0015**	-0.324	5.4	1.40E+09	1.07E+10	1.40E+09	7.07E+09
2.00E+07	36	6	31.2	4.50E+08	**0.0015**	0.324	5.4	4.50E+08	**-0.0015**	-0.324	5.4	1.52E+09	9.69E+09	1.52E+09	6.02E+09
2.00E+07	36	6	33.6	4.50E+08	**0.0015**	0.324	5.4	4.50E+08	**-0.0015**	-0.324	5.4	1.63E+09	8.39E+09	1.63E+09	4.71E+09
2.00E+07	36	6	36	4.50E+08	**0.0015**	0.324	5.4	4.50E+08	**-0.0015**	-0.324	5.4	1.75E+09	6.83E+09	1.75E+09	3.16E+09
2.00E+07	36	6	38.4	4.50E+08	**0.0015**	0.324	5.4	4.50E+08	**-0.0015**	-0.324	5.4	1.87E+09	5.02E+09	1.87E+09	1.35E+09
2.00E+07	36	6	40.8	4.50E+08	**0.0015**	0.324	5.4	4.50E+08	**-0.0015**	-0.324	5.4	1.98E+09	2.96E+09	1.98E+09	-7.16E+08
2.00E+07	36	6	43.2	4.50E+08	**0.0015**	0.324	5.4	4.50E+08	**-0.0015**	-0.324	5.4	2.10E+09	6.43E+08	2.10E+09	-3.03E+09
2.00E+07	36	6	45.6	4.50E+08	**0.0015**	0.324	5.4	4.50E+08	**-0.0015**	-0.324	5.4	2.22E+09	-1.92E+09	2.22E+09	-5.60E+09

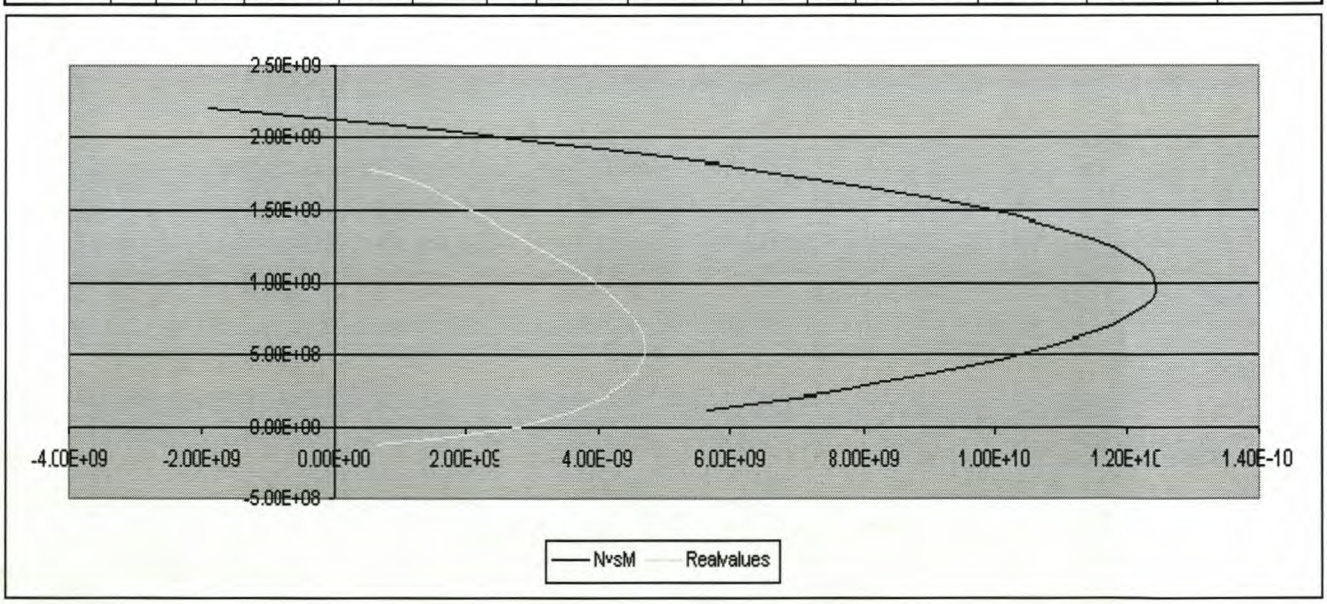

for 20m-level									Sign convention					Sonder staal	
fcu	h	b	x	fs1	%As1	As1	d'	fs2	%As2	As2	d	N	M	N	M
2.00E+07	32	6	2.13	4.50E+08	**0.0015**	0.288	4.8	4.50E+08	**-0.002**	-0.384	4.8	6.05E+07	4.95E+09	1.04E+08	1.56E+09
2.00E+07	32	6	4.27	4.50E+08	**0.0015**	0.288	4.8	4.50E+08	**-0.002**	-0.384	4.8	1.64E+08	6.31E+09	2.07E+08	2.93E+09
2.00E+07	32	6	6.40	4.50E+08	**0.0015**	0.288	4.8	4.50E+08	**-0.002**	-0.384	4.8	2.68E+08	7.48E+09	3.11E+08	4.09E+09
2.00E+07	32	6	8.53	4.50E+08	**0.0015**	0.288	4.8	4.50E+08	**-0.002**	-0.384	4.8	3.72E+08	8.44E+09	4.15E+08	5.06E+09
2.00E+07	32	6	10.6	4.50E+08	**0.0015**	0.288	4.8	4.50E+08	**-0.002**	-0.384	4.8	4.75E+08	9.21E+09	5.18E+08	5.82E+09
2.00E+07	32	6	12.8	4.50E+08	**0.0015**	0.288	4.8	4.50E+08	**-0.002**	-0.384	4.8	5.79E+08	9.77E+09	6.22E+08	6.39E+09
2.00E+07	32	6	14.9	4.50E+08	**0.0015**	0.288	4.8	4.50E+08	**-0.002**	-0.384	4.8	6.83E+08	1.01E+10	7.26E+08	6.75E+09
2.00E+07	32	6	17.0	4.50E+08	**0.0015**	0.288	4.8	4.50E+08	**-0.002**	-0.384	4.8	7.86E+08	1.03E+10	8.29E+08	6.92E+09
2.00E+07	32	6	19.2	4.50E+08	**0.0015**	0.288	4.8	4.50E+08	**-0.002**	-0.384	4.8	8.90E+08	1.03E+10	9.33E+08	6.88E+09
2.00E+07	32	6	21.3	4.50E+08	**0.0015**	0.288	4.8	4.50E+08	**-0.002**	-0.384	4.8	9.94E+08	1.00E+10	1.04E+09	6.65E+09
2.00E+07	32	6	23.4	4.50E+08	**0.0015**	0.288	4.8	4.50E+08	**-0.002**	-0.384	4.8	1.10E+09	9.61E+09	1.14E+09	6.22E+09
2.00E+07	32	6	25.6	4.50E+08	**0.0015**	0.288	4.8	4.50E+08	**-0.002**	-0.384	4.8	1.20E+09	8.97E+09	1.24E+09	5.59E+09
2.00E+07	32	6	27.7	4.50E+08	**0.0015**	0.288	4.8	4.50E+08	**-0.002**	-0.384	4.8	1.30E+09	8.14E+09	1.35E+09	4.76E+09
2.00E+07	32	6	29.8	4.50E+08	**0.0015**	0.288	4.8	4.50E+08	**-0.002**	-0.384	4.8	1.41E+09	7.11E+09	1.45E+09	3.73E+09
2.00E+07	32	6	32.0	4.50E+08	**0.0015**	0.288	4.8	4.50E+08	**-0.002**	-0.384	4.8	1.51E+09	5.88E+09	1.56E+09	2.49E+09
2.00E+07	32	6	34.1	4.50E+08	**0.0015**	0.288	4.8	4.50E+08	**-0.002**	-0.384	4.8	1.62E+09	4.45E+09	1.66E+09	1.06E+09
2.00E+07	32	6	36.2	4.50E+08	**0.0015**	0.288	4.8	4.50E+08	**-0.002**	-0.384	4.8	1.72E+09	2.82E+09	1.76E+09	-5.65E+08
2.00E+07	32	6	38.4	4.50E+08	**0.0015**	0.288	4.8	4.50E+08	**-0.002**	-0.384	4.8	1.82E+09	9.92E+08	1.87E+09	-2.39E+09
2.00E+07	32	6	40.5	4.50E+08	**0.0015**	0.288	4.8	4.50E+08	**-0.002**	-0.384	4.8	1.93E+09	-1.04E+09	1.97E+09	-4.42E+09

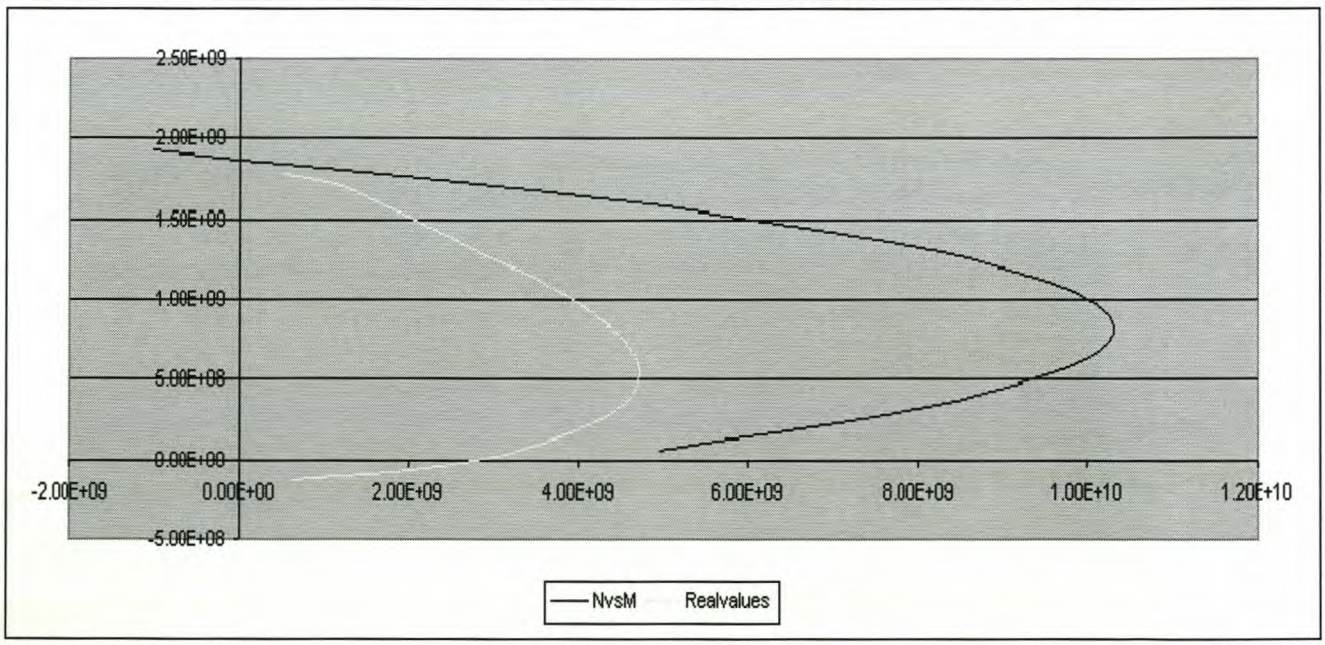

for 30m-level									Sign convention					Sonder staal	
fcu	h	b	x	fs1	%As1	As1	d'	fs2	%As2	As2	d	N	M	N	M
2.30E+07	28	6	1.87	4.50E+08	**0.0015**	0.252	4.2	4.50E+08	**-0.0025**	-0.42	4.2	2.87E+07	4.34E+09	1.04E+08	1.38E+09
2.30E+07	28	6	3.73	4.50E+08	**0.0015**	0.252	4.2	4.50E+08	**-0.0025**	-0.42	4.2	1.33E+08	5.54E+09	2.09E+08	2.58E+09
2.30E+07	28	6	5.60	4.50E+08	**0.0015**	0.252	4.2	4.50E+08	**-0.0025**	-0.42	4.2	2.37E+08	6.57E+09	3.13E+08	3.60E+09
2.30E+07	28	6	7.47	4.50E+08	**0.0015**	0.252	4.2	4.50E+08	**-0.0025**	-0.42	4.2	3.42E+08	7.41E+09	4.17E+08	4.45E+09
2.30E+07	28	6	9.33	4.50E+08	**0.0015**	0.252	4.2	4.50E+08	**-0.0025**	-0.42	4.2	4.46E+08	8.09E+09	5.22E+08	5.12E+09
2.30E+07	28	6	11.2	4.50E+08	**0.0015**	0.252	4.2	4.50E+08	**-0.0025**	-0.42	4.2	5.50E+08	8.59E+09	6.26E+08	5.62E+09
2.30E+07	28	6	13.0	4.50E+08	**0.0015**	0.252	4.2	4.50E+08	**-0.0025**	-0.42	4.2	6.55E+08	8.91E+09	7.30E+08	5.94E+09
2.30E+07	28	6	14.9	4.50E+08	**0.0015**	0.252	4.2	4.50E+08	**-0.0025**	-0.42	4.2	7.59E+08	9.05E+09	8.35E+08	6.09E+09
2.30E+07	28	6	16.8	4.50E+08	**0.0015**	0.252	4.2	4.50E+08	**-0.0025**	-0.42	4.2	8.63E+08	9.03E+09	9.39E+08	6.06E+09
2.30E+07	28	6	18.6	4.50E+08	**0.0015**	0.252	4.2	4.50E+08	**-0.0025**	-0.42	4.2	9.68E+08	8.82E+09	1.04E+09	5.86E+09
2.30E+07	28	6	20.5	4.50E+08	**0.0015**	0.252	4.2	4.50E+08	**-0.0025**	-0.42	4.2	1.07E+09	8.44E+09	1.15E+09	5.48E+09
2.30E+07	28	6	22.4	4.50E+08	**0.0015**	0.252	4.2	4.50E+08	**-0.0025**	-0.42	4.2	1.18E+09	7.88E+09	1.25E+09	4.92E+09
2.30E+07	28	6	24.2	4.50E+08	**0.0015**	0.252	4.2	4.50E+08	**-0.0025**	-0.42	4.2	1.28E+09	7.15E+09	1.36E+09	4.19E+09
2.30E+07	28	6	26.1	4.50E+08	**0.0015**	0.252	4.2	4.50E+08	**-0.0025**	-0.42	4.2	1.38E+09	6.24E+09	1.46E+09	3.28E+09
2.30E+07	28	6	28.0	4.50E+08	**0.0015**	0.252	4.2	4.50E+08	**-0.0025**	-0.42	4.2	1.49E+09	5.16E+09	1.56E+09	2.20E+09
2.30E+07	28	6	29.8	4.50E+08	**0.0015**	0.252	4.2	4.50E+08	**-0.0025**	-0.42	4.2	1.59E+09	3.90E+09	1.67E+09	9.37E+08
2.30E+07	28	6	31.7	4.50E+08	**0.0015**	0.252	4.2	4.50E+08	**-0.0025**	-0.42	4.2	1.70E+09	2.47E+09	1.77E+09	-4.98E+08
2.30E+07	28	6	33.6	4.50E+08	**0.0015**	0.252	4.2	4.50E+08	**-0.0025**	-0.42	4.2	1.80E+09	8.55E+08	1.88E+09	-2.11E+09
2.30E+07	28	6	35.4	4.50E+08	**0.0015**	0.252	4.2	4.50E+08	**-0.0025**	-0.42	4.2	1.91E+09	-9.31E+08	1.98E+09	-3.89E+09

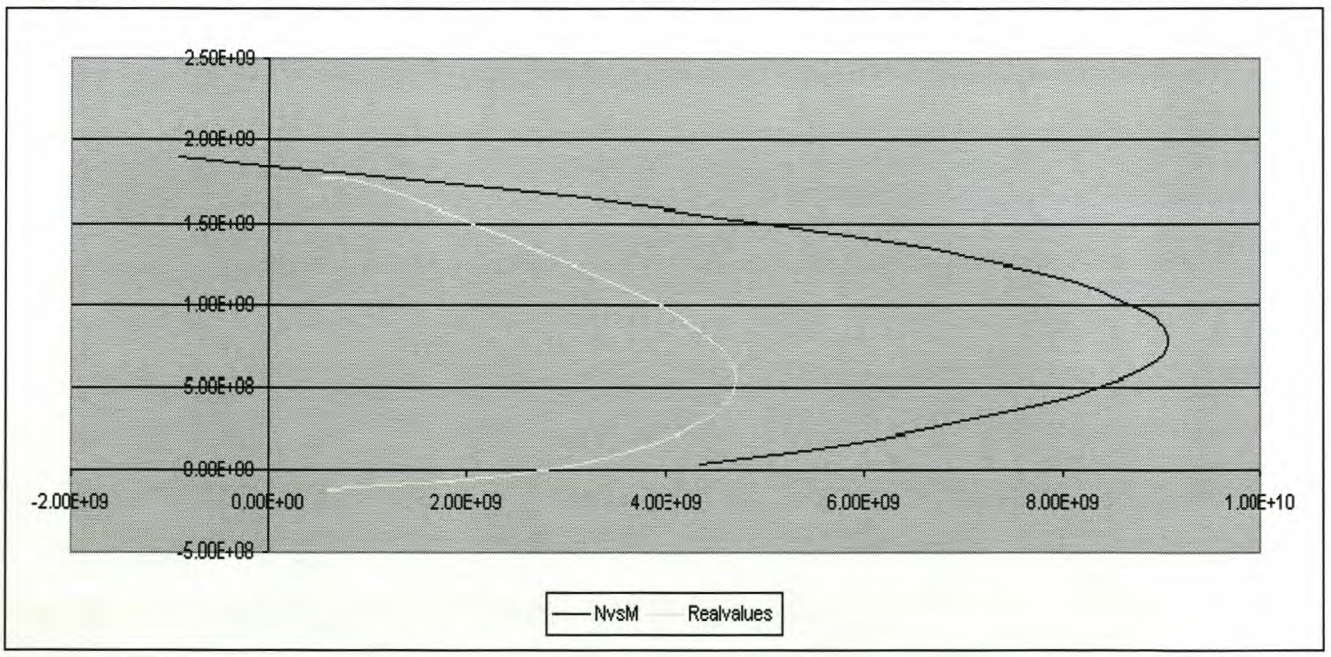

for 40m-level									Sign convention					Sonder staal	
fcu	h	b	x	fs1	%As1	As1	d'	fs2	%As2	As2	d	N	M	N	M
2.70E+07	24	6	1.60	4.50E+08	**0.0015**	0.216	3.6	4.50E+08	**-0.003**	-0.432	3.6	7.78E+06	3.64E+09	1.05E+08	1.19E+09
2.70E+07	24	6	3.20	4.50E+08	**0.0015**	0.216	3.6	4.50E+08	**-0.003**	-0.432	3.6	1.13E+08	4.67E+09	2.10E+08	2.22E+09
2.70E+07	24	6	4.80	4.50E+08	**0.0015**	0.216	3.6	4.50E+08	**-0.003**	-0.432	3.6	2.18E+08	5.56E+09	3.15E+08	3.11E+09
2.70E+07	24	6	6.40	4.50E+08	**0.0015**	0.216	3.6	4.50E+08	**-0.003**	-0.432	3.6	3.23E+08	6.29E+09	4.20E+08	3.84E+09
2.70E+07	24	6	8.00	4.50E+08	**0.0015**	0.216	3.6	4.50E+08	**-0.003**	-0.432	3.6	4.28E+08	6.87E+09	5.25E+08	4.42E+09
2.70E+07	24	6	9.60	4.50E+08	**0.0015**	0.216	3.6	4.50E+08	**-0.003**	-0.432	3.6	5.33E+08	7.30E+09	6.30E+08	4.85E+09
2.70E+07	24	6	11.20	4.50E+08	**0.0015**	0.216	3.6	4.50E+08	**-0.003**	-0.432	3.6	6.38E+08	7.58E+09	7.35E+08	5.13E+09
2.70E+07	24	6	12.8	4.50E+08	**0.0015**	0.216	3.6	4.50E+08	**-0.003**	-0.432	3.6	7.43E+08	7.70E+09	8.40E+08	5.25E+09
2.70E+07	24	6	14.4	4.50E+08	**0.0015**	0.216	3.6	4.50E+08	**-0.003**	-0.432	3.6	8.48E+08	7.68E+09	9.45E+08	5.23E+09
2.70E+07	24	6	16.0	4.50E+08	**0.0015**	0.216	3.6	4.50E+08	**-0.003**	-0.432	3.6	9.53E+08	7.50E+09	1.05E+09	5.05E+09
2.70E+07	24	6	17.6	4.50E+08	**0.0015**	0.216	3.6	4.50E+08	**-0.003**	-0.432	3.6	1.06E+09	7.17E+09	1.15E+09	4.72E+09
2.70E+07	24	6	19.2	4.50E+08	**0.0015**	0.216	3.6	4.50E+08	**-0.003**	-0.432	3.6	1.16E+09	6.69E+09	1.26E+09	4.24E+09
2.70E+07	24	6	20.8	4.50E+08	**0.0015**	0.216	3.6	4.50E+08	**-0.003**	-0.432	3.6	1.27E+09	6.06E+09	1.36E+09	3.61E+09
2.70E+07	24	6	22.4	4.50E+08	**0.0015**	0.216	3.6	4.50E+08	**-0.003**	-0.432	3.6	1.37E+09	5.28E+09	1.47E+09	2.83E+09
2.70E+07	24	6	24.0	4.50E+08	**0.0015**	0.216	3.6	4.50E+08	**-0.003**	-0.432	3.6	1.48E+09	4.34E+09	1.57E+09	1.89E+09
2.70E+07	24	6	25.6	4.50E+08	**0.0015**	0.216	3.6	4.50E+08	**-0.003**	-0.432	3.6	1.58E+09	3.26E+09	1.68E+09	8.08E+08
2.70E+07	24	6	27.2	4.50E+08	**0.0015**	0.216	3.6	4.50E+08	**-0.003**	-0.432	3.6	1.69E+09	2.02E+09	1.78E+09	-4.29E+08
2.70E+07	24	6	28.8	4.50E+08	**0.0015**	0.216	3.6	4.50E+08	**-0.003**	-0.432	3.6	1.79E+09	6.31E+08	1.89E+09	-1.82E+09
2.70E+07	24	6	30.4	4.50E+08	**0.0015**	0.216	3.6	4.50E+08	**-0.003**	-0.432	3.6	1.90E+09	-9.10E+08	1.99E+09	-3.36E+09

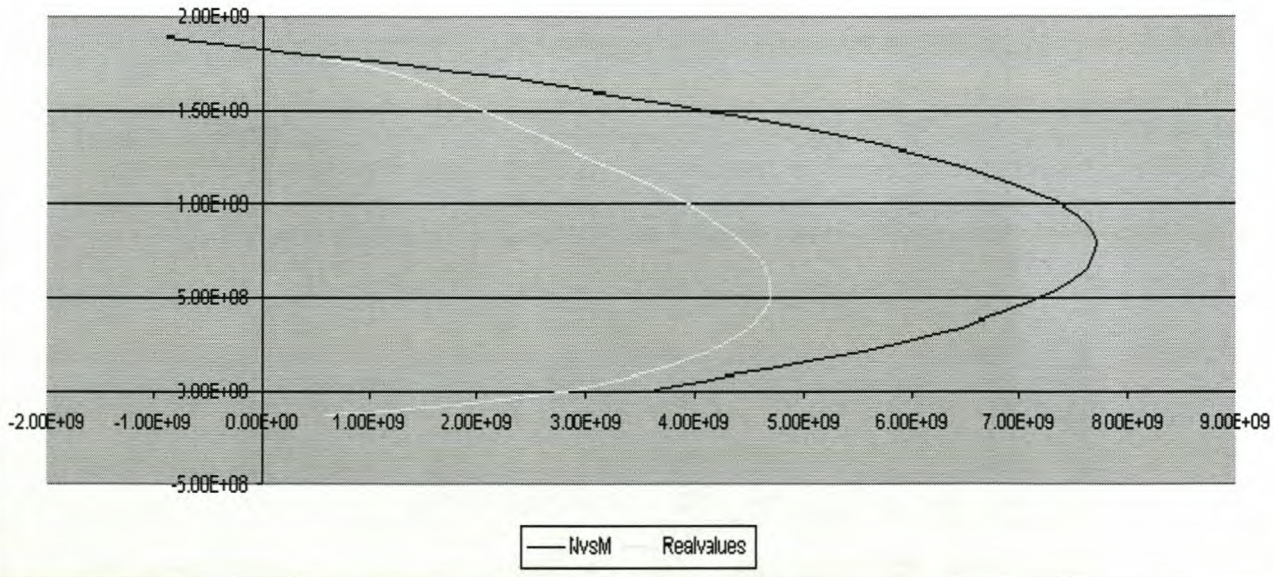

for 50m-level									Sign convention					Sonder staal	
fcu	h	b	x	fs1	%As1	As1	d'	fs2	%As2	As2	d	N	M	N	M
3.00E+07	20	6	1.33	4.50E+08	**0.0035**	0.42	3	4.50E+08	**-0.004**	-0.48	3	7.02E+07	3.75E+09	9.72E+07	9.16E+08
3.00E+07	20	6	2.67	4.50E+08	**0.0035**	0.42	3	4.50E+08	**-0.004**	-0.48	3	1.67E+08	4.55E+09	1.94E+08	1.71E+09
3.00E+07	20	6	4.00	4.50E+08	**0.0035**	0.42	3	4.50E+08	**-0.004**	-0.48	3	2.65E+08	5.23E+09	2.92E+08	2.40E+09
3.00E+07	20	6	5.33	4.50E+08	**0.0035**	0.42	3	4.50E+08	**-0.004**	-0.48	3	3.62E+08	5.80E+09	3.89E+08	2.96E+09
3.00E+07	20	6	6.67	4.50E+08	**0.0035**	0.42	3	4.50E+08	**-0.004**	-0.48	3	4.59E+08	6.25E+09	4.86E+08	3.41E+09
3.00E+07	20	6	8.00	4.50E+08	**0.0035**	0.42	3	4.50E+08	**-0.004**	-0.48	3	5.56E+08	6.58E+09	5.83E+08	3.74E+09
3.00E+07	20	6	9.33	4.50E+08	**0.0035**	0.42	3	4.50E+08	**-0.004**	-0.48	3	6.53E+08	6.79E+09	6.80E+08	3.96E+09
3.00E+07	20	6	10.6	4.50E+08	**0.0035**	0.42	3	4.50E+08	**-0.004**	-0.48	3	7.51E+08	6.89E+09	7.78E+08	4.05E+09
3.00E+07	20	6	12.0	4.50E+08	**0.0035**	0.42	3	4.50E+08	**-0.004**	-0.48	3	8.48E+08	6.87E+09	8.75E+08	4.03E+09
3.00E+07	20	6	13.3	4.50E+08	**0.0035**	0.42	3	4.50E+08	**-0.004**	-0.48	3	9.45E+08	6.73E+09	9.72E+08	3.90E+09
3.00E+07	20	6	14.6	4.50E+08	**0.0035**	0.42	3	4.50E+08	**-0.004**	-0.48	3	1.04E+09	6.48E+09	1.07E+09	3.64E+09
3.00E+07	20	6	16.0	4.50E+08	**0.0035**	0.42	3	4.50E+08	**-0.004**	-0.48	3	1.14E+09	6.11E+09	1.17E+09	3.27E+09
3.00E+07	20	6	17.3	4.50E+08	**0.0035**	0.42	3	4.50E+08	**-0.004**	-0.48	3	1.24E+09	5.62E+09	1.26E+09	2.79E+09
3.00E+07	20	6	18.6	4.50E+08	**0.0035**	0.42	3	4.50E+08	**-0.004**	-0.48	3	1.33E+09	5.02E+09	1.36E+09	2.18E+09
3.00E+07	20	6	20.0	4.50E+08	**0.0035**	0.42	3	4.50E+08	**-0.004**	-0.48	3	1.43E+09	4.30E+09	1.46E+09	1.46E+09
3.00E+07	20	6	21.3	4.50E+08	**0.0035**	0.42	3	4.50E+08	**-0.004**	-0.48	3	1.53E+09	3.46E+09	1.56E+09	6.24E+08
3.00E+07	20	6	22.6	4.50E+08	**0.0035**	0.42	3	4.50E+08	**-0.004**	-0.48	3	1.63E+09	2.50E+09	1.65E+09	-3.31E+08
3.00E+07	20	6	24.0	4.50E+08	**0.0035**	0.42	3	4.50E+08	**-0.004**	-0.48	3	1.72E+09	1.43E+09	1.75E+09	-1.40E+09
3.00E+07	20	6	25.3	4.50E+08	**0.0035**	0.42	3	4.50E+08	**-0.004**	-0.48	3	1.82E+09	2.43E+08	1.85E+09	-2.59E+09
3.00E+07	20	6	26.6	4.50E+08	**0.0035**	0.42	3	4.50E+08	**-0.004**	-0.48	3	1.92E+09	-1.06E+09	1.94E+09	-3.90E+09

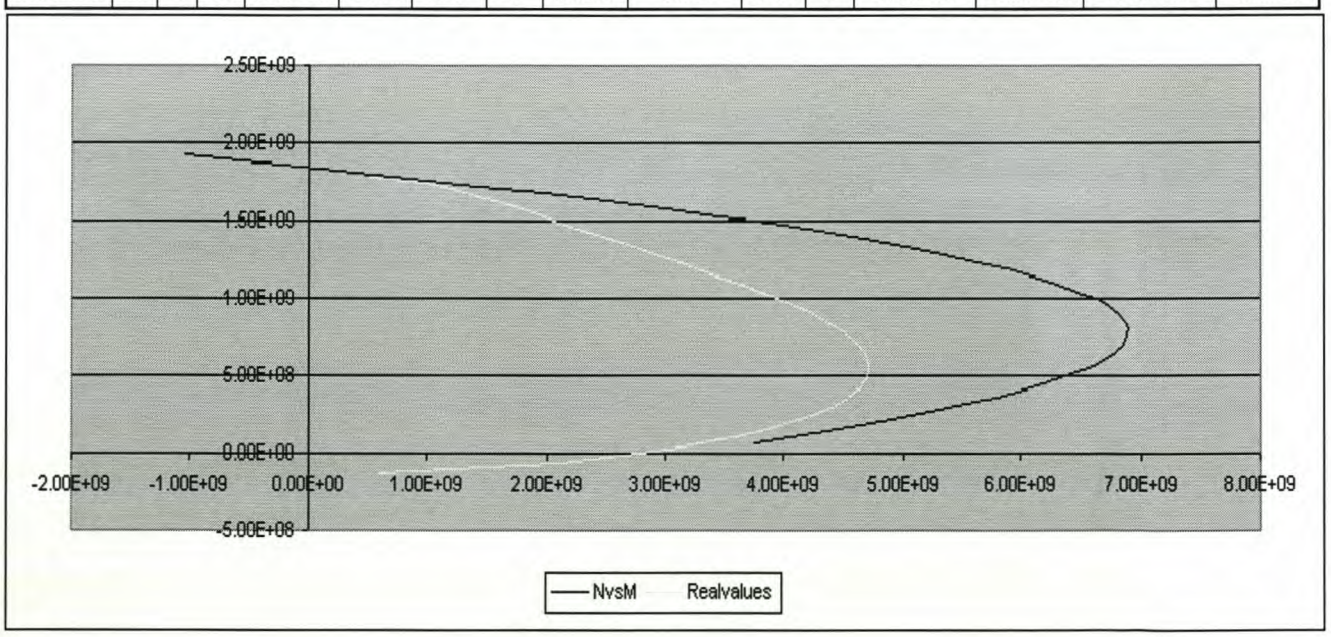

for 60m-level									Sign convention					Sonder staal	
fcu	h	b	x	fs1	%As1	As1	d'	fs2	%As2	As2	d	N	M	N	M
2.50E+07	16	6	1.07	4.50E+08	**0.015**	1.44	2.4	4.50E+08	**-0.007**	-0.672	2.4	4.10E+08	5.81E+09	6.48E+07	4.88E+08
2.50E+07	16	6	2.13	4.50E+08	**0.015**	1.44	2.4	4.50E+08	**-0.007**	-0.672	2.4	4.75E+08	6.24E+09	1.30E+08	9.15E+08
2.50E+07	16	6	3.20	4.50E+08	**0.015**	1.44	2.4	4.50E+08	**-0.007**	-0.672	2.4	5.40E+08	6.60E+09	1.94E+08	1.28E+09
2.50E+07	16	6	4.27	4.50E+08	**0.015**	1.44	2.4	4.50E+08	**-0.007**	-0.672	2.4	6.05E+08	6.90E+09	2.59E+08	1.58E+09
2.50E+07	16	6	5.33	4.50E+08	**0.015**	1.44	2.4	4.50E+08	**-0.007**	-0.672	2.4	6.70E+08	7.14E+09	3.24E+08	1.82E+09
2.50E+07	16	6	6.40	4.50E+08	**0.015**	1.44	2.4	4.50E+08	**-0.007**	-0.672	2.4	7.34E+08	7.32E+09	3.89E+08	2.00E+09
2.50E+07	16	6	7.47	4.50E+08	**0.015**	1.44	2.4	4.50E+08	**-0.007**	-0.672	2.4	7.99E+08	7.43E+09	4.54E+08	2.11E+09
2.50E+07	16	6	8.53	4.50E+08	**0.015**	1.44	2.4	4.50E+08	**-0.007**	-0.672	2.4	8.64E+08	7.48E+09	5.18E+08	2.16E+09
2.50E+07	16	6	9.60	4.50E+08	**0.015**	1.44	2.4	4.50E+08	**-0.007**	-0.672	2.4	9.29E+08	7.47E+09	5.83E+08	2.15E+09
2.50E+07	16	6	10.6	4.50E+08	**0.015**	1.44	2.4	4.50E+08	**-0.007**	-0.672	2.4	9.94E+08	7.40E+09	6.48E+08	2.08E+09
2.50E+07	16	6	11.7	4.50E+08	**0.015**	1.44	2.4	4.50E+08	**-0.007**	-0.672	2.4	1.06E+09	7.27E+09	7.13E+08	1.94E+09
2.50E+07	16	6	12.8	4.50E+08	**0.015**	1.44	2.4	4.50E+08	**-0.007**	-0.672	2.4	1.12E+09	7.07E+09	7.78E+08	1.75E+09
2.50E+07	16	6	13.8	4.50E+08	**0.015**	1.44	2.4	4.50E+08	**-0.007**	-0.672	2.4	1.19E+09	6.81E+09	8.42E+08	1.49E+09
2.50E+07	16	6	14.9	4.50E+08	**0.015**	1.44	2.4	4.50E+08	**-0.007**	-0.672	2.4	1.25E+09	6.49E+09	9.07E+08	1.16E+09
2.50E+07	16	6	16.0	4.50E+08	**0.015**	1.44	2.4	4.50E+08	**-0.007**	-0.672	2.4	1.32E+09	6.10E+09	9.72E+08	7.80E+08
2.50E+07	16	6	17.0	4.50E+08	**0.015**	1.44	2.4	4.50E+08	**-0.007**	-0.672	2.4	1.38E+09	5.65E+09	1.04E+09	3.33E+08
2.50E+07	16	6	18.1	4.50E+08	**0.015**	1.44	2.4	4.50E+08	**-0.007**	-0.672	2.4	1.45E+09	5.15E+09	1.10E+09	-1.77E+08
2.50E+07	16	6	19.2	4.50E+08	**0.015**	1.44	2.4	4.50E+08	**-0.007**	-0.672	2.4	1.51E+09	4.57E+09	1.17E+09	-7.48E+08
2.50E+07	16	6	20.2	4.50E+08	**0.015**	1.44	2.4	4.50E+08	**-0.007**	-0.672	2.4	1.58E+09	3.94E+09	1.23E+09	-1.38E+09
2.50E+07	16	6	21.3	4.50E+08	**0.015**	1.44	2.4	4.50E+08	**-0.007**	-0.672	2.4	1.64E+09	3.24E+09	1.30E+09	-2.08E+09
2.50E+07	16	6	22.4	4.50E+08	**0.015**	1.44	2.4	4.50E+08	**-0.007**	-0.672	2.4	1.71E+09	2.48E+09	1.36E+09	-2.84E+09

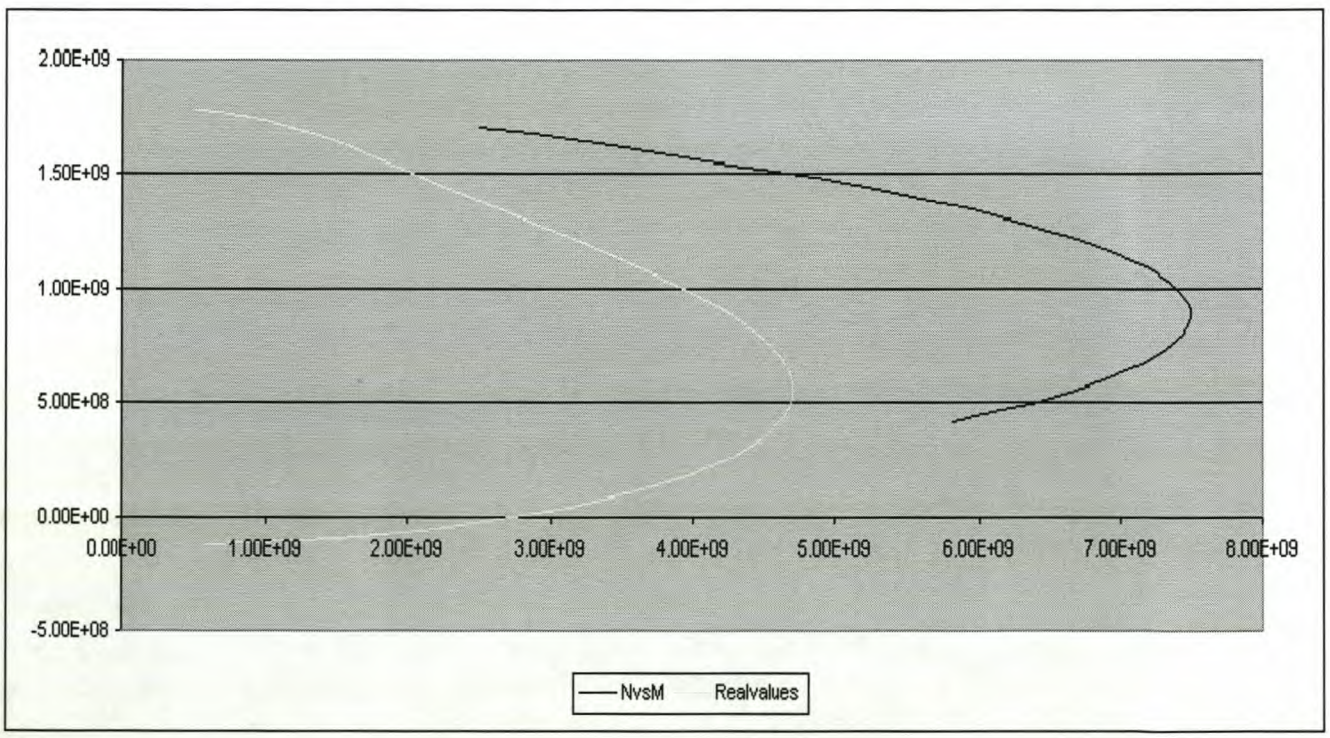

x=70m									Sign convention					Sonder staal	
fcu	h	b	x	fs1	%As1	As1	d'	fs2	%As2	As2	d	N	M	N	M
3.50E+07	7.6	13	0.51	4.50E+08	**0.013**	1.255	1.14	4.50E+08	**-0.017**	-1.640	1.14	-8.25E+07	3.79E+09	9.12E+07	3.27E+08
3.50E+07	7.6	13	1.01	4.50E+08	**0.013**	1.255	1.14	4.50E+08	**-0.017**	-1.640	1.14	8.69E+06	4.08E+09	1.82E+08	6.12E+08
3.50E+07	7.6	13	1.52	4.50E+08	**0.013**	1.255	1.14	4.50E+08	**-0.017**	-1.640	1.14	9.99E+07	4.32E+09	2.74E+08	8.55E+08
3.50E+07	7.6	13	2.03	4.50E+08	**0.013**	1.255	1.14	4.50E+08	**-0.017**	-1.640	1.14	1.91E+08	4.52E+09	3.65E+08	1.06E+09
3.50E+07	7.6	13	2.53	4.50E+08	**0.013**	1.255	1.14	4.50E+08	**-0.017**	-1.640	1.14	2.82E+08	4.68E+09	4.56E+08	1.22E+09
3.50E+07	7.6	13	3.04	4.50E+08	**0.013**	1.255	1.14	4.50E+08	**-0.017**	-1.640	1.14	3.74E+08	4.80E+09	5.47E+08	1.33E+09
3.50E+07	7.6	13	3.55	4.50E+08	**0.013**	1.255	1.14	4.50E+08	**-0.017**	-1.640	1.14	4.65E+08	4.88E+09	6.38E+08	1.41E+09
3.50E+07	7.6	13	4.05	4.50E+08	**0.013**	1.255	1.14	4.50E+08	**-0.017**	-1.640	1.14	5.56E+08	4.91E+09	7.30E+08	1.45E+09
3.50E+07	7.6	13	4.56	4.50E+08	**0.013**	1.255	1.14	4.50E+08	**-0.017**	-1.640	1.14	6.47E+08	4.90E+09	8.21E+08	1.44E+09
3.50E+07	7.6	13	5.07	4.50E+08	**0.013**	1.255	1.14	4.50E+08	**-0.017**	-1.640	1.14	7.38E+08	4.86E+09	9.12E+08	1.39E+09
3.50E+07	7.6	13	5.57	4.50E+08	**0.013**	1.255	1.14	4.50E+08	**-0.017**	-1.640	1.14	8.30E+08	4.77E+09	1.00E+09	1.30E+09
3.50E+07	7.6	13	6.08	4.50E+08	**0.013**	1.255	1.14	4.50E+08	**-0.017**	-1.640	1.14	9.21E+08	4.63E+09	1.09E+09	1.17E+09
3.50E+07	7.6	13	6.59	4.50E+08	**0.013**	1.255	1.14	4.50E+08	**-0.017**	-1.640	1.14	1.01E+09	4.46E+09	1.19E+09	9.94E+08

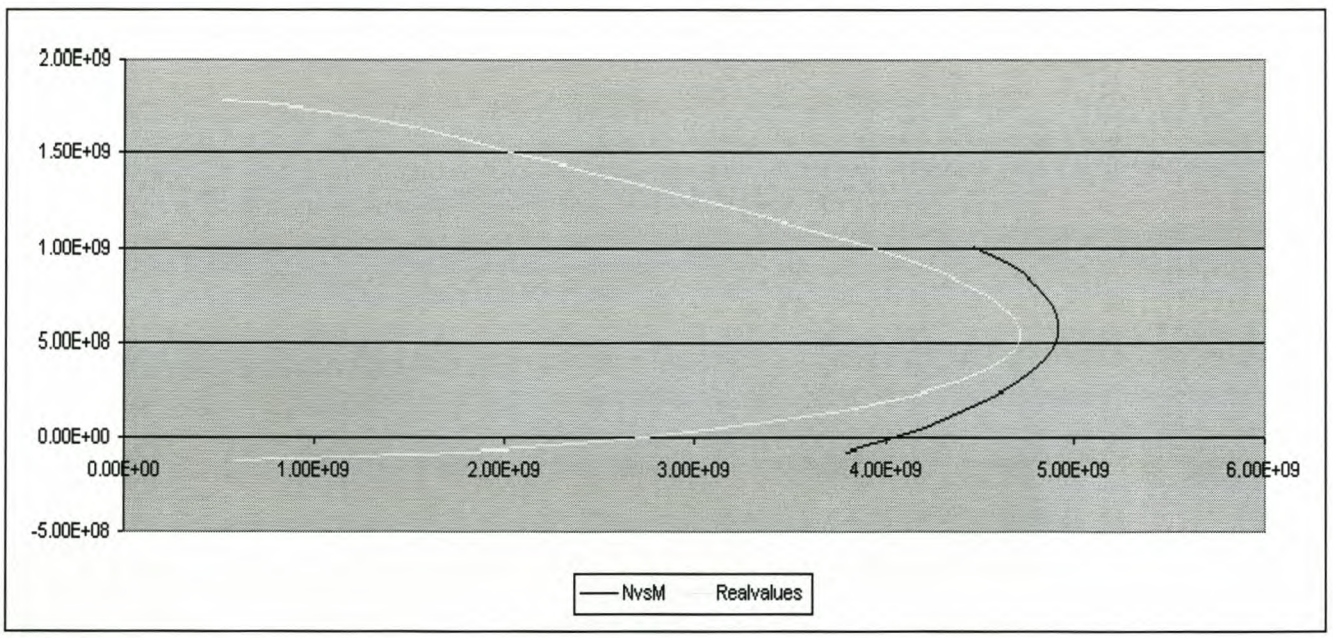

x=80m									Sign convention					Sonder staal	
fcu	h	b	x	fs1	%As1	As1	d'	fs2	%As2	As2	d	N	M	N	M
3.50E+07	5	19	0.33	4.50E+08	**0.023**	2.223	0.75	4.50E+08	**-0.027**	-2.609	0.75	-8.26E+07	4.02E+09	9.13E+07	2.15E+08
3.50E+07	5	19	0.67	4.50E+08	**0.023**	2.223	0.75	4.50E+08	**-0.027**	-2.609	0.75	8.70E+06	4.21E+09	1.83E+08	4.03E+08
3.50E+07	5	19	1.00	4.50E+08	**0.023**	2.223	0.75	4.50E+08	**-0.027**	-2.609	0.75	1.00E+08	4.37E+09	2.74E+08	5.63E+08
3.50E+07	5	19	1.33	4.50E+08	**0.023**	2.223	0.75	4.50E+08	**-0.027**	-2.609	0.75	1.91E+08	4.50E+09	3.65E+08	6.96E+08
3.50E+07	5	19	1.67	4.50E+08	**0.023**	2.223	0.75	4.50E+08	**-0.027**	-2.609	0.75	2.83E+08	4.61E+09	4.57E+08	8.01E+08
3.50E+07	5	19	2.00	4.50E+08	**0.023**	2.223	0.75	4.50E+08	**-0.027**	-2.609	0.75	3.74E+08	4.68E+09	5.48E+08	8.79E+08
3.50E+07	5	19	2.33	4.50E+08	**0.023**	2.223	0.75	4.50E+08	**-0.027**	-2.609	0.75	4.65E+08	4.73E+09	6.39E+08	9.29E+08
3.50E+07	5	19	2.67	4.50E+08	**0.023**	2.223	0.75	4.50E+08	**-0.027**	-2.609	0.75	5.57E+08	4.76E+09	7.31E+08	9.52E+08
3.50E+07	5	19	3.00	4.50E+08	**0.023**	2.223	0.75	4.50E+08	**-0.027**	-2.609	0.75	6.48E+08	4.75E+09	8.22E+08	9.48E+08
3.50E+07	5	19	3.33	4.50E+08	**0.023**	2.223	0.75	4.50E+08	**-0.027**	-2.609	0.75	7.39E+08	4.72E+09	9.13E+08	9.16E+08
3.50E+07	5	19	3.67	4.50E+08	**0.023**	2.223	0.75	4.50E+08	**-0.027**	-2.609	0.75	8.31E+08	4.66E+09	1.00E+09	8.56E+08
3.50E+07	5	19	4.00	4.50E+08	**0.023**	2.223	0.75	4.50E+08	**-0.027**	-2.609	0.75	9.22E+08	4.57E+09	1.10E+09	7.69E+08
3.50E+07	5	19	4.33	4.50E+08	**0.023**	2.223	0.75	4.50E+08	**-0.027**	-2.609	0.75	1.01E+09	4.46E+09	1.19E+09	6.55E+08
3.50E+07	5	19	4.67	4.50E+08	**0.023**	2.223	0.75	4.50E+08	**-0.027**	-2.609	0.75	1.10E+09	4.32E+09	1.28E+09	5.13E+08
3.50E+07	5	19	5.00	4.50E+08	**0.023**	2.223	0.75	4.50E+08	**-0.027**	-2.609	0.75	1.20E+09	4.15E+09	1.37E+09	3.43E+08
3.50E+07	5	19	5.33	4.50E+08	**0.023**	2.223	0.75	4.50E+08	**-0.027**	-2.609	0.75	1.29E+09	3.95E+09	1.46E+09	1.46E+08
3.50E+07	5	19	5.67	4.50E+08	**0.023**	2.223	0.75	4.50E+08	**-0.027**	-2.609	0.75	1.38E+09	3.73E+09	1.55E+09	-7.78E+07
3.50E+07	5	19	6.00	4.50E+08	**0.023**	2.223	0.75	4.50E+08	**-0.027**	-2.609	0.75	1.47E+09	3.48E+09	1.64E+09	-3.30E+08

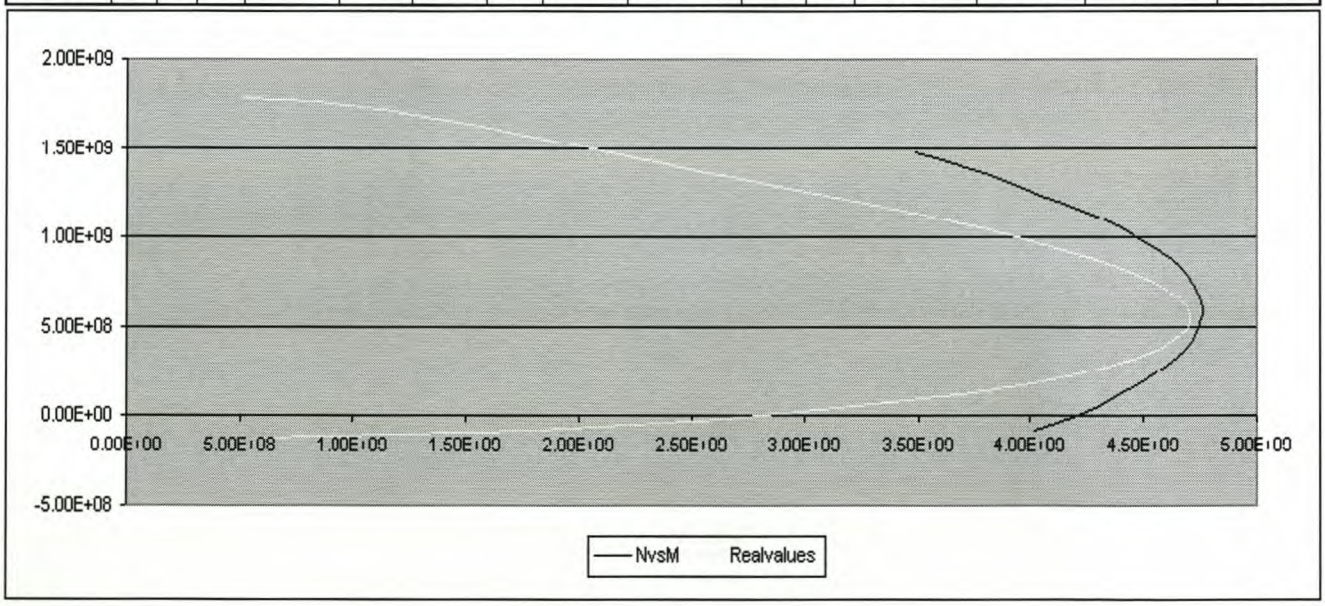

x=85m									Sign convention					Sonder staal	
fcu	h	b	x	fs1	%As1	As1	d'	fs2	%As2	As2	d	N	M	N	M
6.00E+07	4.1	26	0.27	4.50E+08	**0.02**	2.132	0.615	4.50E+08	**-0.03**	-3.198	0.615	-3.07E+08	3.78E+09	1.73E+08	3.34E+08
6.00E+07	4.1	26	0.55	4.50E+08	**0.02**	2.132	0.615	4.50E+08	**-0.03**	-3.198	0.615	-1.34E+08	4.07E+09	3.45E+08	6.25E+08
6.00E+07	4.1	26	0.82	4.50E+08	**0.02**	2.132	0.615	4.50E+08	**-0.03**	-3.198	0.615	3.84E+07	4.31E+09	5.18E+08	8.73E+08
6.00E+07	4.1	26	1.09	4.50E+08	**0.02**	2.132	0.615	4.50E+08	**-0.03**	-3.198	0.615	2.11E+08	4.52E+09	6.91E+08	1.08E+09
6.00E+07	4.1	26	1.37	4.50E+08	**0.02**	2.132	0.615	4.50E+08	**-0.03**	-3.198	0.615	3.84E+08	4.68E+09	8.63E+08	1.24E+09
6.00E+07	4.1	26	1.64	4.50E+08	**0.02**	2.132	0.615	4.50E+08	**-0.03**	-3.198	0.615	5.56E+08	4.80E+09	1.04E+09	1.36E+09
6.00E+07	4.1	26	1.91	4.50E+08	**0.02**	2.132	0.615	4.50E+08	**-0.03**	-3.198	0.615	7.29E+08	4.88E+09	1.21E+09	1.44E+09
6.00E+07	4.1	26	2.19	4.50E+08	**0.02**	2.132	0.615	4.50E+08	**-0.03**	-3.198	0.615	9.02E+08	4.92E+09	1.38E+09	1.48E+09
6.00E+07	4.1	26	2.46	4.50E+08	**0.02**	2.132	0.615	4.50E+08	**-0.03**	-3.198	0.615	1.07E+09	4.91E+09	1.55E+09	1.47E+09
6.00E+07	4.1	26	2.73	4.50E+08	**0.02**	2.132	0.615	4.50E+08	**-0.03**	-3.198	0.615	1.25E+09	4.86E+09	1.73E+09	1.42E+09
6.00E+07	4.1	26	3.01	4.50E+08	**0.02**	2.132	0.615	4.50E+08	**-0.03**	-3.198	0.615	1.42E+09	4.77E+09	1.90E+09	1.33E+09
6.00E+07	4.1	26	3.28	4.50E+08	**0.02**	2.132	0.615	4.50E+08	**-0.03**	-3.198	0.615	1.59E+09	4.63E+09	2.07E+09	1.19E+09
6.00E+07	4.1	26	3.55	4.50E+08	**0.02**	2.132	0.615	4.50E+08	**-0.03**	-3.198	0.615	1.77E+09	4.46E+09	2.24E+09	1.01E+09
6.00E+07	4.1	26	3.83	4.50E+08	**0.02**	2.132	0.615	4.50E+08	**-0.03**	-3.198	0.615	1.94E+09	4.24E+09	2.42E+09	7.95E+08
6.00E+07	4.1	26	4.10	4.50E+08	**0.02**	2.132	0.615	4.50E+08	**-0.03**	-3.198	0.615	2.11E+09	3.97E+09	2.59E+09	5.32E+08
6.00E+07	4.1	26	4.37	4.50E+08	**0.02**	2.132	0.615	4.50E+08	**-0.03**	-3.198	0.615	2.28E+09	3.67E+09	2.76E+09	2.27E+08
6.00E+07	4.1	26	4.65	4.50E+08	**0.02**	2.132	0.615	4.50E+08	**-0.03**	-3.198	0.615	2.46E+09	3.32E+09	2.94E+09	-1.21E+08
6.00E+07	4.1	26	4.92	4.50E+08	**0.02**	2.132	0.615	4.50E+08	**-0.03**	-3.198	0.615	2.63E+09	2.93E+09	3.11E+09	-5.11E+08
6.00E+07	4.1	26	5.19	4.50E+08	**0.02**	2.132	0.615	4.50E+08	**-0.03**	-3.198	0.615	2.80E+09	2.50E+09	3.28E+09	-9.44E+08

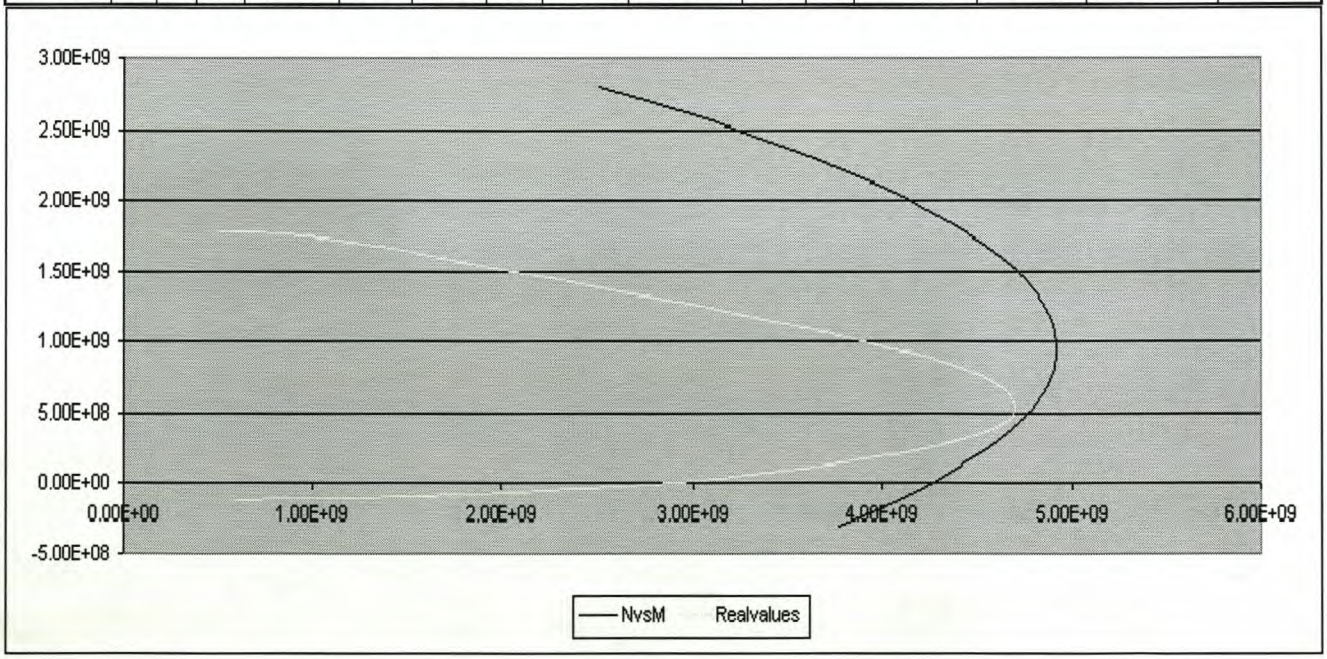

x=90m									Sign convention					Sonder staal	
fcu	h	b	x	fs1	%As1	As1	d'	fs2	%As2	As2	d	N	M	N	M
9.50E+07	2.2	26	0.15	4.50E+08	**0.03**	1.716	0.33	4.50E+08	**-0.03**	-1.716	0.33	1.47E+08	1.34E+09	1.47E+08	1.52E+08
9.50E+07	2.2	26	0.29	4.50E+08	**0.03**	1.716	0.33	4.50E+08	**-0.03**	-1.716	0.33	2.93E+08	1.47E+09	2.93E+08	2.85E+08
9.50E+07	2.2	26	0.44	4.50E+08	**0.03**	1.716	0.33	4.50E+08	**-0.03**	-1.716	0.33	4.40E+08	1.59E+09	4.40E+08	3.98E+08
9.50E+07	2.2	26	0.59	4.50E+08	**0.03**	1.716	0.33	4.50E+08	**-0.03**	-1.716	0.33	5.87E+08	1.68E+09	5.87E+08	4.92E+08
9.50E+07	2.2	26	0.73	4.50E+08	**0.03**	1.716	0.33	4.50E+08	**-0.03**	-1.716	0.33	7.34E+08	1.76E+09	7.34E+08	5.66E+08
9.50E+07	2.2	26	0.88	4.50E+08	**0.03**	1.716	0.33	4.50E+08	**-0.03**	-1.716	0.33	8.80E+08	1.81E+09	8.80E+08	6.21E+08
9.50E+07	2.2	26	1.03	4.50E+08	**0.03**	1.716	0.33	4.50E+08	**-0.03**	-1.716	0.33	1.03E+09	1.85E+09	1.03E+09	6.57E+08
9.50E+07	2.2	26	1.17	4.50E+08	**0.03**	1.716	0.33	4.50E+08	**-0.03**	-1.716	0.33	1.17E+09	1.86E+09	1.17E+09	6.73E+08
9.50E+07	2.2	26	1.32	4.50E+08	**0.03**	1.716	0.33	4.50E+08	**-0.03**	-1.716	0.33	1.32E+09	1.86E+09	1.32E+09	6.70E+08
9.50E+07	2.2	26	1.47	4.50E+08	**0.03**	1.716	0.33	4.50E+08	**-0.03**	-1.716	0.33	1.47E+09	1.84E+09	1.47E+09	6.47E+08
9.50E+07	2.2	26	1.61	4.50E+08	**0.03**	1.716	0.33	4.50E+08	**-0.03**	-1.716	0.33	1.61E+09	1.79E+09	1.61E+09	6.05E+08
9.50E+07	2.2	26	1.76	4.50E+08	**0.03**	1.716	0.33	4.50E+08	**-0.03**	-1.716	0.33	1.76E+09	1.73E+09	1.76E+09	5.44E+08
9.50E+07	2.2	26	1.91	4.50E+08	**0.03**	1.716	0.33	4.50E+08	**-0.03**	-1.716	0.33	1.91E+09	1.65E+09	1.91E+09	4.63E+08
9.50E+07	2.2	26	2.05	4.50E+08	**0.03**	1.716	0.33	4.50E+08	**-0.03**	-1.716	0.33	2.05E+09	1.55E+09	2.05E+09	3.62E+08
9.50E+07	2.2	26	2.20	4.50E+08	**0.03**	1.716	0.33	4.50E+08	**-0.03**	-1.716	0.33	2.20E+09	1.43E+09	2.20E+09	2.43E+08
9.50E+07	2.2	26	2.35	4.50E+08	**0.03**	1.716	0.33	4.50E+08	**-0.03**	-1.716	0.33	2.35E+09	1.29E+09	2.35E+09	1.04E+08
9.50E+07	2.2	26	2.49	4.50E+08	**0.03**	1.716	0.33	4.50E+08	**-0.03**	-1.716	0.33	2.49E+09	1.13E+09	2.49E+09	-5.50E+07
9.50E+07	2.2	26	2.64	4.50E+08	**0.03**	1.716	0.33	4.50E+08	**-0.03**	-1.716	0.33	2.64E+09	9.56E+08	2.64E+09	-2.33E+08
9.50E+07	2.2	26	2.79	4.50E+08	**0.03**	1.716	0.33	4.50E+08	**-0.03**	-1.716	0.33	2.79E+09	7.59E+08	2.79E+09	-4.30E+08
9.50E+07	2.2	26	2.93	4.50E+08	**0.03**	1.716	0.33	4.50E+08	**-0.03**	-1.716	0.33	2.93E+09	5.42E+08	2.93E+09	-6.47E+08

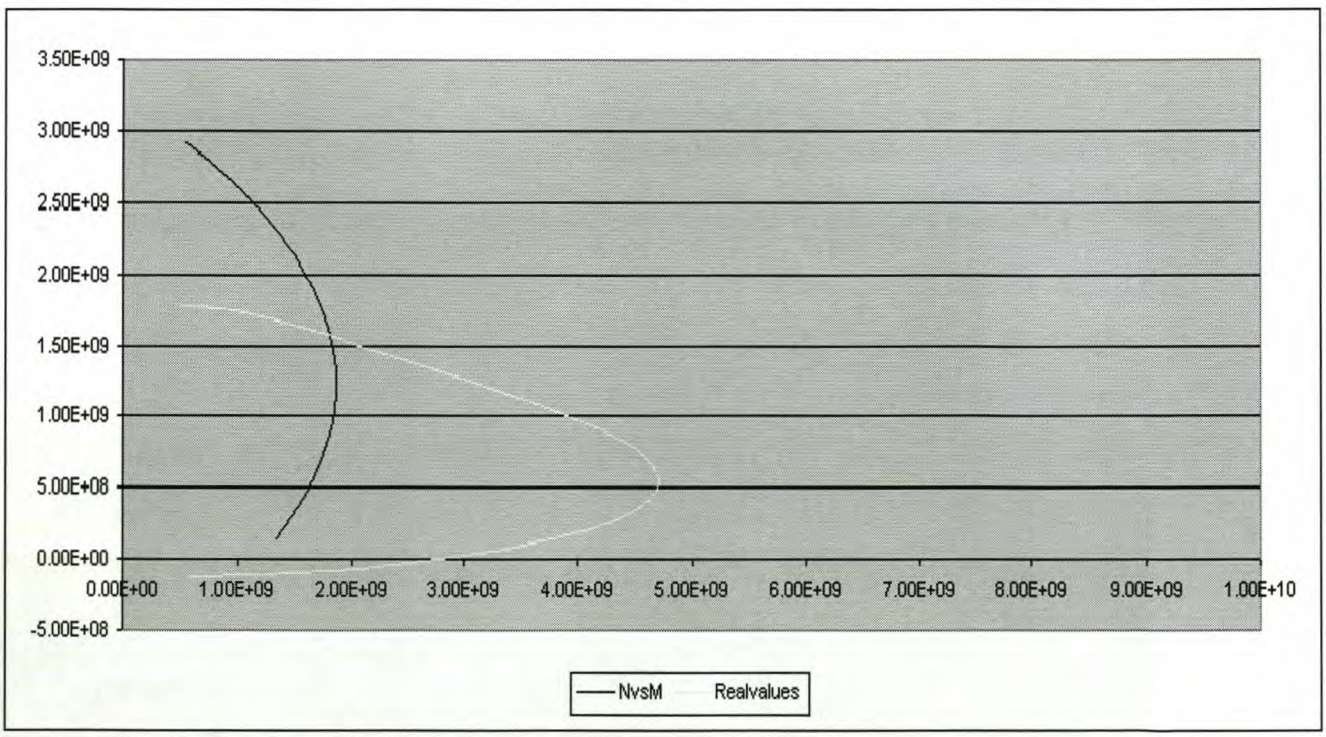

This last one displays the fact that the transfer section is needed!!

APPENDIX G: Rough Cost Estimation For Concepts

Concept 2: 40 meter height

			Volume			Cost/m^3		Cost	
Virtual Area	Area	Width	Concrete	Steel	MPa	Concrete	Steel	Concrete	Steel
1.25	49.8625	6	299.175	0.448763	7	R 628.92	R 36,895.00	R 188,157.14	R 16,557.11
11	438.79	6	2632.74	3.94911	9.5	R 630.00	R 36,895.00	R 1,658,626.20	R 145,702.41
13.5	538.515	6	3231.09	4.846635	12.1	R 653.00	R 36,895.00	R 2,109,901.77	R 178,816.60
7.5	299.175	6	1795.05	2.692575	14.62	R 676.00	R 36,895.00	R 1,213,453.80	R 99,342.55
5	199.45	6	1196.7	1.79505	17.15	R 699.00	R 36,895.00	R 836,493.30	R 66,228.37
4	159.56	6	957.36	1.43604	19.67	R 722.00	R 36,895.00	R 691,213.92	R 52,982.70
2	79.78	6	478.68	0.71802	22.2	R 752.00	R 36,895.00	R 359,967.36	R 26,491.35
1.25	49.8625	6	299.175	0.448763	24.73	R 783.00	R 36,895.00	R 234,254.03	R 16,557.11
0.25	9.9725	6	59.835	0.089753	27.26	R 820.00	R 36,895.00	R 49,064.70	R 3,311.44
0.1	3.989	6	23.934	0.035901	29.79	R 870.00	R 36,895.00	R 20,822.58	R 1,324.57
0.1	3.989	6	23.934	0.035901	32.32	R 915.00	R 36,895.00	R 21,899.61	R 1,324.57
45.95							**Totals**	**R 7,383,854.41**	**R 608,638.77**
									R 7,992,493.18

Concept 2: 150 meter height

			Volume			Cost/m^3		Cost	
Virtual Area	Area	Width	Concrete	Steel	MPa	Concrete	Steel	Concrete	Steel
21	934.2669	6	5605.601	8.408402	11.76	R 650.00	R 36,895.00	R 3,643,640.65	R 310,227.99
44	1957.512	6	11745.07	17.6176	13.7	R 670.00	R 36,895.00	R 7,869,196.90	R 650,001.35
9	400.4001	6	2402.401	3.603601	15.63	R 685.00	R 36,895.00	R 1,645,644.69	R 132,954.86
7	311.4223	6	1868.534	2.802801	17.57	R 705.00	R 36,895.00	R 1,317,316.47	R 103,409.34
81							**Totals**	**R 14,475,798.71**	**R 1,196,593.55**
									R 15,672,392.25

Concept 2: 300 meter height

			Volume			Cost/m^3		Cost	
Virtual Area	Area	Width	Concrete	Steel	MPa	Concrete	Steel	Concrete	Steel
15	1958.988	6	11753.93	17.63089	12.83	R 662.00	R 36,895.00	R 7,781,101.66	R 650,491.69
25	3264.98	6	19589.88	29.38482	14.71	R 675.00	R 36,895.00	R 13,223,169.00	R 1,084,152.93
9	1175.393	6	7052.356	10.57853	16.59	R 693.00	R 36,895.00	R 4,887,282.71	R 390,294.86
2.5	326.498	6	1958.988	2.938482	18.48	R 715.00	R 36,895.00	R 1,400,676.42	R 108,415.29
1	130.5992	6	783.5951	1.175393	20.36	R 734.00	R 36,895.00	R 575,158.80	R 43,366.12
1.5	195.8988	6	1175.393	1.763089	22.25	R 755.00	R 36,895.00	R 887,421.72	R 65,049.17
54							**Totals**	**R 28,754,810.31**	**R 2,341,770.07**
									R 31,096,580.38

Concept 1: 40 meter length

			Volume			Cost/m^3		Cost	
Virtual Area	**Area**	**Width**	**Concrete**	**Steel**	**MPa**	**Concrete**	**Steel**	**Concrete**	**Steel**
9.75	277.29	6	1663.74	2.49561	7.78	R 628.92	R 36,895.00	R 1,046,359.36	R 92,075.53
11.5	327.06	6	1962.36	2.94354	19.11	R 628.92	R 36,895.00	R 1,234,167.45	R 108,601.91
10.5	298.62	6	1791.72	2.68758	30.22	R 667.00	R 36,895.00	R 1,195,077.24	R 99,158.26
11	312.84	6	1877.04	2.81556	41.56	R 712.00	R 36,895.00	R 1,336,452.48	R 103,880.09
5.5	156.42	6	938.52	1.40778	52.89	R 772.00	R 36,895.00	R 724,537.44	R 51,940.04
2.6	73.944	6	443.664	0.665496	64.11	R 848.00	R 36,895.00	R 376,227.07	R 24,553.47
2	56.88	6	341.28	0.51192	75.33	R 941.00	R 36,895.00	R 321,144.48	R 18,887.29
1.7	48.348	6	290.088	0.435132	86.67	R 1,060.00	R 36,895.00	R 307,493.28	R 16,054.20
2	56.88	6	341.28	0.51192	97.78	R 1,200.00	R 36,895.00	R 409,536.00	R 18,887.29
2	56.88	6	341.28	0.51192	109.13	R 1,390.00	R 36,895.00	R 474,379.20	R 18,887.29
2	56.88	6	341.28	0.51192	120.38	R 1,600.00	R 36,895.00	R 546,048.00	R 18,887.29
1	28.44	6	170.64	0.25596	131.62	R 1,900.00	R 36,895.00	R 324,216.00	R 9,443.64
1	28.44	6	170.64	0.25596	142.89	R 2,300.00	R 36,895.00	R 392,472.00	R 9,443.64
1	28.44	6	170.64	0.25596	154.13	R 2,900.00	R 36,895.00	R 494,856.00	R 9,443.64
63.55							**Totals**	**R 9,182,966.00**	**R 600,143.59**
									R 9,783,109.59

The values highlighted in the Concept 1 tables are not readily available commercially. A simple exponential extrapolation was used to determine the concrete cost at these high stress values. The table below displays the extrapolation.

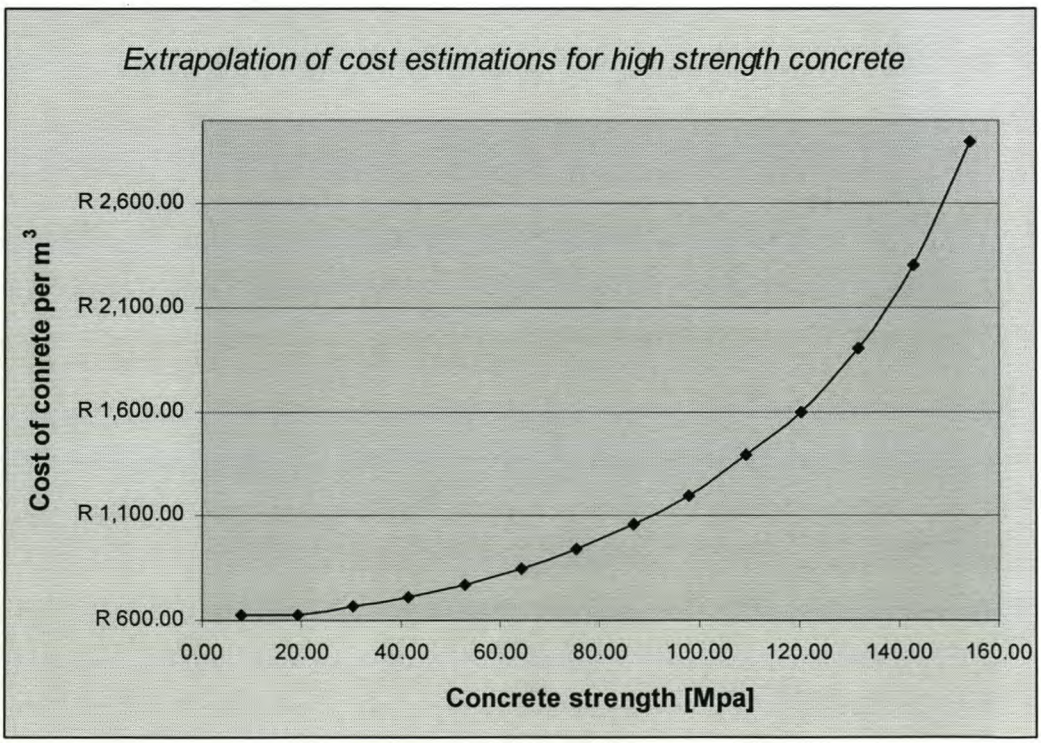

Concept 1: medium height, 40 meter length

			Volume			Cost/m^3		Cost	
Virtual Area	**Area**	**Width**	**Concrete**	**Steel**	**MPa**	**Concrete**	**Steel**	**Concrete**	**Steel**
9	400.4001	6	2402.401	3.603601	7.78	R 628.92	R 36,895.00	R 1,510,918.04	R 132,954.86
7.5	333.6668	6	2002.001	3.003001	19.11	R 628.92	R 36,895.00	R 1,259,098.47	R 110,795.72
8	355.9112	6	2135.467	3.203201	30.22	R 667.00	R 36,895.00	R 1,424,356.49	R 118,182.10
11	489.3779	6	2936.267	4.404401	41.56	R 712.00	R 36,895.00	R 2,090,622.10	R 162,500.37
6.5	289.1779	6	1735.067	2.602601	52.89	R 772.00	R 36,895.00	R 1,339,471.72	R 96,022.96
4	177.9556	6	1067.734	1.6016	64.11	R 848.00	R 36,895.00	R 905,438.43	R 59,091.03
3	133.4667	6	800.8002	1.2012	75.33	R 941.00	R 36,895.00	R 753,552.99	R 44,318.27
2	88.9778	6	533.8668	0.8008	86.67	R 1,060.00	R 36,895.00	R 565,898.81	R 29,545.52
1	44.4889	6	266.9334	0.4004	97.78	R 1,200.00	R 36,895.00	R 320,320.08	R 14,772.76
0.5	22.24445	6	133.4667	0.2002	109.13	R 1,390.00	R 36,895.00	R 185,518.71	R 7,386.38
52.5							**Totals**	**R 10,355,195.84**	**R 775,569.98**
									R 11,130,765.82

Concept 1: medium height, 32 meter length

			Volume			Cost/m^3		Cost	
Virtual Area	**Area**	**Width**	**Concrete**	**Steel**	**MPa**	**Concrete**	**Steel**	**Concrete**	**Steel**
1	40.96	6	245.76	0.36864	2.22	R 628.92	R 36,895.00	R 154,563.38	R 13,600.97
5.8	237.568	6	1425.408	2.138112	7.78	R 628.92	R 36,895.00	R 896,467.60	R 78,885.64
6	245.76	6	1474.56	2.21184	19.11	R 628.92	R 36,895.00	R 927,380.28	R 81,605.84
7.5	307.2	6	1843.2	2.7648	30.22	R 667.00	R 36,895.00	R 1,229,414.40	R 102,007.30
10	409.6	6	2457.6	3.6864	41.56	R 712.00	R 36,895.00	R 1,749,811.20	R 136,009.73
5	204.8	6	1228.8	1.8432	52.89	R 772.00	R 36,895.00	R 948,633.60	R 68,004.86
3	122.88	6	737.28	1.10592	64.11	R 848.00	R 36,895.00	R 625,213.44	R 40,802.92
1.7	69.632	6	417.792	0.626688	75.33	R 941.00	R 36,895.00	R 393,142.27	R 23,121.65
2	81.92	6	491.52	0.73728	86.67	R 1,060.00	R 36,895.00	R 521,011.20	R 27,201.95
0.2	8.192	6	49.152	0.073728	97.78	R 1,200.00	R 36,895.00	R 58,982.40	R 2,720.19
42.2							**Totals**	**R 7,504,619.77**	**R 573,961.05**
									R 8,078,580.82

Note: approximations as to the exact geometry and the volumes of specific strength characteristic material are made in the determination of the volume.